

1 **Air Pollution Scenario over Pakistan: Characterization and Ranking of Extremely**  
2 **Polluted Cities using Long-Term Concentrations of Aerosols and Trace Gases**

3 Muhammad Bilal<sup>1</sup>, Alaa Mhawish<sup>1</sup>, Janet E. Nichol<sup>2</sup>, Zhongfeng Qiu<sup>1,\*</sup>, Majid Nazeer<sup>3</sup>, Md. Arfan  
4 Ali<sup>1</sup>, Gerrit de Leeuw<sup>4,5,6,7</sup>, Robert C. Levy<sup>8</sup>, Yu Wang<sup>1</sup>, Yang Chen<sup>9</sup>, Lunche Wang<sup>10</sup>, Yuan Shi<sup>11</sup>,  
5 Max P. Bleiweiss<sup>12</sup>, Usman Mazhar<sup>13</sup>, Luqman Atique<sup>14</sup>, and Song Ke<sup>15</sup>

6 <sup>1</sup> Lab of Environmental Remote Sensing (LERS), School of Marine Sciences, Nanjing University of Information  
7 Science and Technology, Nanjing, 210044, China.

8 <sup>2</sup> Department of Geography, School of Global Studies, University of Sussex, Brighton BN19RH, UK.

9 <sup>3</sup> Key Laboratory of Digital Land and Resources, East China University of Technology, Nanchang 330013, China.

10 <sup>4</sup> Royal Netherlands Meteorological Institute (KNMI), R & D Satellite Observations, 3730AE De Bilt, The  
11 Netherlands.

12 <sup>5</sup> School of Atmospheric Physics, Nanjing University of Information Science and Technology, Nanjing, 210044,  
13 China.

14 <sup>6</sup> Aerospace Information Research Institute, Chinese Academy of Sciences (AirCAS), No.20 Datun Road, Chaoyang  
15 District, Beijing 100101, China

16 <sup>7</sup> School of Environment Science and Spatial Informatics, University of Mining and Technology, Xuzhou, Jiangsu  
17 221116, China.

18 <sup>8</sup> Climate and Radiation Laboratory, NASA Goddard Space Flight Center, Greenbelt, MD, USA.

19 <sup>9</sup> State Key Laboratory of Information Engineering in Surveying, Mapping and Remote Sensing, Wuhan University,  
20 Wuhan 430079, China.

21 <sup>10</sup> Laboratory of Critical Zone Evolution, School of Earth Sciences, China University of Geosciences, Wuhan  
22 430074, China.

23 <sup>11</sup> Institute of Future Cities, The Chinese University of Hong Kong, Hong Kong SAR, China.

24 <sup>12</sup> Department of Entomology, Plant Pathology and Weed Science, New Mexico State University, Las Cruces, NM  
25 88003, USA.

26 <sup>13</sup> School of Earth Sciences, Zhejiang University, Hangzhou 310027, China.

27 <sup>14</sup> School of Remote Sensing & Geomatics Engineering, Nanjing University of Information Science and  
28 Technology, Nanjing 210044, China.

29 <sup>15</sup> Geological Survey of Jiangsu Province, Nanjing, 210018, China.

30 \*Corresponding author: Zhongfeng Qiu ([zhongfeng.qiu@nuist.edu.cn](mailto:zhongfeng.qiu@nuist.edu.cn))

## Research Highlights:

- Lahore, Gujranwala, and Okara are the most polluted city based on  $PM_{2.5}$
- Jhang, Multan, and Vehari are the most polluted cities based on AOD
- Aerosols, nighttime lights, population, cropland, and fire show same spatial patterns
- Pakistan's entire population is exposed to long-term  $PM_x$  ( $x = 1, 2.5, \& 10$ )
- Pakistan's air quality is mainly affected by local anthropogenic sources

## 31 **Abstract**

32 Pakistan ranks third in the world in terms of mortality attributable to air pollution, with  
33 aerosol mass concentrations ( $PM_{2.5}$ ) consistently well above WHO (World Health Organization)  
34 air quality guidelines (AQG). However, regulation is dependent on a sparse network of air quality  
35 monitoring stations and insufficient ground data. This study utilizes long-term observations of  
36 aerosols and trace gases to characterize and rank the air pollution scenarios and pollution  
37 characteristics of 80 selected cities in Pakistan. Datasets used include (1) the Aqua and Terra  
38 (AquaTerra) MODIS (Moderate Resolution Imaging Spectroradiometer) Level 2 Collection 6.1  
39 merged Dark Target and Deep Blue (DTB) aerosol optical depth (AOD) retrieval products; (2) the  
40 CAMS (Copernicus Atmosphere Monitoring Service) reanalysis  $PM_1$ ,  $PM_{2.5}$ , and  $PM_{10}$  data; (3) the  
41 MERRA-2 (Modern-Era Retrospective analysis for Research and Applications, Version 2)  
42 reanalysis  $PM_{2.5}$  data, (4) the OMI (Ozone Monitoring Instrument) tropospheric vertical column  
43 density (TVCD) of nitrogen dioxide ( $NO_2$ ), and VCD of sulfur dioxide ( $SO_2$ ) in the Planetary  
44 Boundary Layer (PBL), (5) the VIIRS (Visible Infrared Imaging Radiometer Suite) Nighttime Lights  
45 data, (6) MODIS Collection 6 Version 2 global monthly fire location data (MCD14ML), (7)  
46 population density, (8) MODIS Level 3 Collection 6 land cover types, (9) AERONET (AErosol  
47 RObotic NETwork) Version 3 Level 2.0 data, and (10) ground-based  $PM_{2.5}$  concentrations from air  
48 quality monitoring stations. Potential Source Contribution Function (PSCF) analyses were  
49 performed by integrating with ground-based  $PM_{2.5}$  concentrations and the NOAA (National  
50 Oceanic and Atmospheric Administration) HYSPLIT (Hybrid Single-Particle Lagrangian Integrated  
51 Trajectory) air parcel back trajectories to identify potential pollution source areas which are

52 responsible for extreme air pollution in Pakistan. Results show that the ranking of the top  
53 polluted cities depends on the type of pollutant considered and the metric used. For example,  
54 Jhang, Multan, and Vehari were characterized as the top three polluted cities in Pakistan when  
55 considering AquaTerra DTB AOD products; for PM<sub>1</sub>, PM<sub>2.5</sub>, and PM<sub>10</sub> Lahore, Gujranwala, and  
56 Okara were the top three; for tropospheric NO<sub>2</sub> VCD Lahore, Rawalpindi, and Islamabad and for  
57 PBL SO<sub>2</sub> VCD Lahore, Mirpur, and Gujranwala. The results demonstrate that Pakistan's entire  
58 population has been exposed to high PM<sub>2.5</sub> concentrations for many years, with a mean annual  
59 value of 54.7 µg/m<sup>3</sup>, over all Pakistan from 2003 to 2020. This value exceeds Pakistan's National  
60 Environmental Quality Standards (Pak-NEQS, i.e., <15 µg/m<sup>3</sup> annual mean) for ambient air  
61 defined by the Pakistan Environmental Protection Agency (Pak-EPA) as well as the WHO Interim  
62 Target-1 (i.e., mean annual PM<sub>2.5</sub> <35 µg/m<sup>3</sup>). The spatial analyses of the concentrations of  
63 aerosols and trace gases in terms of population density, nighttime lights, land cover types, and  
64 fire location data, and the PSCF analysis indicate that Pakistan's air quality is strongly affected by  
65 anthropogenic sources inside of Pakistan, with contributions from surrounding countries.  
66 Statistically significant positive (increasing) trends in PM<sub>1</sub>, PM<sub>2.5</sub>, PM<sub>10</sub>, tropospheric NO<sub>2</sub> VCD,  
67 and SO<sub>2</sub> VCD were observed in ~89%, ~67%, ~48%, 91%, and ~88% of the Pakistani cities (80  
68 cities), respectively. This comprehensive analysis of aerosol and trace gas levels, their  
69 characteristics in spatio-temporal domains, and their trends over Pakistan, is the first of its kind.  
70 Results will be helpful to the Ministry of Climate Change (Government of Pakistan), Pak-EPA,  
71 SUPARCO (Pakistan Space and Upper Atmosphere Research Commission), policymakers, and the  
72 local research community to mitigate air pollution and its effects on human health.

73 **Keywords:** MODIS; AOD; CAMS; MERRA-2; PM<sub>1</sub>; PM<sub>2.5</sub>; PM<sub>10</sub>; OMI; NO<sub>2</sub>; SO<sub>2</sub>; PSCF; Pakistan



74 **Highlights:**

- 75 • Lahore, Gujranwala, and Okara are the most polluted city based on PM<sub>2.5</sub>
- 76 • Jhang, Multan, and Vehari are the most polluted cities based on AOD
- 77 • Aerosols, nighttime lights, population, cropland, and fire show same spatial patterns
- 78 • Pakistan's entire population is exposed to long-term PM<sub>x</sub> (x = 1, 2.5, & 10)
- 79 • Pakistan's air quality is mainly affected by local anthropogenic sources

80 **1. Introduction**

81 With the rapid increase in population and overexploitation of natural resources, air pollution  
82 is a serious global environmental concern. According to the World Health Organization (WHO  
83 2018a), air pollution levels are dangerously high worldwide as 9 out of 10 people breathe polluted  
84 air, and each year 7 million deaths are caused by outdoor and indoor aerosol pollutants. Outdoor  
85 (ambient) air pollution is due to high concentrations of different species including airborne  
86 particulate matter (PM), ozone (O<sub>3</sub>), nitrogen dioxide (NO<sub>2</sub>), volatile organic compounds (VOC),  
87 carbon monoxide (CO), and sulfur dioxide (SO<sub>2</sub>), which have adverse health effects (Mannucci  
88 and Franchini 2017). Although air pollution is a global problem, the latest WHO air quality  
89 database reveals that 97% of affected cities are in low- and middle-income countries with more  
90 than 100,000 inhabitants (WHO 2018b). Air pollution is endemic to Pakistan, being listed among  
91 low- and middle-income countries as well as being the most urbanized of its South Asian  
92 counterparts (77.42 million or 36.37 % of the urban population, with 2.52 % annual growth rate)  
93 (UNDP 2019). Purohit et al. (2013) predicted that under current emission control standards, air

94 pollution would decrease life expectancy by more than 100 months by 2030. The Health Effects  
95 Institute (2019) reported that since 1990, Pakistan's entire population has been exposed to PM<sub>2.5</sub>  
96 (the integrated dry mass of aerosol particulates with an aerodynamic diameter less than 2.5 µm)  
97 annual mean concentrations of 58 µg/m<sup>3</sup> in 2017, levels exceeding WHO Interim Target-1 (i.e.,  
98 <35 µg/m<sup>3</sup>). Pakistan ranks third in the world in terms of mortality attributable to air pollution,  
99 with an annual loss of 128,000 lives (Government of Pakistan 2019). Recently, on October 30,  
100 2019, the Air Quality Index (AQI) was 484 in Lahore (the second-largest city with the highest  
101 urbanization rate of 6.12 percent per annum), well above the threshold of 300 for "hazardous"  
102 level (Amnesty International 2019). The winter of 2019-2020 witnessed a spate of smog, which  
103 compelled authorities in Punjab to close schools for an extended period. The formation of this  
104 smog was fueled by the buildup of anthropogenic aerosols having 65% of sources within Pakistan.  
105 The principal cause for smog formation is NO<sub>x</sub>, which is emitted primarily from Pakistan's 23.6  
106 million transport vehicles (58%), followed by industry and power, which accounts for 34% of  
107 emissions (Amnesty International 2019; Government of Pakistan 2019; UNDP 2019). According  
108 to the Pakistan Air Quality Initiative (PAQI), Lahore, Peshawar, Islamabad, and Karachi are the  
109 most polluted cities where air quality does not meet WHO air quality guidelines during autumn  
110 and winter (PAQI 2018). Air pollution monitoring throughout Pakistan is challenging due to  
111 sparsely distributed air quality monitoring stations, though several remote sensing studies have  
112 been conducted.

113 Satellite observations provide spatial distributions of column-integrated concentrations  
114 which are related to the near-surface concentrations through meteorological and physico-  
115 chemical processes, thus complementing local ground-based observations. Gupta et al. (2013)

116 analyzed MODIS (Moderate Resolution Imaging Spectroradiometer) AOD (Aerosol Optical Depth)  
117 retrievals over Lahore and Karachi from 2001 to 2010 and reported higher aerosol loadings near  
118 the city center than outside the city. Tariq et al. (2016) analyzed ground-based and satellite-based  
119 aerosol optical properties over Lahore during intense haze events in October 2013 and reported  
120 crop residue burning and urban-industrial emissions as the main sources of high AOD levels. Bilal  
121 et al. (2016) evaluated the performance of the Aqua-MODIS (MYD04) level 2 aerosol products  
122 over Lahore and Karachi from 2007 to 2013, and recommended the use of Dark Target (DT) and  
123 Deep Blue (DB) algorithms over Karachi and Lahore, respectively, for regional air quality  
124 applications, as these cities have different land cover characteristics and aerosol types. Other  
125 remote sensing studies have been conducted on atmospheric trace gases, such as ozone (O<sub>3</sub>),  
126 nitrogen dioxide (NO<sub>2</sub>), sulfur dioxide (SO<sub>2</sub>), and carbon dioxide CO<sub>2</sub>, as well as their trends over  
127 time (Khokhar et al. 2016; Khokhar et al. 2015; Tariq and Ali 2015; ul-Haq et al. 2017; ul-Haq et  
128 al. 2014; Ul-Haq et al. 2015). Zhang et al. (2020) conducted the first study of the vertical  
129 distribution of aerosol optical properties over Pakistan using CALIPSO (Cloud-Aerosol Lidar and  
130 Infrared Pathfinder Satellite Observation) data.

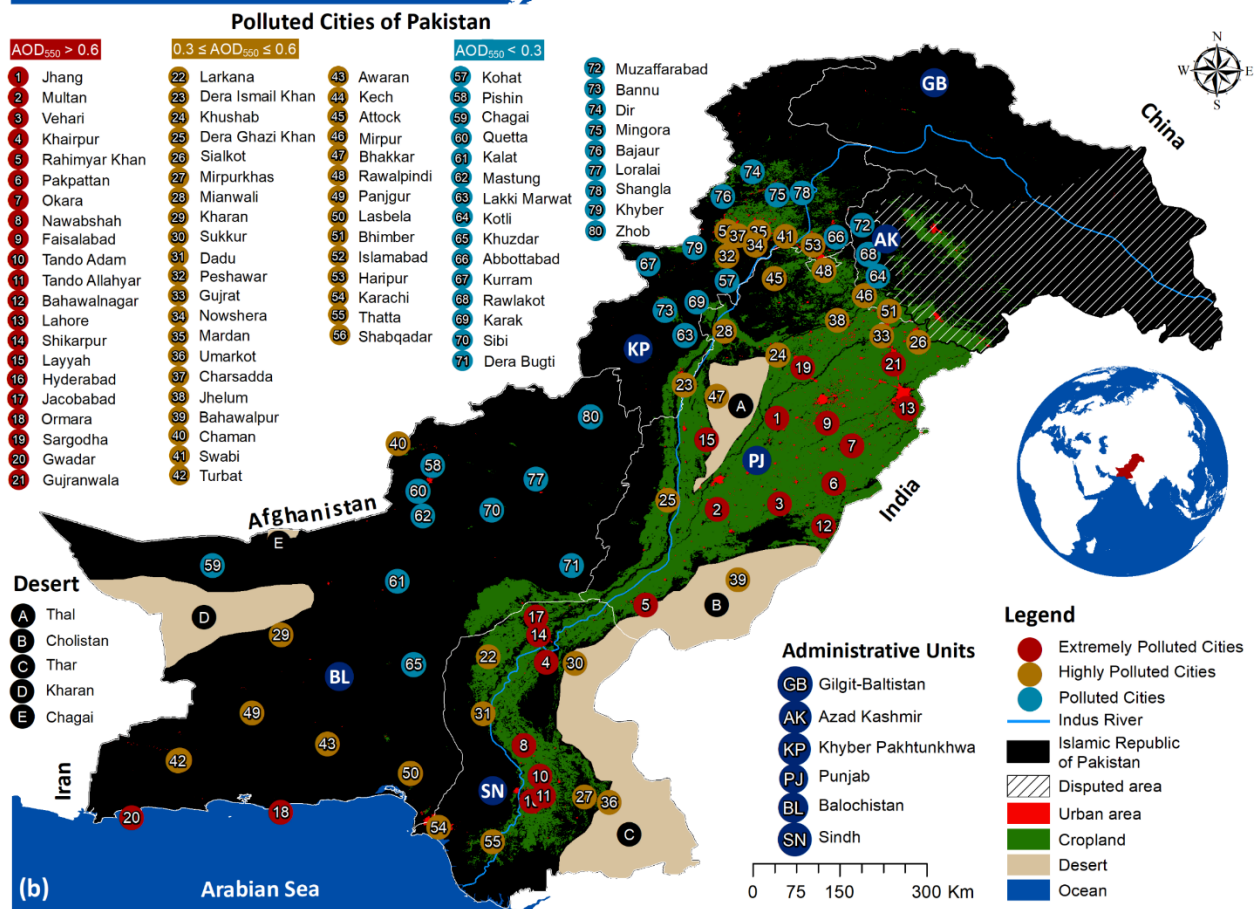
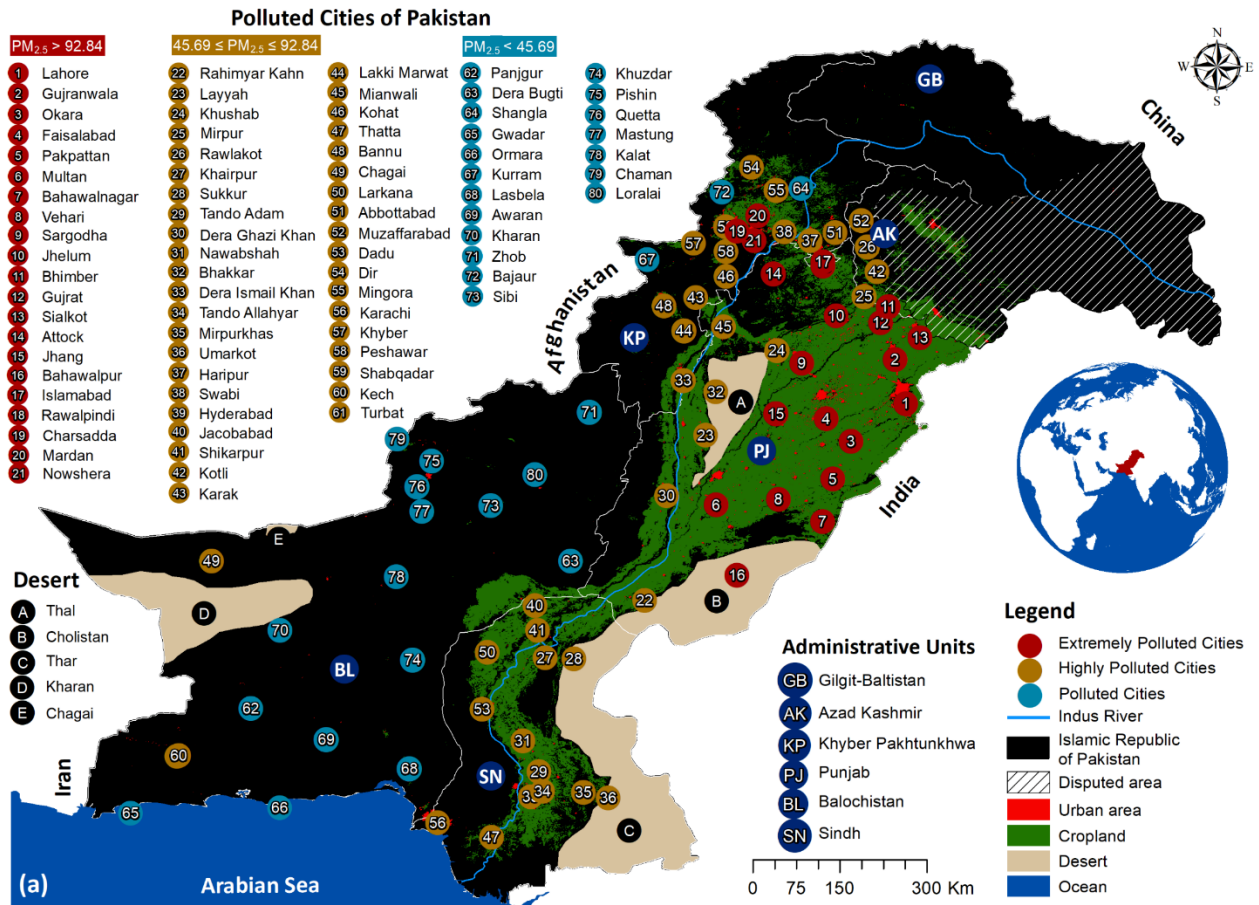
131 Cities are areas of high activity, and every city is a huge source of local anthropogenic aerosols  
132 and trace gases from industrial and human activities, which can impact air quality, visibility, and  
133 alter the physico-chemical properties of the atmosphere at local, regional, and global scales.  
134 Although several studies of AOD and atmospheric trace gases have been conducted over  
135 Pakistan, no study has encompassed different particle fractions (PM<sub>x</sub>, x = 1, 2.5, and 10) on the  
136 national scale, i.e., the dry mass of ultrafine particles with an aerodynamic diameter less than 1  
137 μm (PM<sub>1</sub>), 2.5 μm (PM<sub>2.5</sub>) and 10 μm (PM<sub>10</sub>). PM<sub>1</sub> is part of PM<sub>2.5</sub>, PM<sub>2.5</sub> is part of PM<sub>10</sub>. It is of

138 great importance to identify the cities most affected by different  $PM_x$  fractions, as they have  
139 different effects on, for instance, health and chemical and physical processes in the atmosphere,  
140 and this is the first study to do so. Moreover, very few studies have investigated the long-term  
141 trends in pollutant concentrations at city level, which can provide additional insights into the link  
142 between concentrations and the changes in emissions. Furthermore, previous studies are not  
143 comprehensive enough to answer questions such as: which are the most and least polluted cities  
144 of Pakistan, and what are the likely pollution sources? Therefore, this study aims (1) to  
145 extensively characterize and rank the extremely polluted cities of Pakistan, considering multiple  
146 sources and aerosol mass fractions, for 80 carefully selected cities, representing almost all major  
147 urban centers of Pakistan, and (2) to identify the likely pollutant sources by performing PSCF  
148 (Potential Source Contribution Function) analysis with the integration of HYSPLIT (Hybrid Single-  
149 Particle Lagrangian Integrated Trajectory) back trajectory and ground-based  $PM_{2.5}$   
150 concentrations. This study is based on long-term combined Aqua and Terra (AquaTerra) MODIS  
151 data from 2003 to 2017, OMI (Ozone Monitoring Instrument) data ( $NO_2$  and  $SO_2$ ) from 2004 to  
152 2019, CAMS (Copernicus Atmosphere Monitoring Service) reanalysis  $PM_1$ ,  $PM_{2.5}$ , and  $PM_{10}$  data  
153 from 2003 to 2019, MERRA-2 (Modern-Era Retrospective analysis for Research and Applications,  
154 Version 2)  $PM_{2.5}$  data from 2003 to 2020, VIIRS (Visible Infrared Imaging Radiometer Suite)  
155 Nighttime Lights from 2012 to 2019, LandScan global population density for 2019, MODIS land  
156 cover type for 2019, MODIS global monthly fire location data from 2003 to 2020, ground-based  
157  $PM_{2.5}$  concentrations from 2018 to 2020, and AERONET (AErosol RObotic NETwork) AOD  
158 measurements from 2006 to 2017. Detailed information on the data used in this study is provided  
159 in Section 3.

## 160 2. Study Area

161 Pakistan, with a population of 212.82 million, is the sixth most populous country in the world.  
162 It lies between 23°35' to 37°05' North and 60°50' to 77°50' East, having a diverse geographical  
163 landscape bordered by China, the Himalayas, India, Afghanistan, Iran, and the Arabian Sea.  
164 Geographically, Pakistan falls into three major regions: the northern highlands, constituting parts  
165 of the Hindu Kush, the Karakoram Range, and the Himalayas; the Indus River basin plain in the  
166 center and east (65% of the total area i.e. 796,096 km<sup>2</sup>); and the Balochistan Plateau in the south  
167 and west (Government of Pakistan 2019). Administratively, Pakistan has six units: Punjab, Sindh,  
168 Khyber Pakhtunkhwa, Balochistan, Azad Kashmir, and Gilgit Baltistan. Punjab is the most  
169 populous (112.38 million; 53%) administrative unit of Pakistan, followed by Sindh (49.05 million;  
170 23%), Khyber Pakhtunkhwa (36.5 million; 17%), and Balochistan (12.7 million; 6%). Balochistan  
171 has the largest area (43.6 %), followed by Punjab (25.8%), Sindh (17.7 %), and Khyber  
172 Pakhtunkhwa (12.78%). Sindh is the most urbanized and industrialized administrative unit of  
173 Pakistan with 52% urban population. Islamabad (2.1 million; 1%) Capital Territory (ICT), a rather  
174 small unit in terms of area (0.1 %), is, in fact, the second most urbanized (50.58%) region of  
175 Pakistan, and has an annual urbanization rate of 4.91 %. Currently, 10 cities in Pakistan have a  
176 population of over one million, and 7 have higher per-capita incomes than the national average  
177 (UNDP 2019). The Pakistan economic survey 2018-19 reports a total cropped area of 22.6 million  
178 hectares, and agricultural contributions of 18.5 % to the GDP, compared with 20.3% from the  
179 industrial sector (Government of Pakistan 2019).

180        This study covers almost all prominent cities in Pakistan including all administrative units and  
181 their capital cities, and the Capital of the country (Figure 1). In summary, the study area analyzes  
182 23 cities from the most populated administrative unit, Punjab; Khyber Pakhtunkhwa is also well-  
183 represented by 19 urban centers; Balochistan is the least populated but the largest administrative  
184 unit, and is represented by 19 cities; 14 other cities exemplify the diversity of Sindh in the South-  
185 East, and 5 cities represent the attractive hilly land of Azad Kashmir.



187 **Figure 1:** Geographical and administrative map of Pakistan including a list of cities used in the  
188 present study. Cities are characterized using (a) yearly mean CAMS (Copernicus Atmosphere  
189 Monitoring Service) reanalysis  $PM_{2.5}$  concentrations ( $\mu\text{g}/\text{m}^3$ ) for the years 2003 and 2020, and  
190 (b) yearly mean AquaTerra MODIS DTB AOD retrievals at 550 nm from 2003 to 2017. Extremely  
191 polluted cities (red color) are defined for  $PM_{2.5} > 92.84$  ( $AOD > 0.6$ ) (3<sup>rd</sup> quartile), highly polluted  
192 cities (brown color) for  $45.69 \leq PM_{2.5} \leq 92.84$  ( $0.3 < AOD < 0.6$ ) (between 3<sup>rd</sup> and 1<sup>st</sup> quartiles),  
193 and polluted cities (purple color) for  $PM_{2.5} < 45.69$  ( $AOD < 0.3$ ) (1<sup>st</sup> quartile) using descriptive  
194 statistics (Table S1). Cities are not defined as low polluted or clean cities as annual mean  $PM_{2.5}$   
195 concentrations for all cities exceed Pakistan's National Environmental Quality Standards (Pak-  
196 NEQS) for ambient air ( $<15 \mu\text{g}/\text{m}^3$  annual mean).

### 197 **3. Dataset**

#### 198 **3.1 AERONET Data**

199 The AERONET (AErosol RObotic NETwork) (Holben et al. 1998; Holben et al. 2001) is a global  
200 network of calibrated Sunphotometers coordinated by NASA (National Aeronautics and Space  
201 Administration) which provides regular measurements of spectral AOD at 340 nm, 380 nm, 440  
202 nm, 500 nm, 675 nm, 870 nm, 1020 nm, and 1640 nm, and AE at 340–440 nm, 380–500 nm, 440–  
203 675 nm, and 500–870 nm at three levels, i.e., Level 1.0 (unscreened), Level 1.5 (cloud-screened),  
204 and Level 2.0 (cloud-screened and quality-assured), under cloud-free skies (Smirnov et al. 2000)  
205 for every 15 minutes with an uncertainty of 0.01–0.02 (Holben et al. 2001). The present study  
206 used Version 3 Level 2.0 AOD at 500 nm ( $AOD_{500}$ ) and AE at 440–675nm ( $AE_{440-675}$ ) (Giles et al.  
207 2019) obtained from the AERONET website (<https://aeronet.gsfc.nasa.gov/>) for the Lahore



208 (31.47987° N, 74.26406° E) and Karachi (24.94574° N, 67.13594° E) sites from 2006 to 2017. The  
209 Lahore and Karachi AERONET sites are located in an urban area, and approximately 20 km away  
210 from the Arabian Sea coast, respectively.

### 211 **3.2 AquaTerra MODIS Data**

212 In the present study, Aqua and Terra MODIS C6.1 L2 aerosol products at 10 km spatial  
213 resolution are obtained from 2003 to 2017 for Pakistan from the LAADS DAAC  
214 (<https://ladsweb.modaps.eosdis.nasa.gov/>). The MODIS aerosol product provides DT AOD  
215 retrievals over land and water surfaces (Levy et al. 2013), and DB AOD retrievals only over land  
216 (Hsu et al. 2013). The DT and DB AOD retrievals for different collections are extensively validated  
217 against Sunphotometer (AERONET) measurements at regional (Bilal et al. 2019b; Bilal et al. 2014;  
218 Che et al. 2019; de Leeuw et al. 2018; Fan et al. 2017; Filonchik et al. 2019; Gupta et al. 2013; He  
219 et al. 2018; Islam et al. 2019; Livingston et al. 2014; Mhawish et al. 2017; More et al. 2013; Nichol  
220 and Bilal 2016; Shen et al. 2018; Shi et al. 2013; Sogacheva et al. 2018; Wang et al. 2017; Wang  
221 et al. 2019; Xiao et al. 2016; Xie et al. 2011) and global scales (Bilal et al. 2018a; Bilal et al. 2017;  
222 Levy et al. 2013; Levy et al. 2010; Mehta et al. 2016; Remer et al. 2013; Sayer et al. 2013; Sayer  
223 et al. 2014; Sayer et al. 2015; Tong et al. 2020). These studies have reported overestimation and  
224 underestimation in DT and DB AOD retrievals respectively, due to error in the estimated surface  
225 reflectance and aerosol scheme used in the inversion methods, but overall their performance is  
226 satisfactory. Previous studies (Bilal et al. 2018a; Bilal and Nichol 2017; Bilal et al. 2017; Bilal et al.  
227 2018b; Mei et al. 2019; Sayer et al. 2014) have also reported different spatial coverage of DT and  
228 DB AOD retrievals over land due to differences in their approaches, i.e., pixel selection criteria,

229 estimation of surface reflectance, and the cloud mask. Therefore, a new merged Scientific Data  
230 Set (SDS: AOD 550 Dark Target Deep Blue Combined) was introduced which contains only the  
231 highest quality DT and DB (DTB) AOD retrievals or their average values (Levy et al. 2013). The  
232 purpose of this new dataset is to improve spatial coverage over land (Levy et al., 2013; Sayer et  
233 al., 2014), i.e., to retrieve AOD in the same image for those regions where either the DT or the  
234 DB algorithm does not achieve a successful retrieval (Bilal et al. 2017; Levy et al. 2013). The  
235 merged DTB AOD retrievals have been validated at regional and global scales (Ali and Assiri 2019;  
236 Bilal et al. 2018a; Bilal and Nichol 2017; Bilal et al. 2017; Sayer et al. 2014; Sogacheva et al. 2018).  
237 However, the new customized method-1 (CM1) (Bilal et al. 2017), which is named Simplified  
238 Merge Scheme (SMS) in the later publications (Bilal et al. 2018a; Bilal et al. 2018b), provides  
239 equally consistent data quality with the combined DTB AOD retrievals available in C6.1, but with  
240 significantly improved spatio-temporal coverage.

### 241 **3.3 CAMS Data**

242 The Copernicus Atmosphere Monitoring Service (CAMS) reanalysis is an atmospheric  
243 composition dataset generated by the European Centre for Medium-Range Weather Forecasts  
244 (ECMWF). The global CAMS model combines satellite-based observations with chemistry-aerosol  
245 modeling using the four-dimensional variational (4D-VAR) data assimilation technique to obtain  
246 the mass concentration of aerosols and trace gases. CAMS uses the MACCity inventory at  $0.5^\circ \times$   
247  $0.5^\circ$  spatial resolution for anthropogenic emissions which covers the period 1960–2010 (Granier  
248 et al. 2011). Detailed information about the model and the emission inventory can be found in  
249 (Flemming et al. 2017; Flemming et al. 2015). In this study, the ground-based mass concentration

250 of particulate matter, including particles with an aerodynamic diameter of less than 1  $\mu\text{m}$  ( $\text{PM}_{10}$ ),  
251 less than 2.5  $\mu\text{m}$  ( $\text{PM}_{2.5}$ ), and less than 10  $\mu\text{m}$  ( $\text{PM}_{10}$ ) was obtained from the CAMS reanalysis data  
252 for the years 2003 and 2020.  $\text{PM}_x$  ( $x = 1, 2.5, \& 10$ ) data were used at two different spatiotemporal  
253 resolutions, i.e., (i) CAMS global reanalysis dataset at  $0.75^\circ \times 0.75^\circ$  spatial resolution and 3-hourly  
254 temporal resolution from 2003 to 2020, and (ii) CAMS near-real time dataset at  $0.125^\circ \times 0.125^\circ$   
255 spatial resolution and 12-hourly temporal resolution from 2018 to 2020 (Inness et al. 2019). The  
256  $\text{PM}_x$  data at  $0.75^\circ$  grid size and 3-hourly temporal resolution were used for long-term climatology  
257 and for characterizing extremely polluted cities, whereas, the CAMS near-real time data at  $0.125^\circ$   
258 grid size and 12-hourly temporal resolution were used for validation against ground-based  $\text{PM}_{2.5}$   
259 concentrations obtained from air quality monitoring stations.

### 260 **3.4 MERRA-2 Reanalysis Data**

261 The MERRA-2 (Modern-Era Retrospective analysis for Research and Applications, Version 2)  
262 atmospheric reanalysis is the latest data released by the NASA GMAO (Global Modeling and  
263 Assimilation Office) in 2017 (Buchard et al. 2017; Randles et al. 2017). The MERRA-2 aerosol  
264 gridded data, i.e., dust, sea salt, sulfate, black carbon, and organic carbon, are simulated with 72  
265 vertical layers from the surface to higher than 80 km using the GEOS-5 (GMAO Earth system  
266 model version 5) model radiatively coupled to the GOCART (Goddard Chemistry Aerosol  
267 Radiation and Transport) model (Chin et al. 2002; Colarco et al. 2010). For anthropogenic  
268 emissions, MERRA-2 uses the EDGAR-4.2 emission inventory at  $0.1^\circ \times 0.1^\circ$  spatial resolution  
269 which covers the period 1970–2008 (Janssens-Maenhout et al. 2013). In this study, the MERRA-  
270 2 aerosol gridded data (dust, sea salt, sulfate, black carbon, and organic carbon) at  $0.5^\circ \times 0.625^\circ$

271 spatial resolution from 2018 to 2020 were used. More details about MERRA-2 reanalysis data can  
272 be found in Randles et al. (2017) and Buchard et al. (2017).

### 273 **3.5 Ground-based PM<sub>2.5</sub> Measurements**

274 Ground-based PM<sub>2.5</sub> measurements were obtained from two different air quality monitoring  
275 networks. Firstly, PM<sub>2.5</sub> data were obtained from 4 air quality stations operated by the US  
276 Consulates in Islamabad, Karachi, Lahore, and Peshawar, and secondly, 54 air quality monitoring  
277 stations operated by PAQI in Lahore (24 stations), Karachi (15), Islamabad (5) Sialkot (3),  
278 Peshawar (2), Rawalpindi (2), Faisalabad (1), Gujranwala (1), and Muridke (1). Due to the lack of  
279 a well-developed and standard air quality network of ground-based PM<sub>2.5</sub> measurements, this  
280 study is limited to only these cities for the validation of CAMS and MERRA-2 reanalysis PM<sub>2.5</sub>  
281 gridded data. PM<sub>2.5</sub> concentrations from the US Consulates are measured by beta gauge  
282 attenuation monitors (BAM-1020; Met One Instruments), hereafter referred to as BAM PM<sub>2.5</sub>  
283 concentrations. To increase social awareness in Pakistan, PAQI provides PM<sub>2.5</sub> data using a  
284 nationwide network of low-cost air quality monitors (IQAir AirVisual Pro), hereafter referred to  
285 as LCM PM<sub>2.5</sub> concentrations. In this study, LCM and BAM PM<sub>2.5</sub> measurements were used for  
286 January 2018–December 2019 and January 2019–February 2021, respectively. More details  
287 about PAQI (LCM) and US Consulates (BAM) PM<sub>2.5</sub> data can be found in Shi et al. (2020) and  
288 Mhawish et al. (2020), respectively.

### 289 **3.6 OMI Data**

290 The Ozone Monitoring Instrument (OMI) onboard the Aura satellite was launched in July 2004  
291 as a part of the A-Train satellite constellation. OMI is a hyperspectral sensor that measures the  
292 radiation reflected from the earth-atmosphere system, in the wavelength range 250–500 nm and  
293 provides daily global coverage at a spatial resolution of  $13 \times 24 \text{ km}^2$  at nadir. The OMI OMAERUV  
294 algorithm utilizes the sensitivity of near-UV spectral regions to aerosol absorption, and it  
295 retrieves absorbing aerosol optical depth (AAOD) at 388nm (Torres et al. 2013; Torres et al. 2007).  
296 Along with the AAOD, the OMAERUV algorithm also provides an ultraviolet Aerosol Index (UVAI),  
297 AOD, and Single Scattering Albedo (SSA). OMI also retrieves the atmospheric trace gases  $\text{O}_3$ ,  $\text{NO}_2$   
298 and  $\text{SO}_2$  (Carn et al. 2017; Krotkov et al. 2017; Krotkov et al. 2016; Li et al. 2017; Li et al. 2013;  
299 Veefkind et al. 2006). In this study, OMAERUV version 3 Level 3 daily cloud-screened (cloud  
300 fraction < 30 %)  $\text{NO}_2$  tropospheric vertical column density (TVCD) (OMNO2e), and  $\text{SO}_2$  VCD in the  
301 planetary boundary layer (PBL) (OMSO2e) gridded at  $0.25^\circ \times 0.25^\circ$  spatial resolution from 2004  
302 to 2019 were used.

### 303 **3.7 Other Supporting Datasets**

304 Other supporting datasets include (i) annual mean VIIRS nighttime lights data  
305 (<https://eogdata.mines.edu/products/vnl/>) from 2012 to 2019 derived from monthly mean data  
306 (Elvidge et al. 2021), (ii) MODIS Collection 6 global monthly Fire Location product (MCD14ML)  
307 from 2003 to 2020 (<https://firms.modaps.eosdis.nasa.gov/download/>), (iv) MODIS Collection 6  
308 Level 3 land cover type product (MCD12Q1) for 2019

309 (<https://ladsweb.modaps.eosdis.nasa.gov/>), and (v) the LandScan population density  
310 (<https://landscan.ornl.gov/>) for 2019 (Rose et al. 2020).

#### 311 **4. Research Methodology**

312 To investigate the air pollution scenario over Pakistan and characterize the extremely  
313 polluted cities, in this study the following methodology was adopted:

314 1. MODIS AOD retrievals were obtained from the Scientific Data Set (SDS) “Optical Depth  
315 Land and Ocean” and “Deep Blue Aerosol Optical Depth 550 Land Best Estimate”. Only  
316 the highest quality-assured DT (QA = 3) and DB (QA ≥ 2) retrievals were used, as  
317 recommended by previous studies (Bilal et al. 2013; Levy et al. 2013; Mhawish et al. 2019;  
318 Sayer et al. 2013). Pakistan has a variety of land cover types, e.g., snow and mountainous  
319 land surface in Northern Pakistan, plain and agricultural land surfaces in Central Pakistan,  
320 and arid and desert land surfaces in southern Pakistan, where the DT and DB algorithms  
321 overestimate and underestimate, respectively. However, the DT algorithm is unable to  
322 provide retrievals over the arid and desert land surfaces of Balochistan. Similar results  
323 were observed and reported in our previous study over Pakistan (Bilal et al. 2016).  
324 Therefore, in the present study, we preferred to generate the combined (merged) DTB  
325 AOD<sub>550</sub> retrievals for both Aqua and Terra MODIS data from 2003 to 2017 using the  
326 customized method-1 (CM1) (Bilal et al. 2017), which in later publications is named  
327 Simplified Merge Scheme (SMS) (Bilal et al. 2018a; Bilal et al. 2018b), i.e., an average of  
328 the DT and DB AOD retrievals or the available one with the highest quality flag (Equation  
329 1), to enhance spatio-temporal coverage.

330

$$331 \quad DTB \ AOD_{550} = \left\{ \begin{array}{ll} \text{if only DT AOD exists} & \rightarrow \quad DT \\ \text{if only DB AOD exists} & \rightarrow \quad DB \\ \text{if both DT and DB AOD exist} & \rightarrow \quad (DT + DB)/2 \end{array} \right\} \quad (1)$$

332

333 2. Aqua and Terra MODIS may not provide complete spatial coverage due to cloud cover.

334 On days when Aqua provides AOD retrievals, Terra may not, and vice-versa. Therefore,

335 for more complete spatial coverage between Aqua and Terra as well as to represent an

336 average air pollution scenario between morning and afternoon times with a single

337 dataset, the combined AquaTerra DTB AOD retrievals were generated from the Aqua DTB

338 and Terra DTB AOD retrievals using SMS/CM1, i.e., an average of the Aqua and Terra DTB

339 AOD retrievals or the available one (Equation 2).

$$340 \quad AquaTerra \ AOD = \left\{ \begin{array}{ll} \text{if only Aqua AOD exists} & \rightarrow \quad Aqua \\ \text{if only Terra AOD exists} & \rightarrow \quad Terra \\ \text{if both Aqua and Terra AOD exist} & \rightarrow \quad (Aqua + Terra)/2 \end{array} \right\} \quad (2)$$

341 3. The AquaTerra DTB AOD retrievals are validated against Sunphotometer AOD

342 measurements obtained for Lahore (31.480° N and 74.264° E) and Karachi (24.946° N and

343 67.136° E) AERONET sites. The AERONET Sunphotometer does not provide AOD at 550

344 nm (AOD<sub>550</sub>), AOD<sub>550</sub> is interpolated using AOD at 500 nm (AOD<sub>500</sub>) and Ångström

345 Exponent at 440-675 nm (AE<sub>440-675</sub>) based on the Ångström Exponent empirical formula

346 (Equation 3) (Eck et al. 1999). Collocated AquaTerra and AERONET AOD retrievals were

347 defined as the average of at least two pixels of DTB within a spatial region of 3 × 3 pixels

348 (at least 2 out of 9 pixels) centered on the AERONET site and the average of at least two  
349 AERONET AOD measurements between 10:00 and 14:30 local solar time.

$$350 \quad AOD_{550} = AOD_{500} \left( \frac{550}{500} \right)^{-AE_{440-667}} \quad (3)$$

351 4. Accuracy and errors are reported using the Pearson correlation coefficient ( $r$ ), the  
352 expected error (EE, Equation 4), and relative mean bias (RMB, Equation 5). The slope ( $\beta$ ,  
353 Equation 6) and intercept ( $\alpha$ , Equation 7) between collocated AquaTerra DTB and  
354 AERONET AOD data are calculated using the reduced major axis (RMA) regression which  
355 incorporates errors in both independent (AERONET) and dependent (MODIS) variables  
356 (Bilal et al. 2019a; Harper 2016). The performance of the Terra and Aqua DT, DB, and DTB  
357 AOD retrievals is evaluated based on (i) highest correlation coefficient ( $r$ ), (ii) highest  
358 number of collocated retrievals ( $N$ ), (iii) the highest percentage of retrievals within the EE,  
359 and (iv) lowest RMB. To evaluate the performance of the collocated retrievals, the  
360 following criteria are utilized (Bilal et al. 2017): the DT, DB, and DTB retrievals are  
361 considered to be of equal quality if the relative difference is within (1) 5% for the  
362 correlation coefficient ( $r$ ), (2) 10% for the collocated retrievals, (3) 10% for the percentage  
363 of retrievals is within the EE, and (4) RMB < 25%.

$$364 \quad EE = \pm (0.05 + 0.20 \times AERONET_{AOD}) \quad (4)$$

365 The upper and lower EE envelopes are calculated using Equations 4a and 4b.

$$366 \quad \text{Upper EE envelope} = AERONET_{AOD} + |EE| \quad (4a)$$



367 
$$\text{Lower EE envelope} = \text{AERONET}_{AOD} - |EE| \quad (4b)$$

368 The percentage of best retrieved MODIS AOD retrievals within the EE is reported using  
 369 Equation 4c.

370 
$$\%EE = \text{AERONET}_{AOD} - |EE| \leq \text{MODIS}_{AOD} \leq \text{AERONET}_{AOD} + |EE| \quad (4c)$$

371 Where  $|EE|$  is the absolute value of EE.

372 
$$\text{RMB} = \frac{(\overline{\text{MODIS}_{AOD}} - \overline{\text{AERONET}_{AOD}})}{\overline{\text{AERONET}_{AOD}}} \times 100 \quad (5)$$

373 Where,  $\overline{\text{MODIS}_{AOD}}$  and  $\overline{\text{AERONET}_{AOD}}$  are the mean of MODIS and AERONET AOD  
 374 retrievals, respectively.  $\text{RMB} > 0$  represents overestimation in MODIS AOD compared to  
 375 AERONET AOD,  $\text{RMB} < 0$  represents underestimation, and  $\text{RMB} = 0$  represents no over- and  
 376 under-estimations.

377 
$$\beta = \frac{\sigma_{\text{MODIS}_{AOD}}}{\sigma_{\text{AERONET}_{AOD}}} \quad (6)$$

378 
$$\alpha = \overline{\text{MODIS}_{AOD}} - \left( \frac{\sigma_{\text{MODIS}_{AOD}}}{\sigma_{\text{AERONET}_{AOD}}} \right) \times \overline{\text{AERONET}_{AOD}} \quad (7)$$

379 Where,  $\beta$ ,  $\alpha$ ,  $\sigma_{\text{MODIS}_{AOD}}$ , and  $\sigma_{\text{AERONET}_{AOD}}$  are the slope, intercept, the standard deviation  
 380 of MODIS AOD, and standard deviation of AERONET AOD, respectively.

381 5. To show the long-term variation of the mean spatial distributions of AquaTerra AOD over  
 382 Pakistan, the AOD retrievals from 2003 to 2017 are used to generate monthly mean

383 spatial AOD maps, and their corresponding pixel counts are calculated for reporting the  
384 retrieval performance of both the DT and DB algorithms.

385 6. To assure the quality of the  $PM_{2.5}$  data, validation of daily average CAMS and MERRA-2  
386  $PM_{2.5}$  data was conducted against in-situ  $PM_{2.5}$  measurements obtained from the air  
387 quality monitoring stations. The performance was evaluated based on the correlation  
388 coefficient ( $r$ ), RMB (Eq. 5), and slope (Eq. 6). MERRA-2  $PM_{2.5}$  concentrations were  
389 calculated based on five aerosol components using Equation 8 (Song et al. 2018), and  
390 CAMS  $PM_{2.5}$  and  $PM_{10}$  concentrations were calculated using Equations 9 and 10 (Rémy et  
391 al. 2019).

392

$$393 \quad PM_{2.5} = [Dust_{2.5}] + [SS_{2.5}] + 1.375 \times [SO_4] + [BC] + 1.6 \times [OC] \quad (8)$$

394 Where,  $Dust_{2.5}$ ,  $SS_{2.5}$ , BC, OC, and  $SO_4$  are the GOCART concentrations of dust, sea salt,  
395 black carbon, organic carbon, and sulfate in particles with a diameter smaller than 2.5  $\mu m$ ,  
396 respectively.

$$397 \quad PM_{2.5} = \rho([SS_1]/4.3 + [SS_2]/4.3 + [DD_1] + [DD_2] + 0.7[OM] + [BC] + 0.7[SU] \\ 398 \quad + 0.7[NI_1] + 0.25[NI_2] + 0.7[AM]) \quad (9)$$

399

$$400 \quad PM_{10} = \rho([SS_1]/4.3 + [SS_2]/4.3 + [DD_1] + [DD_2] + 0.4[DD_3] + [OM] + [BC] \\ 401 \quad + [SU] + [NI_1] + [NI_2] + [AM]) \quad (10)$$

402 Where  $[SS_{1,2}]$  = sea salt aerosol,  $[DD_{1,2,3}]$  = desert dust,  $[NI_{1,2}]$  = nitrate,  $[OM]$  = organic  
403 matter,  $[BC]$  = black carbon,  $[SU]$  = sulfate, and  $[AM]$  = ammonium (concentrations in  
404 particles with a diameter smaller than  $2.5 \mu\text{m}$  from the CAMS model).

405 7. To characterize extremely polluted cities in Pakistan, the DTB AOD retrieved from  
406 AquaTerra, the  $PM_{1,}$   $PM_{2.5,}$  and  $PM_{10}$  from CAMS data, and the  $SO_2$  VCD and  $NO_2$  TVCD  
407 from OMI are used. Polluted months as well as years, for the corresponding polluted  
408 cities, are also characterized based on each pollutant.

409 8. To assess recent changes in the concentrations of atmospheric constituents, the non-  
410 parametric Mann Kendal test (Kendall and Gibbons 1990; Mann 1945) associated with  
411 Theil-Sen's slope (Sen 1968; Theil 1992) was used to estimate and detect trends over the  
412 main cities of Pakistan from 2003 to 2020. The non-parametric Mann Kendal test is often  
413 used to detect monotonic trends in a time series and is also suitable for non-normally  
414 distributed data, or if the data have some missing observations such as environmental  
415 data. Further, the bootstrapping technique was used to eliminate serial autocorrelation  
416 in the monthly mean aggregated time series data and increase the robustness of the test  
417 (Hamed and Ramachandra Rao 1998; Salmi et al. 2002). The significance of the calculated  
418 trend was assessed using the two-tailed test method at a 95% confidence interval.

419 9. The NOAA (National Oceanic and Atmospheric Administration) HYSPLIT (Hybrid Single-  
420 Particle Lagrangian Integrated Trajectory Model) (Stein et al. 2015), a complete transport,  
421 dispersion, and chemical transformation model, is used for back trajectory analysis to  
422 determine the origin of air masses (Fleming et al. 2012) and highlight the possible sources  
423 of aerosol pollutants affecting the air quality of Pakistan using the PSCF (Potential Source

424 Contribution Function) analysis. In this study, 72 hours HYSPLIT backward trajectories at  
425 the height of 500 m above the ground level (AGL) were computed for every 6 hours at  
426 seasonal scales from March 2020 to February 2021 using the GDAS (Global Data  
427 Assimilation System) meteorological data at  $1^\circ \times 1^\circ$  spatial resolution (available at  
428 <ftp://arlftp.arlhq.noaa.gov/pub/archives/gdas1>). The PSCF analysis was performed for 4  
429 cities selected because of the availability of ground-based  $PM_{2.5}$  measurements from the  
430 air quality stations operated by the US Consulates, namely, Peshawar, Islamabad, Lahore,  
431 and Karachi. The height of 500 m AGL has been reported very useful as it is the  
432 approximate height of the mixing layer (Begum et al. 2005). The backward trajectory  
433 clustering and investigation of the origins of the particulate matter at the receptor  
434 locations were studied using Meteoinfo TrajStat software (Version 2.0, available at  
435 <http://meteothink.org/products/trajstat.html>) (Wang et al. 2009) in conjunction with  
436 HYSPLIT and Geographic Information System (GIS).

437 The PSCF analysis was performed using 24-hour average ground-based  $PM_{2.5}$   
438 concentrations over a grid with a resolution of  $0.5^\circ$ , for the days that exceeded the Pak-  
439 NEQS 24-hour air quality standards ( $35 \mu\text{g}/\text{m}^3$ ). The PSCF value for a specific grid cell was  
440 calculated on the assumption that the trajectory endpoint is located within a cell (i, j) and  
441 the trajectory is assumed to collect pollutants emitted from different pocket emission  
442 sources within that cell (i, j). The PSCF value can be interpreted as a conditional probability  
443 describing the potential contributions of a grid cell to the high  $PM_{2.5}$  loadings at the  
444 receptor site. The error associated with the trajectory is proportional to the distance from

445 the receptor location (Begum et al. 2005). The PSCF value for the  $ij^{th}$  grid cell can be  
446 computed using Equation 11:

$$447 \quad PSCF(i, j) = m_{ij}/n_{ij} \quad (11)$$

448 Where,  $n_{ij}$  represents the number of endpoints that fall or pass through the  $ij^{th}$  cell  
449 and  $m_{ij}$  denotes for the number of endpoints in the  $ij^{th}$  cell having a higher pollutant  
450 concentration than the 24-hour Pak-NEQS. The uncertainty arising due to small  $n_{ij}$  is  
451 reduced by multiplying an arbitrary weight function  $W_{i,j}$ , which is multiplied into the  
452 PSCF. In this case, the weight function is given in Equation (12):

$$453 \quad W_{i,j} = \begin{cases} \text{if } n_{ij} > 3\bar{n} \rightarrow 1.00 \\ \text{if } 1.5\bar{n} < n_{ij} \leq 3\bar{n} \rightarrow 0.70 \\ \text{if } \bar{n} < n_{ij} \leq 1.5\bar{n} \rightarrow 0.42 \\ \text{if } n_{ij} \leq \bar{n} \rightarrow 0.15 \end{cases} \quad (12)$$

454 Where  $\bar{n}$  denotes the average number of endpoints per cell, which is calculated for each  
455 cell that has at least one endpoint. Therefore, the Weighted PSCF is expressed as Equation  
456 (13):

$$457 \quad WPSCF = W_{i,j} \times PSCF(i, j) \quad (13)$$

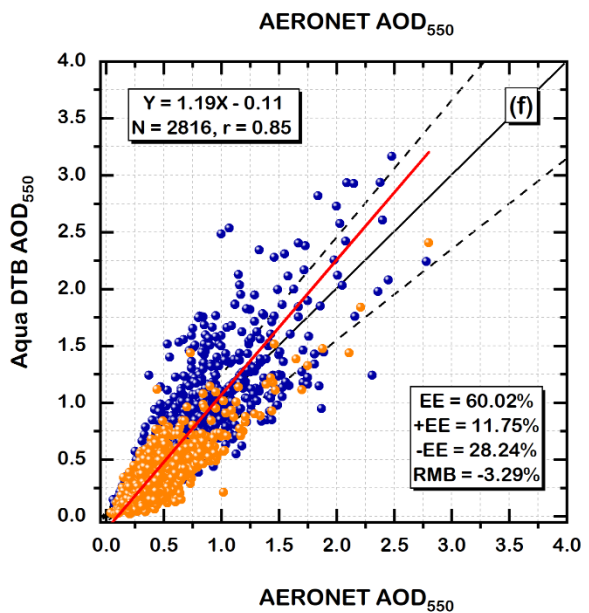
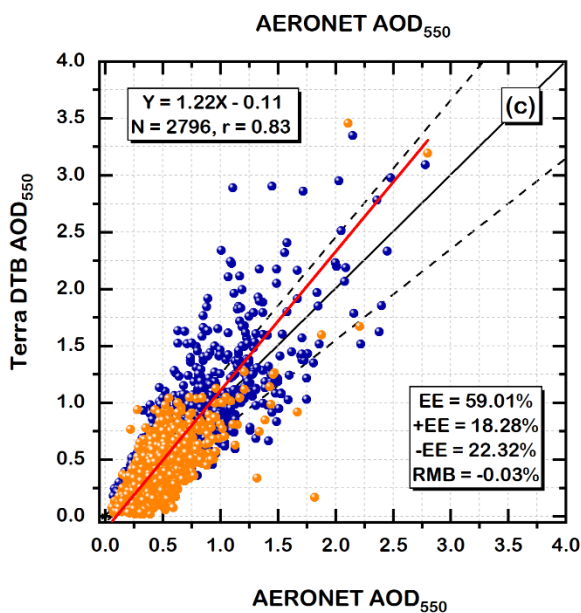
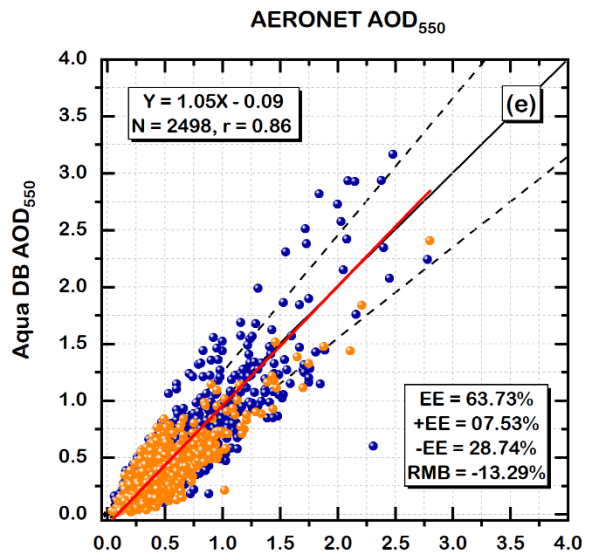
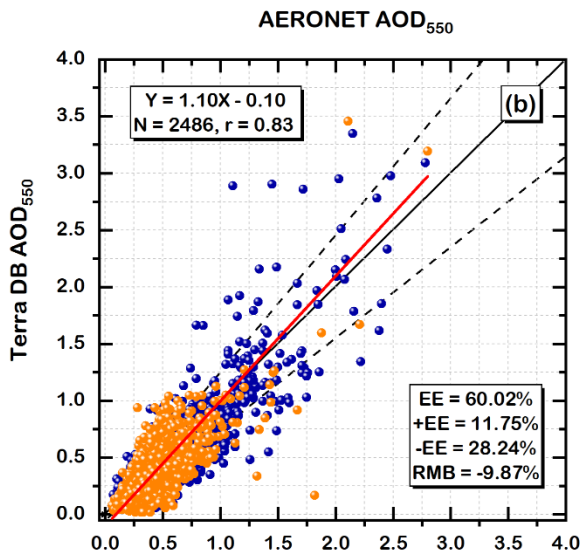
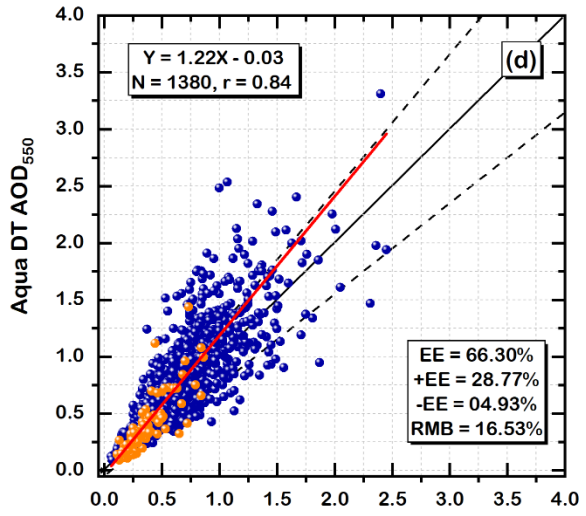
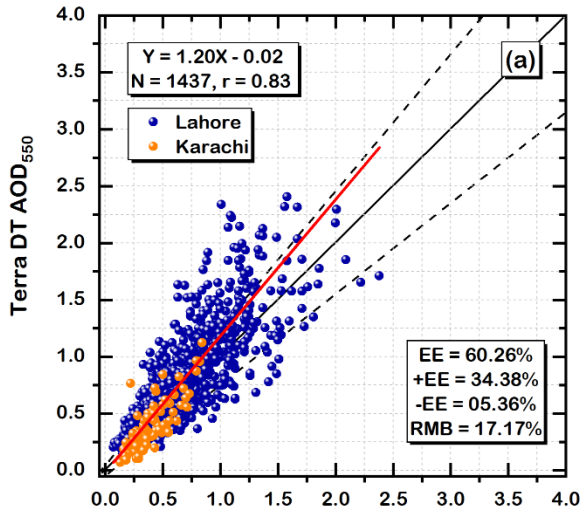
## 458 **5. Results and Discussion**

### 459 **5.1 Aqua and Terra MODIS AOD data**

#### 460 **5.1.1 Validation of AOD products against AERONET**

461 The MODIS AOD data used in this paper were evaluated by comparison with the AERONET  
462 AOD data over Lahore and Karachi. The scatterplots in Figure 2 show that Terra DT (Figure 2a),

463 DB (Figure 2b), and DTB (Figure 2c) retrieved AOD are equally correlated ( $r = 0.83$ ) with AERONET-  
464 derived AOD, and have the same percentage of retrievals within the EE. However, the number of  
465 collocated observations for DTB ( $N = 2796$ ) is significantly higher than for DT ( $N = 1437$ ) and DB  
466 ( $N = 2486$ ) i.e., 94.6% and 12.5% more data are available from DTB than from DT and DB,  
467 respectively. The AOD retrieved from DT is significantly overestimated (RMB = 17.17%), with  
468 34.38% of the data are above the EE (+EE). DB underestimates the AOD (RMB = -9.87%) with  
469 28.24% of the data below the EE (-EE). These uncertainties appear to be averaged out in the DTB  
470 AOD product, as the overestimations and underestimations are fewer than for DT and DB,  
471 individually. Furthermore, the RMB (-0.03%) is significantly improved, being 99.9% and 99.8%  
472 lower than for DT and DB, respectively. These results indicate the better performance of the Terra  
473 DTB AOD product as compared to DT and DB over Pakistan. Similar to Terra, the performance of  
474 the Aqua DTB AOD product (Figure 2f) is much better than for DT (Figure 2d) and DB (Figure 2e)  
475 products, with a significantly higher number of collocated AOD values and lower RMB. However,  
476 Aqua performs equally as Terra in terms of correlation and the percentage of retrievals within  
477 the EE. It is important to mention that a larger number of both DT and DB AOD retrieval products  
478 was available for Lahore than for Karachi and also that DB provides a greater number of AOD  
479 retrievals over Pakistan than DT. Based on the superior performance of the Aqua and Terra DTB  
480 AOD retrievals, the merged AquaTerra DTB AOD product was generated for further analysis (see  
481 Figure S1 in the supplementary data for the validation of AquaTerra DTB AOD retrievals).



483 **Figure 2:** Validation of Terra and Aqua DT, DB, and DTB AOD products versus AERONET Version  
484 3 Level 2.0 AOD measured in Lahore (for location, see no. 1 in Fig. 1a) and Karachi (for location,  
485 see no. 56 in Fig. 1a) from 2006 to 2017. The red line represents the regression line, the solid  
486 black line represents the identity line, and the dashed black lines represent the upper and lower  
487 EE envelopes. The orange points represent AOD pairs at Karachi, the blue dots at Lahore.

### 488 **5.1.2 Spatial distribution of AOD retrievals**

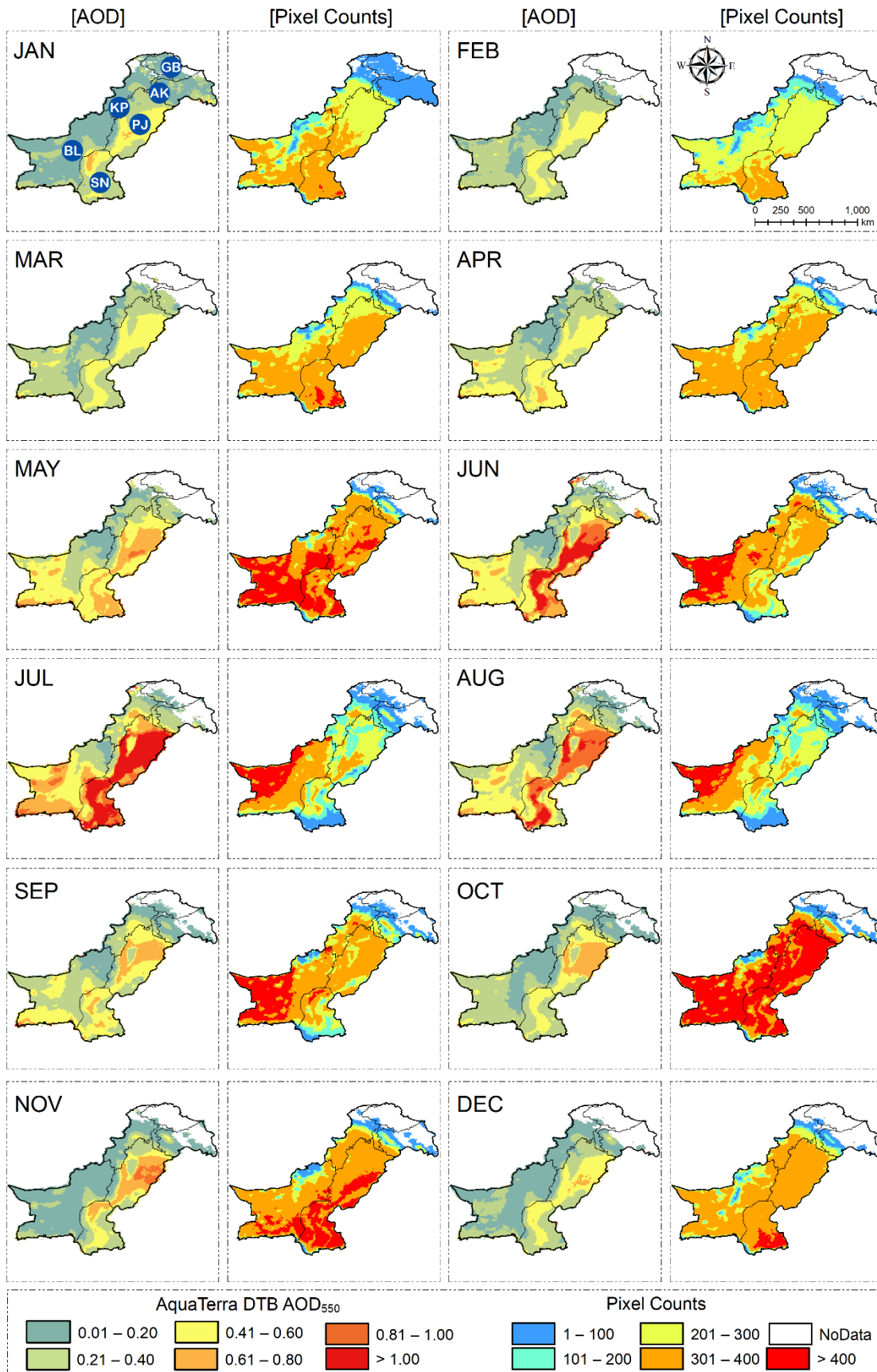
489 Figure 3 shows the spatial distributions of the monthly mean AquaTerra DTB AOD over  
490 Pakistan together with the corresponding pixel counts (PC) averaged over the years 2003 - 2017.  
491 Significant monthly variations in both AOD and PC are observed. AOD retrievals are missing over  
492 the Gilgit-Baltistan and Jammu & Kashmir (disputed territory) throughout the year, except for  
493 January, as the DT and DB algorithms do not provide AOD retrievals over high mountain regions  
494 and snow-covered surfaces. The presence of AOD retrievals during January is because the DB  
495 algorithm does not use the MODIS snow mask product directly, and the internal snow/cloud  
496 mask does not work well over these regions. Surprisingly, high AOD values  $> 1.0$  are observed  
497 during June and July over the Northwestern region of Khyber Pakhtunkhwa, which is a high  
498 mountainous region with permanent snow cover. These high AOD values over snow-covered  
499 regions could be due to an error in the internal snow/cloud mask of the DB algorithm which has  
500 missed these pixels during preprocessing; DT does discard bright pixels during preprocessing.  
501 AOD  $> 1.0$  is observed in July followed by June and August over Punjab and Sindh, mainly  
502 attributed to hygroscopic growth of the aerosol particles during summer relative humidity is high,  
503 similar to other reports using MODIS and MISR aerosol products (Mehta et al. 2016; Mhawish et



504 al. 2021). Most of the major cities of Punjab and Sindh are surrounded by cropland, and the  
505 results show that high AOD over Pakistan follows the same spatial pattern as that of the cropland.  
506 The AOD over cropland is significantly higher than over non-agricultural (i.e., mainly desert)  
507 regions throughout the year, even during late spring and summer when dust storms are  
508 considered a major source of aerosols over Punjab and Sindh. Local production of anthropogenic  
509 aerosols from urban and industrial emissions and agricultural pre- and post-harvest burning may  
510 be responsible for the high pollution levels over the region. Over Balochistan, especially over the  
511 desert areas, the AOD is low compared to that in Punjab and Sindh, but still higher than over  
512 other administrative units. Over Punjab, the highest AOD values are observed during the post-  
513 harvest seasons, i.e., throughout September to November, peaking in November, probably due  
514 to biomass (crop residue) burning activities (Jethva et al. 2019; Mhawish et al. 2021). However,  
515 if the high AOD levels would only be due to locally produced aerosols, the spatial patterns during  
516 each month should be similar, but they are not. Therefore, the transboundary transport of  
517 aerosols may contribute to Pakistan's deteriorating air quality. This is confirmed by the well-  
518 known smog episodes, occurring every year over Punjab due to both local production of aerosols  
519 from crop residue burning and across the border, during which atmospheric visibility is reduced  
520 to a few meters in both urban and rural areas. Overall, much higher AOD levels were observed in  
521 Pakistan during June, July, and August (summer), followed by September, October, and  
522 November (autumn), March, April, and May (spring), and December, January, and February  
523 (winter). The higher AOD in the summer is attributed to several reasons, including (i) hygroscopic  
524 growth of aerosol particles, due to high relative humidity, which increases the extinction  
525 efficiency of the atmospheric aerosols (Dickerson et al. 1997; Li and Wang 2014), (ii) the

526 enhancement of secondary aerosol formation rate due to faster photochemical reactions during  
527 higher temperatures (Jacob and Winner 2009; Kulmala et al. 2020), and (iii) the larger  
528 contribution of natural aerosols (mainly dust) during the summer monsoon (Mhawish et al.  
529 2021).

530 Figure 3 shows a distinct pattern of PC which suggests that the DT and DB algorithms do not  
531 perform equally temporally or spatially. For example, between 2003 to 2017, from late spring to  
532 early autumn, a large number of AOD retrievals (> 400) per pixel are available over Balochistan  
533 and some parts of Punjab, and from late autumn to early spring, a large number of AOD retrievals  
534 (> 400) per pixel are available over Sindh and some parts of Punjab. This could be attributed to  
535 the seasonality in the surface albedo due to changes in vegetation cover and/or the presence of  
536 cloud cover. Only October provides favorable conditions to both the DT and DB algorithms, when  
537 more than 400 AOD retrievals are available over Pakistan from both algorithms, except for Gilgit-  
538 Baltistan and disputed areas, due to high surface albedo for snow/ice surfaces.



540 **Figure 3:** Monthly mean spatial distributions of AquaTerra DTB AOD<sub>550</sub> and the total number of  
541 corresponding Pixel Counts (PC) over Pakistan, both averaged over the years from 2003 to  
542 2017. The six units in Pakistan are indicated in the upper-left figure: GB = Gilgit-Baltistan, AK=  
543 Azad Kashmir, KP = Khyber Pakhtunkhwa, PJ = Punjab, BL = Balochistan, and SN = Sindh.

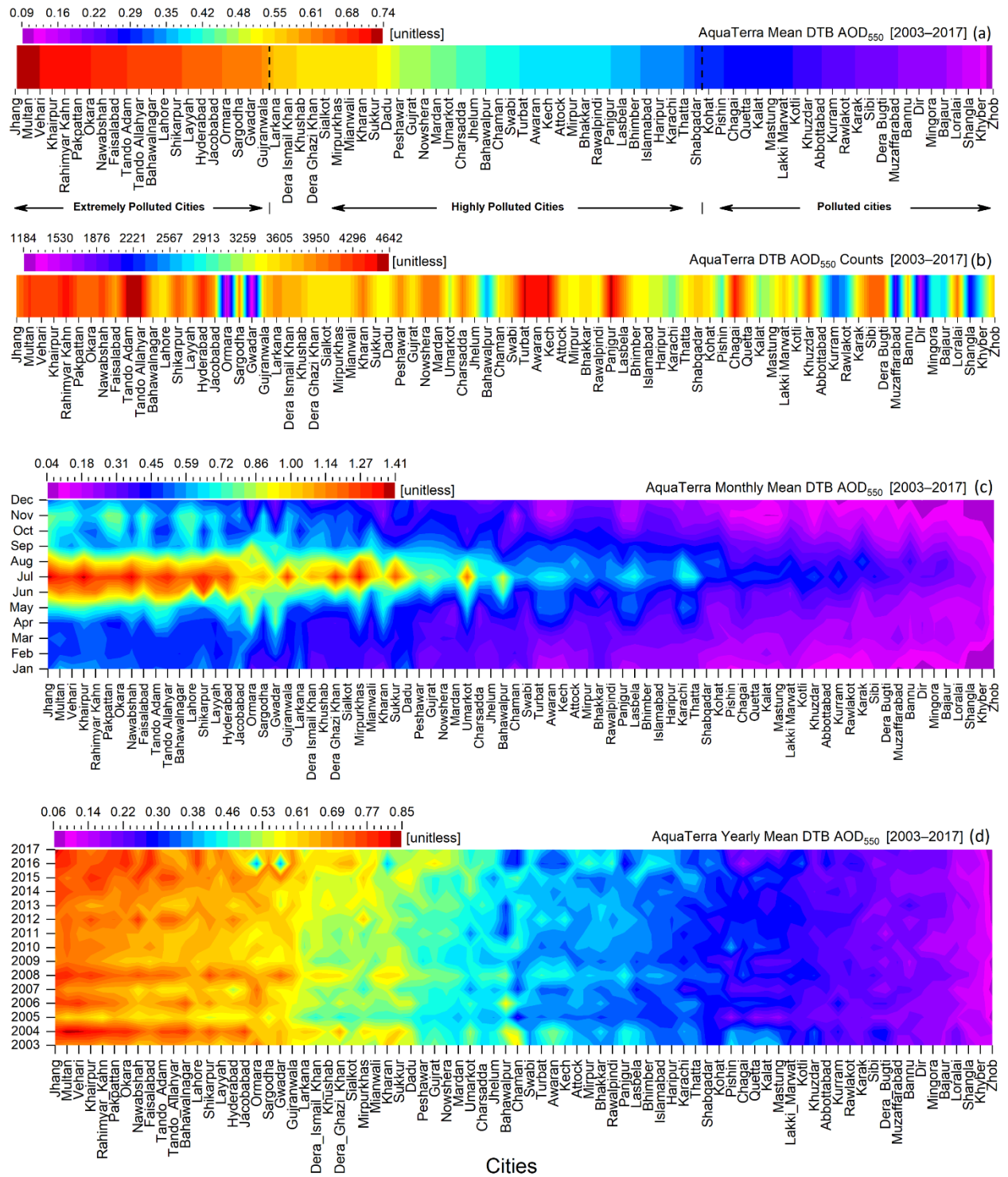
### 544 5.1.3 Characterization of extremely polluted cities using MODIS data

545 Figure 4a shows the mean AOD<sub>550</sub> retrievals for 80 cities (Figure 1) obtained from the annual  
546 mean AquaTerra DTB AOD<sub>550</sub> images and categorizes the extremely polluted to polluted cities.  
547 The thresholds for polluted and extremely polluted cities are defined based on the values of first  
548 (Q1) and third (Q3) quartiles respectively, and these quartiles are calculated by analyzing  
549 descriptive statistics (Table S1) for the AOD values extracted for 80 cities. Highly polluted cities  
550 are defined based on the AOD range between the first and third quartiles. For example, AOD <  
551 0.3 (1<sup>st</sup> quartile) represents polluted cities,  $0.3 \leq \text{AOD} \leq 0.6$  (between 1<sup>st</sup> and 3<sup>rd</sup> quartiles)  
552 represents highly polluted cities and AOD > 0.6 represents extremely polluted cities (3<sup>rd</sup> quartile).  
553 A total of 21 cities fall within the category of extremely polluted cities (Punjab: 12, Sindh: 7, and  
554 Balochistan: 2), 35 cities in the category of moderately polluted cities (Punjab: 11, Sindh 7,  
555 Balochistan: 7, Khyber Pakhtunkhwa: 8, Azad Kashmir: 2), and 24 cities in the category of low  
556 polluted cities (Punjab: 0, Sindh 0, Balochistan: 10, Khyber Pakhtunkhwa: 11, Azad Kashmir: 3).  
557 The top 3 polluted cities are Jhang, Multan, and Vehari in Punjab, as Punjab is the most urbanized  
558 and populated administrative unit (Figures 1b and 4a), with more vehicles and industries, and  
559 also faces severe smog episodes and dust storms, resulting in extremely high AOD levels over the  
560 region. Along with anthropogenic aerosols produced locally from cropland, urban and industrial

561 emissions, regional transport of aerosols may be responsible for Punjab's severe air pollution  
562 problems which will be investigated using the PSCF analysis based on the HYSPLIT air parcel back  
563 trajectory analysis and BAM PM<sub>2.5</sub> concentrations (see section 5.7).

564 Figure 4b shows the pixel counts (PC) of the daily AOD retrievals for each city from 2003 to  
565 2017. Results show a large number of PC for most cities, indicating that the characterization of  
566 extremely polluted to polluted cities is based on a large number of PC, which supports the results  
567 in Figure 4a and provides confidence in the use of merged AquaTerra DTB AOD products for  
568 quantitative research applications over Pakistan. However, it is noted that the lowest number of  
569 PC is observed for the coastal (Ormara and Gwadar) and mountainous (Dir) cities, where the  
570 inversion scheme of both the DT and DB algorithms needs to be improved.

571 The monthly mean AOD retrievals are plotted to identify the high and low polluted months  
572 in Pakistan (Figure 4c). The months of June, July, and August are by far the most polluted, with  
573 AOD > 1.20 for extremely polluted cities. A similar pattern of monthly variation in AOD is  
574 observed for all other cities, though at lower pollution levels. As mentioned in section 5.1.2, these  
575 months may be affected by aerosol pollutants from local sources such as agricultural land, urban  
576 and industrial regions, and deserts. Figure 4d, showing inter-annual variations, indicates very high  
577 AOD levels for extremely polluted cities throughout the last two decades, with annual mean AOD  
578 > 0.60, and with the most polluted years being 2004, 2006, 2008, 2016, and 2017.



580 **Figure 4:** Characterization of extremely polluted to polluted cities in Pakistan using AquaTerra  
581 DTB AOD<sub>550</sub> products from 2003 to 2017. (a) polluted cities based on mean AOD, (b) pixel  
582 counts, (c) polluted months based on mean AOD, and (d) polluted years based on mean AOD.

## 583 **5.2 CAMS and MERRA-2 reanalysis data**

### 584 **5.2.1 Validation of PM<sub>2.5</sub> reanalysis data**

585 Previous studies have evaluated the uncertainties in both CAMS and MERRA-2 PM<sub>2.5</sub>  
586 reanalysis data compared to ground-based PM<sub>2.5</sub> measurements (Cuevas et al. 2015; He et al.  
587 2019; Song et al. 2018; Ukhov et al. 2020). Recently, Ukhov et al. (2020) reported overestimation  
588 in CAMS PM<sub>2.5</sub> over the middle east and west Asia which have been attributed to the deficient  
589 size distribution of the emitted dust. Additionally, significant underestimation in MERRA-2 PM<sub>2.5</sub>  
590 was reported over China and India (He et al. 2019; Navinya et al. 2020; Song et al. 2018) which  
591 could be due to the lack of nitrate concentrations in the reanalysis data and underestimation of  
592 OC emission for urban/suburban areas (Buchard et al. 2016; Provencal et al. 2017).

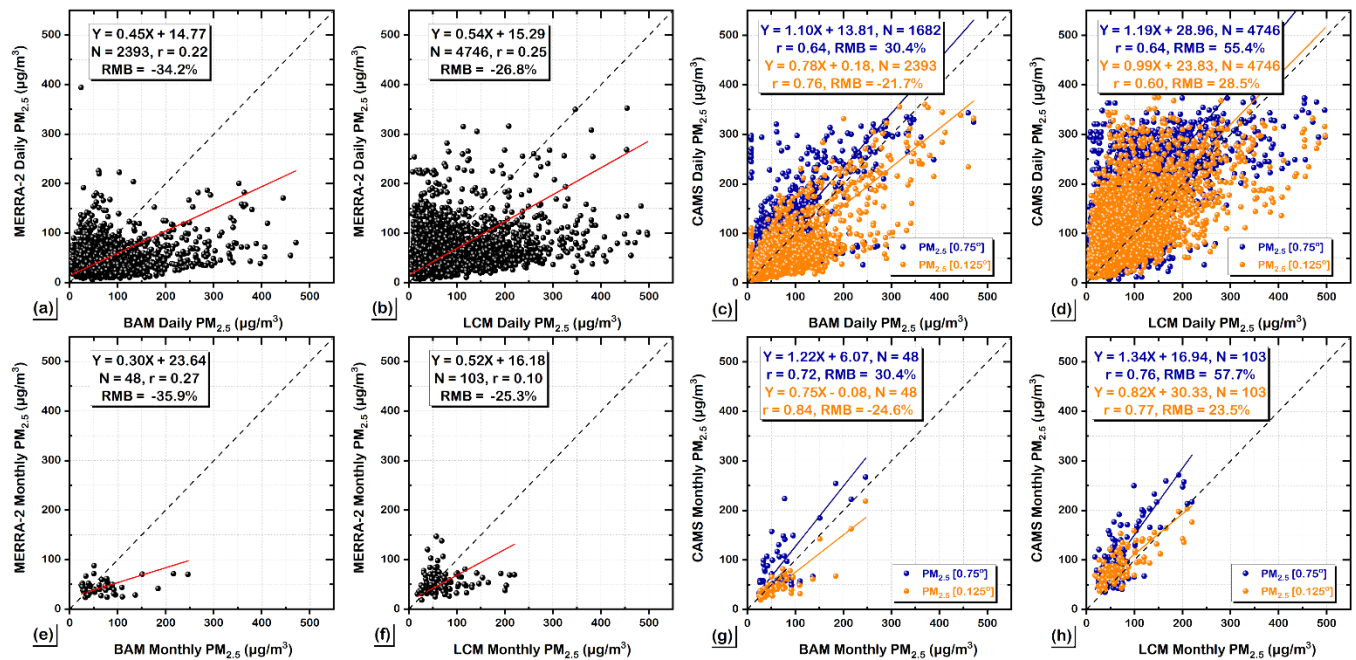
593 The MERRA-2 and CAMS PM<sub>2.5</sub> reanalysis data over Pakistan were evaluated by comparison  
594 with BAM (beta gauge attenuation monitor) PM<sub>2.5</sub> concentrations for 2019-2020 provided by the  
595 US Consulates and with LCM (low-cost monitor) PM<sub>2.5</sub> concentrations for 2018-2019 provided by  
596 PAQI. The scatterplots in Figure 5 show a significant underestimation of both daily (Figures 5a  
597 and 5b) and monthly (Figures 5e and 5f) MERRA-2 PM<sub>2.5</sub> concentrations compared to both BAM  
598 and LCM PM<sub>2.5</sub> measurements: for the daily data the slopes are 0.45 and 0.54 and the RMB are -  
599 34.2% and -26.8%, respectively, and for the monthly data the slopes are 0.30 and 0.52 with -

600 35.9% to 25.3%, respectively. The results also show the weak correlation of MERRA-2 PM<sub>2.5</sub> data  
601 with both BAM and LCM daily ( $r = 0.22$  and  $0.25$ , respectively) and monthly ( $r = 0.10$  and  $0.27$ ,  
602 respectively) PM<sub>2.5</sub> data. The weak correlation suggests that MERRA-2 PM<sub>2.5</sub> data based on the  
603 GOCART aerosol module is unable to accurately reproduce the temporal variations in PM<sub>2.5</sub>. A  
604 significant underestimation of MERRA-2 PM<sub>2.5</sub> data was also reported over China (He et al. 2019;  
605 Song et al. 2018) and India (Navinya et al. 2020), but over Pakistan, the correlation is even  
606 weaker. Moreover, the grid size of MERRA2 ( $0.5^\circ \times 0.625^\circ$  grid size) could introduce errors due  
607 to heterogeneity within the large area that affects the correlation with the in-situ measurements.

608 In comparison with the MERRA-2 data, the correlation coefficients of the CAMS daily (Figures  
609 5c and 5d) and monthly (Figures 5g and 5h) PM<sub>2.5</sub> data versus ground-based in situ PM<sub>2.5</sub>  
610 measurements are substantially higher for both BAM and LCM. However, the data in Figure 5  
611 show significant deviations of the CAMS-estimated PM<sub>2.5</sub> from the ground-based PM<sub>2.5</sub> values,  
612 with over- or under-estimation depending on grid size. For example, CAMS overestimates PM<sub>2.5</sub>  
613 at the  $0.75^\circ$  grid size by 30.4% in comparison with the daily BAM data and by 55.4% in comparison  
614 with the daily LCM data. For monthly data, these percentages are 30.4% and 57.4%. In contrast,  
615 CAMS underestimates PM<sub>2.5</sub> at the  $0.125^\circ$  grid size in comparison with BAM data and  
616 overestimates in comparison with LCM data. These results suggest that grid size and ground-  
617 based PM<sub>2.5</sub> measurement methods (BAM and LCM) play an important role in the  
618 overestimation/underestimation of CAMS PM<sub>2.5</sub> data. For illustration, in comparison with the  
619 BAM PM<sub>2.5</sub> measurements, CAMS data are overestimated for one grid ( $0.75^\circ$ ) and  
620 underestimated for another grid ( $0.125^\circ$ ), and CAMS PM<sub>2.5</sub> data at the same grid size ( $0.125^\circ$ ) are  
621 underestimated when compared with data measured using the BAM method and overestimated



622 when compared with data measured using the LCM method. It is worth mentioning that both  
623 MERRA-2 and CAMS simulate 5 types of fine particulate matter components (dust, sea salt,  
624 sulfate, organic carbon, and black carbon), but nitrate concentrations are not included. If the lack  
625 of nitrate concentrations is the main reason for underestimation in MERRA PM<sub>2.5</sub> data, as  
626 reported by previous studies (Buchard et al. 2016; He et al. 2019; Provencal et al. 2017; Song et  
627 al. 2018), then underestimation should be observed in CAMS PM<sub>2.5</sub> data at 0.75° grid size, but  
628 this is not the case. Therefore, the exact reasons for underestimation in both MERRA-2 and CAMS  
629 as well as overestimation in CAMS data should be thoroughly investigated in future studies. The  
630 results show a higher correlation for CAMS monthly data (Figures 5g and 5h) compared to the  
631 daily data (Figures 5c and 5d). Although CAMS monthly data at 0.75° grid size show  
632 overestimation, they have a good correlation coefficient ( $r = 0.72\text{--}0.76$ ) with ground-based PM<sub>2.5</sub>  
633 measurements and could be useful for characterizing pollution levels in the cities of Pakistan  
634 compared to the MERRA-2. The comparisons in Figure 5 do not provide a strong reason for  
635 choosing one data set over the other. We have selected the CAMS data at the 0.75° grid taking  
636 into account the deviation in the CAMS data observed in this evaluation, in addition to the large  
637 scatter in individual data points which adds uncertainty.



638

639

**Figure 5:** Validation of MERRA-2 and CAMS PM<sub>2.5</sub> reanalysis data against BAM (beta gauge

640

attenuation monitor) PM<sub>2.5</sub> concentrations for 2019-2020 provided by the US Consulates and

641

LCM (low-cost monitor) PM<sub>2.5</sub> concentrations for 2018-2019 provided by PAQI. Where, (a)

642

MERRA-2 daily PM<sub>2.5</sub> vs. BAM daily PM<sub>2.5</sub>, (b) MERRA-2 daily PM<sub>2.5</sub> vs. LCM daily PM<sub>2.5</sub>, (c) CAMS

643

daily PM<sub>2.5</sub> vs. BAM daily PM<sub>2.5</sub>, (d) CAMS daily PM<sub>2.5</sub> vs. LCM daily PM<sub>2.5</sub>, (e) MERRA-2 monthly

644

PM<sub>2.5</sub> vs. BAM monthly PM<sub>2.5</sub>, (f) MERRA-2 monthly PM<sub>2.5</sub> vs. LCM monthly PM<sub>2.5</sub>, (g) CAMS

645

monthly PM<sub>2.5</sub> vs. BAM monthly PM<sub>2.5</sub>, and (h) CAMS monthly PM<sub>2.5</sub> vs. LCM monthly PM<sub>2.5</sub>. The

646

dashed line in each figure is the identity line and the blue and orange solid lines are the fit lines

647

with parameters presented in the legends.

648

### 5.2.2 Characterization of extremely polluted cities using PM<sub>1</sub> and PM<sub>2.5</sub> concentrations

649

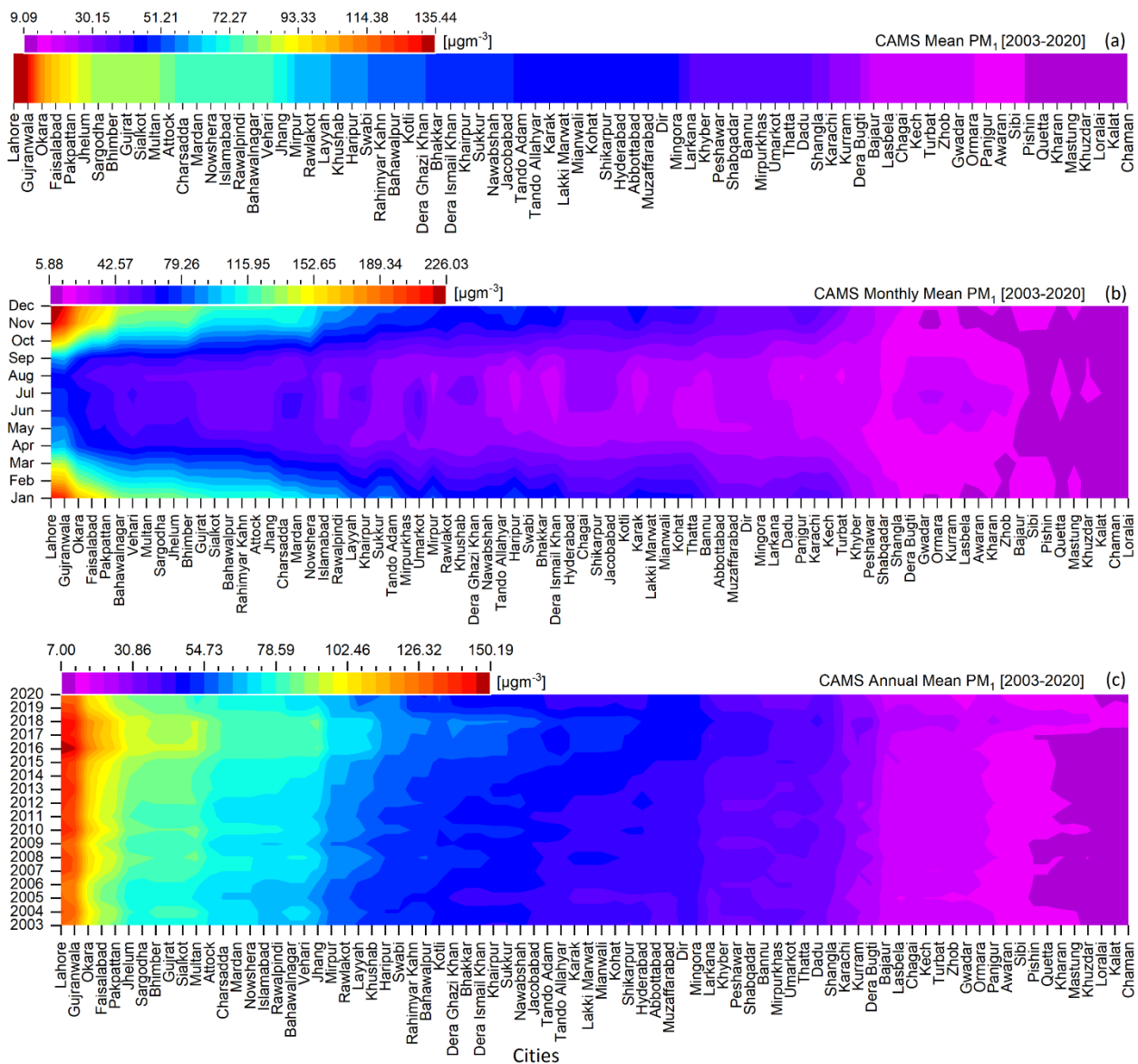
PM<sub>1</sub> and PM<sub>2.5</sub> are fine particulate matter associated with human health issues. PM<sub>1</sub> is more

650

harmful than PM<sub>2.5</sub> as it can reach deeper into the lungs and affect the respiratory system (Liu et

651 al. 2013; Meng et al. 2013). A previous study over China reported that most health issues  
652 associated with PM<sub>2.5</sub> were mainly due to greater contributions of PM<sub>1</sub> in PM<sub>2.5</sub> (Chen et al. 2017).  
653 The ranking of extremely polluted to polluted cities in Pakistan according to annual mean CAMS  
654 PM<sub>1</sub> concentrations from 2003 to 2020 in Figure 6a indicates that the top 10 extremely polluted  
655 cities are Lahore (135.44 µg/m<sup>3</sup>), Gujranwala (131.99 µg/m<sup>3</sup>), Okara (107.72 µg/m<sup>3</sup>), Faisalabad  
656 (98.96 µg/m<sup>3</sup>), Pakpattan (94.06 µg/m<sup>3</sup>), Jhelum (85.51 µg/m<sup>3</sup>), Sargodha (84.30 µg/m<sup>3</sup>), Bhimber  
657 (83.99 µg/m<sup>3</sup>), Gujrat (83.99 µg/m<sup>3</sup>), and Sialkot (83.99 µg/m<sup>3</sup>). Similarly, the top 10 extremely  
658 polluted cities (Figure 7a) ranked according to PM<sub>2.5</sub> concentrations are Lahore (170.53 µg/m<sup>3</sup>),  
659 Gujranwala (163.63 µg/m<sup>3</sup>), Okara (139.43 µg/m<sup>3</sup>), Faisalabad (129.85 µg/m<sup>3</sup>), Pakpattan (126.97  
660 µg/m<sup>3</sup>), Multan (113.09 µg/m<sup>3</sup>), Bahawalnagar (110.81 µg/m<sup>3</sup>), Vehari (110.81 µg/m<sup>3</sup>), Sargodha  
661 (109.81 µg/m<sup>3</sup>), and Jhelum (107.68 µg/m<sup>3</sup>). The WHO air quality guidelines (AQG) are not yet  
662 defined for PM<sub>1</sub> as PM<sub>1</sub> is not as widely monitored as PM<sub>2.5</sub>, therefore the WHO recommended  
663 AQG for PM<sub>2.5</sub> (<10 µg/m<sup>3</sup> annual mean) and Pak-NEQS for PM<sub>2.5</sub> (<15 µg/m<sup>3</sup> annual mean) are  
664 used for comparison purposes. Not a single city in Pakistan falls within the PM<sub>2.5</sub> standards  
665 defined by Pak-NEQS and WHO, and the values of PM<sub>1</sub> and PM<sub>2.5</sub> respectively for the top 10 cities  
666 are 5.6 (8.4) to 9.0 (13.5) times and 7.2 (10.8) to 11.4 (17.1) times greater than the Pak-NEQS  
667 (WHO AQG). For PM<sub>1</sub> and PM<sub>2.5</sub>, 9 out of 10, and 10 out of 10 cities respectively, are in Punjab.  
668 The extremely high pollution level may be due to emissions from local anthropogenic activities,  
669 confirming the results of a previous modeling study that suggested local anthropogenic activities  
670 as the major cause of high particulate concentrations in Pakistan (Shi et al. 2020). All major cities  
671 selected in this study (80 cities) are exposed to PM<sub>2.5</sub> concentrations during a long period of time  
672 (Figures 1a and 7a), which exceed the Pak-NEQS (<15 µg/m<sup>3</sup>) and 68, 73, and 80, out of 80 cities

673 exceeded the WHO Interim Target-1 ( $<35 \mu\text{g}/\text{m}^3$ ), Target-2 ( $<25 \mu\text{g}/\text{m}^3$ ), and Target-3 ( $<15$   
 674  $\mu\text{g}/\text{m}^3$ ), respectively. These exceedances are set in strong perspective against the much lower  
 675 recommended WHO AQG for  $\text{PM}_{2.5}$  of  $10 \mu\text{g}/\text{m}^3$ . These results suggest that the top polluted cities  
 676 are extremely hazardous for human health, as an increase of  $\text{PM}_{2.5}$  by  $10 \mu\text{g}/\text{m}^3$  can increase  
 677 mortality, lung cancer, and cardiopulmonary diseases by 8%, 6%, and 4%, respectively, due to  
 678 long-term exposure to fine particulates (Pope et al. 2002).



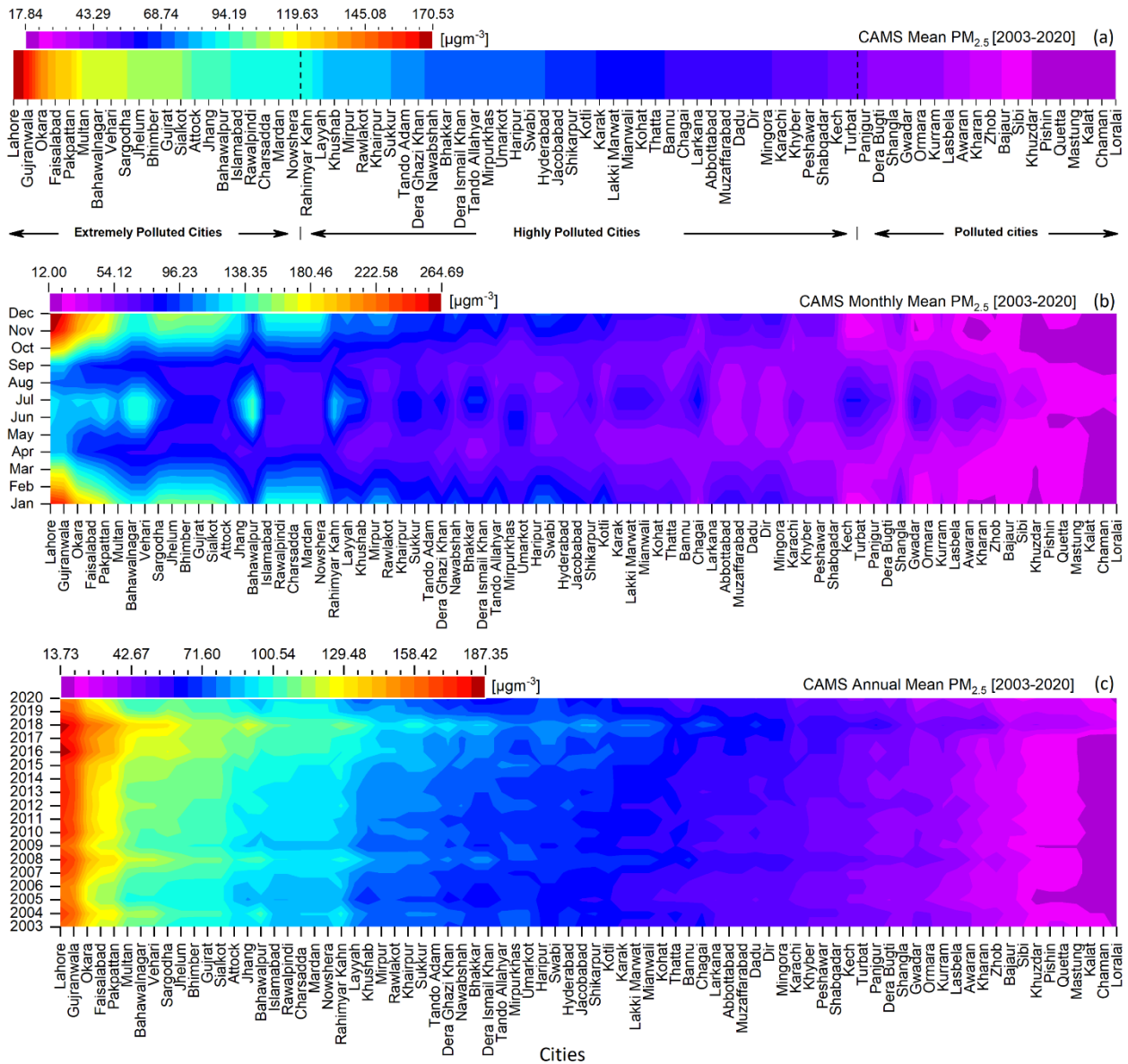
679

680 **Figure 6:** Ranking of extremely polluted to polluted cities in Pakistan according to annual mean  
681 CAMS PM<sub>1</sub> concentrations from 2003 to 2020. Where (a) polluted cities based on yearly mean  
682 PM<sub>1</sub> averaged over the years 2003-2020, (b) polluted months based on PM<sub>1</sub> averaged over the  
683 years 2003-2020, and (c) polluted years based on yearly mean PM<sub>1</sub>.

684 Figures 6b and 7b show months with the highest levels of PM<sub>1</sub> and PM<sub>2.5</sub>, averaged over the  
685 years 2003-2020, for the extremely polluted cities. The higher PM<sub>1</sub> and PM<sub>2.5</sub> concentrations were  
686 observed in cold months (October to February) with the maximum concentrations in December  
687 and January, while warmer months (March to September) showed lower PM<sub>x</sub> concentrations.  
688 The high levels of fine particulates in October and November may be attributed to both cross-  
689 border transport of aerosol produced from biomass burning activities (from India) as well as  
690 locally produced aerosols by anthropogenic activities. As the highest values of fine particulates  
691 were observed in December and January which are not the main months of biomass burning  
692 activities, these are not likely the main source of the high levels of fine particulates pervasive  
693 across these highly polluted cities. At this time of year, less surface heating and less turbulence  
694 due to lower intensity of solar irradiation lead to stable and shallow boundary layers.  
695 Furthermore, with higher concentrations of light-absorbing aerosols, mainly BC, the atmospheric  
696 stability increases due to local heating near the top of the boundary layer, induced by BC, which  
697 further lowers the boundary layer height (BLH) (Ding et al. 2016). Stable atmospheric conditions  
698 that imply low BLH together with low wind speed, both limiting aerosol transport, lead to the  
699 accumulation of aerosols and enhancement of particle concentrations near the surface. As a  
700 result, anthropogenic aerosols such as those produced from fossil fuel combustion and other  
701 urban and industrial activities may linger for long periods (Mhawish et al. 2020). In October and

702 November, both local and remote (cross-border) biomass (crop residue) burning activities  
703 coupled with stable atmospheric conditions have been recognized to cause severe haze and smog  
704 episodes, especially over Punjab (Mhawish et al. 2020; Tariq et al. 2015; Tariq et al. 2016). The  
705 formation of secondary inorganic aerosol during haze episodes is also responsible for higher  
706 PM<sub>2.5</sub> concentrations as reported from recent studies over China (Nichol et al. 2020; Zhang et al.  
707 2018). An increase in PM<sub>2.5</sub> concentrations was observed in June and July, and PM<sub>1</sub>  
708 concentrations slightly increased in July. This means that PM<sub>2.5</sub> exhibited two peaks: the first in  
709 winter and the second in summer, whereas a single peak in winter was observed for PM<sub>1</sub>. The  
710 second PM<sub>2.5</sub> peak in summer may be attributed to the fine particulates from dust, as dust storm  
711 activities are very common in Pakistan during summer, as well as local anthropogenic activities.  
712 The lower peak of PM<sub>2.5</sub> in the summer, compared to winter, may be due to the unstable  
713 atmospheric conditions due to the higher surface heating by solar irradiation, leading to the  
714 generation of strong turbulence with rising air and thus strong mixing conditions which promote  
715 the vertical dispersion of pollutants.

716 The annual mean concentrations of PM<sub>1</sub> (Figure 6c) and PM<sub>2.5</sub> (Figure 7c) show strong inter-  
717 annual variations with distinct PM<sub>x</sub> levels and very poor air quality conditions throughout the last  
718 two decades. The annual mean mass concentrations in extremely polluted cities range from 63  
719 µg/m<sup>3</sup> to 150.19 µg/m<sup>3</sup> for PM<sub>1</sub> and from 85 µg/m<sup>3</sup> to 187.35 µg/m<sup>3</sup> for PM<sub>2.5</sub>, which are 4.2  
720 (6.3)–10 (15) and 5.7 (8.5)–12.5 (18.7) times greater than the Pak-NEQS (WHO AQG),  
721 respectively.



722

723

Figure 7: As Figure 6, but for PM<sub>2.5</sub>.

724

### 5.2.3 Characterization of extremely polluted cities using PM<sub>10</sub> concentrations

725

Figure 8a shows the ranking of polluted cities according to PM<sub>10</sub> concentrations. The PM<sub>10</sub>

726

fraction with an aerodynamic diameter larger than PM<sub>2.5</sub> (PM<sub>10</sub>-PM<sub>2.5</sub>), i.e. the mass

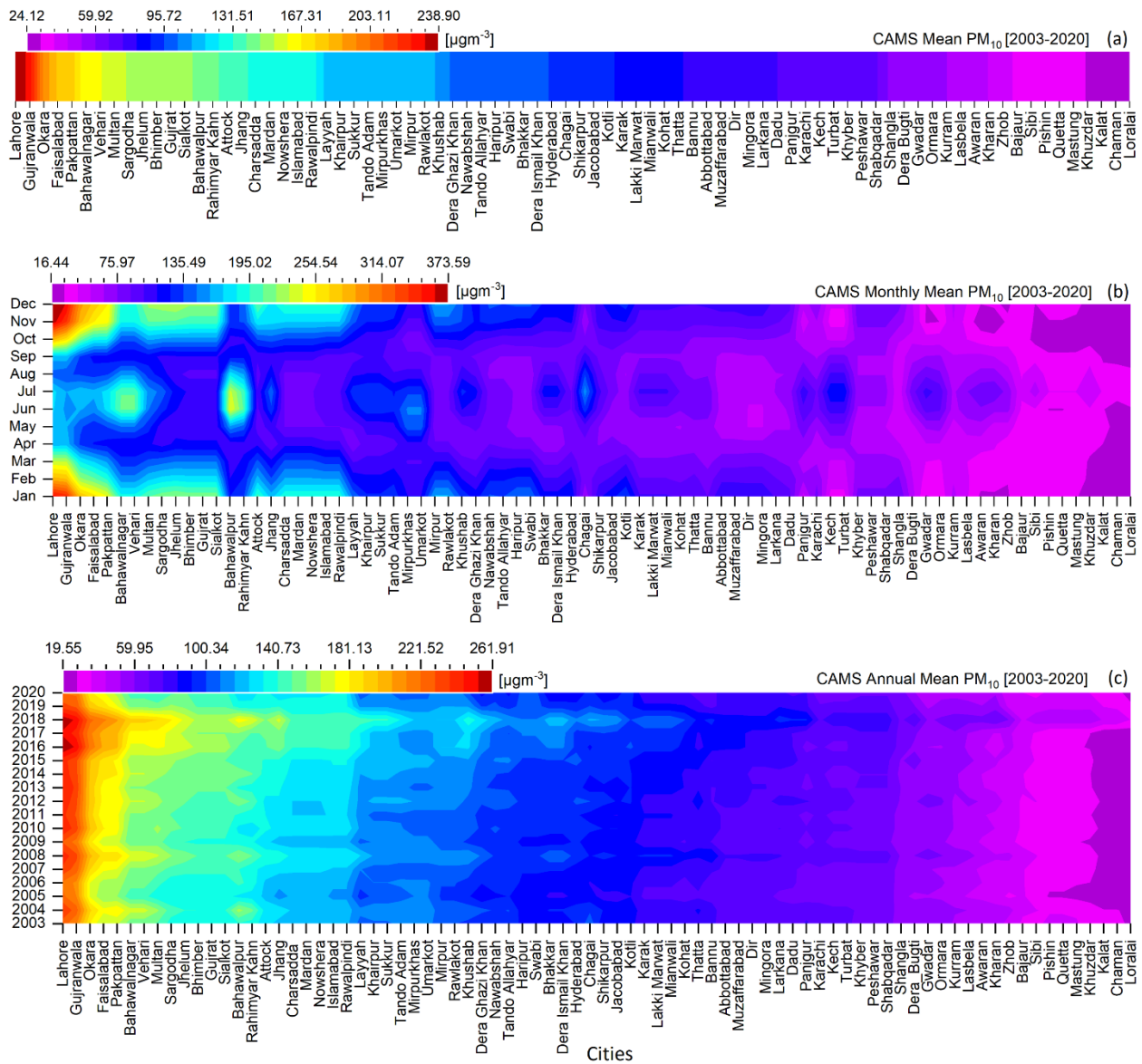
727

concentration of coarse particles, mainly originates from natural sources such as desert dust and

728 resuspended soil particles. The top 10 most polluted cities according to the PM<sub>10</sub> concentrations  
729 are Lahore (238.9 µg/m<sup>3</sup>), Gujranwala (229.1 µg/m<sup>3</sup>), Okara (194.5 µg/m<sup>3</sup>), Faisalabad (180.6  
730 µg/m<sup>3</sup>), Pakpattan (177.9 µg/m<sup>3</sup>), Bahawalnagar (160.6 µg/m<sup>3</sup>), Vehari (160.6 µg/m<sup>3</sup>), Multan  
731 (157.5 µg/m<sup>3</sup>), Sargodha (152.3 µg/m<sup>3</sup>), and Jhelum (149.7 µg/m<sup>3</sup>). PM<sub>10</sub> concentrations are 1.2  
732 to 11.9 times higher than the WHO AQG for PM<sub>10</sub> (20 µg/m<sup>3</sup> annual mean) for all the cities shown  
733 in Figure 8a, suggesting that very poor air quality conditions, hazardous for human life, prevail in  
734 all Pakistani cities. Overall, the PM<sub>10</sub> temporal trend pattern is very similar to that for PM<sub>2.5</sub>, i.e.,  
735 December is the month with the highest PM<sub>10</sub> concentrations, followed by January. In summer,  
736 July is the most polluted month followed by June (Figure 8b). Similar to the PM<sub>2.5</sub> variations, PM<sub>10</sub>  
737 also exhibited peaks in both winter and summer. The higher concentrations during the winter  
738 months (i.e. December and January) may be due to increased anthropogenic emission activities  
739 along with stable atmospheric conditions (stagnant conditions, and shallower boundary layer).  
740 Despite the abundance of coarse particulate matter in spring and summer seasons which are  
741 transported from the arid and semiarid regions, the strong convection combined with a deeper  
742 boundary layer enhances the dispersion of the near-surface pollutant that decreases the PM<sub>10</sub>  
743 concentrations along with the wet deposition during the rainy summer season. The pre-harvest,  
744 harvesting, and post-harvest burning activities along with meteorological conditions such as low  
745 wind speed and low boundary layer height may contribute to higher surface PM<sub>10</sub> levels  
746 especially during October and November as these activities produce both fine (PM<sub>1</sub> and PM<sub>2.5</sub>)  
747 and coarse (PM<sub>10</sub>) particles as reported by (Jain et al. 2020; Singh et al. 2017) over South Asia and  
748 by Le Blond et al. (2017) over South American countries.



749 Similar to the annual mean PM<sub>2.5</sub> variations (Figure 7c), the annual mean PM<sub>10</sub> concentrations  
 750 also show distinct interannual variations for all cities (Figure 8c), and severe air pollution levels  
 751 were observed throughout the last two decades. According to these findings, Pakistani people  
 752 are not only exposed to long-term PM<sub>2.5</sub> but also to PM<sub>10</sub> concentrations exceeding the WHO  
 753 recommended AQG for PM<sub>10</sub> (<20 µg/m<sup>3</sup>). Overall, these results suggested that Pakistani cities  
 754 are a severe threat to human life due to extremely poor air quality conditions.



755

756

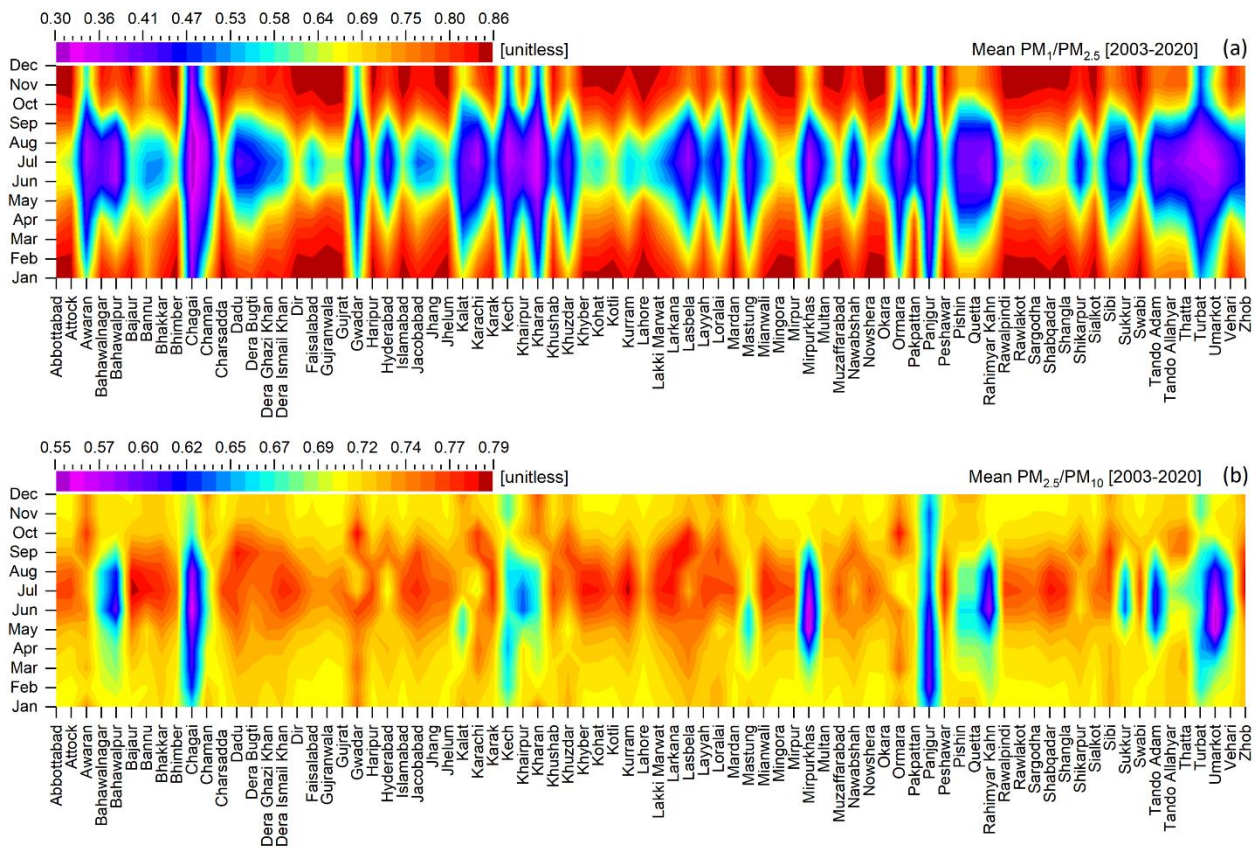
**Figure 8:** As Figure 6, but for  $PM_{10}$ .

757 **5.2.4  $PM_1/PM_{2.5}$  and  $PM_{2.5}/PM_{10}$  ratios**

758 The  $PM_x$  ratios are very useful for understanding the contributions among particulate size, as  
759 revealed by a study in China where  $PM_1$  contributed nearly 80% of  $PM_{2.5}$  (Wang et al. 2015),  
760 which would have consequences for human health. Over Pakistan, the  $PM_1/PM_{2.5}$  (Figure 9a) and  
761  $PM_{2.5}/PM_{10}$  (Figure 9b) ratios are lower than those observed over China (Wang et al. 2015),  
762 indicating lower contributions of  $PM_1$  to  $PM_{2.5}$  and  $PM_{2.5}$  to  $PM_{10}$ . However, the pattern of ratios  
763 is similar to that observed for China, i.e., the  $PM_1/PM_{2.5}$  ratios are higher than  $PM_{2.5}/PM_{10}$  ratios.  
764 Relatively higher  $PM_1/PM_{2.5}$  ratios (>75%) are observed from October to March (Figure 9a),  
765 indicating a larger fraction of  $PM_1$  in  $PM_{2.5}$  due to more anthropogenic activities. The directly  
766 emitted  $PM_1$  from the automobile and combustion of fossil fuel, and indirectly by formation from  
767 precursor gases, are most likely higher from October to March, leading to the enhanced  
768  $PM_1/PM_{2.5}$  ratio. This also suggests that the  $PM_{2.5}$  concentrations from October to March are  
769 driven by emissions from combustion and secondary aerosols formation (Jain et al. 2020).  
770 However, low  $PM_1/PM_{2.5}$  ratios are observed from April to September in most of the cities, and  
771 low ratios during all months are observed in the cities located in Balochistan, indicating a lower  
772 contribution of  $PM_1$  to  $PM_{2.5}$ , which is mainly dominated by the larger particles especially during  
773 summer (June, July, and August) which not contributed to  $PM_1$ .

774 Figure 9b shows large contributions of  $PM_{2.5}$  to  $PM_{10}$  throughout the year with maximum  
775 contributions during summer as indicated by the large  $PM_{2.5}/PM_{10}$  ratios. This suggests that the  
776 air quality in these cities is mainly (and significantly) influenced by fine particulates, largely from

777 anthropogenic sources. The large  $PM_{2.5}/PM_{10}$  ratios in Gwadar and Ormara (Figure 9b), coastal  
 778 cities in Balochistan, throughout the year suggest that also in these coastal cities the PM is  
 779 dominated by  $PM_{2.5}$  particles, which indicates that the  $PM_{10}$  is driven by  $PM_{2.5}$  which is highly  
 780 influenced by anthropogenic sources. Gwadar has the deepest seaport in the world and the ship-  
 781 based emissions may be one of the sources of fine anthropogenic particles throughout the year.  
 782 However, lower  $PM_{2.5}/PM_{10}$  ratios are observed for other cities located in Balochistan, indicating  
 783 the greater influence of coarse particulates (mainly desert dust).



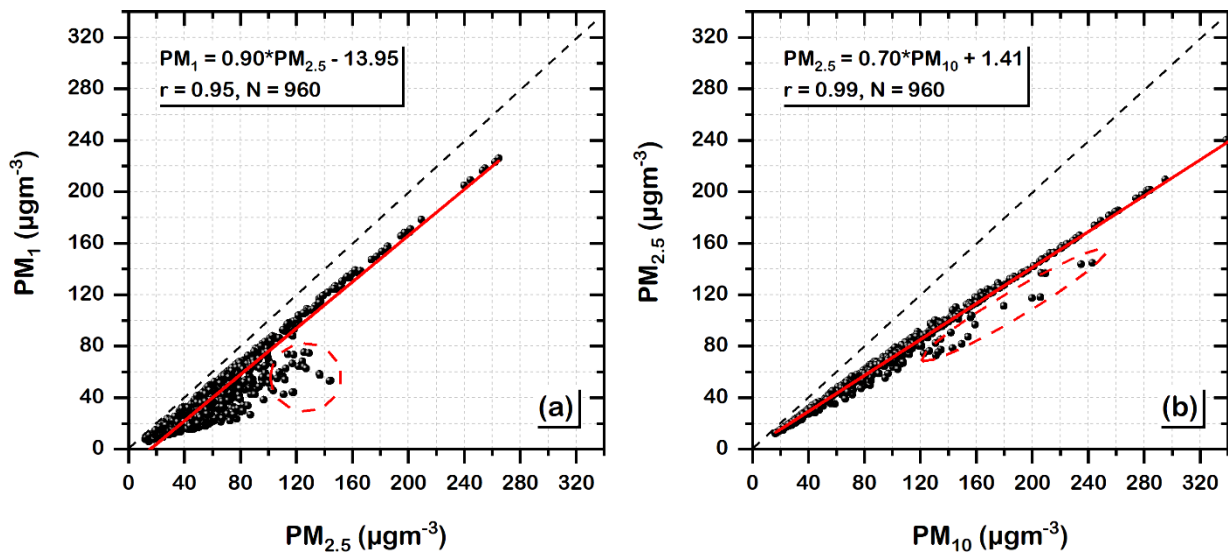
784

785

**Figure 9:** (a) Monthly mean ratios of  $PM_1/PM_{2.5}$  and (b)  $PM_{2.5}/PM_{10}$ .

786

787 Scatter plots of  $PM_1$  vs.  $PM_{2.5}$  (Figure 10a) and  $PM_{2.5}$  vs.  $PM_{10}$  (Figure 10b) show that the  $PM_x$   
788 fractions over Pakistan are well-correlated, with Pearson's correlation coefficients ( $r$ ) of 0.95 and  
789 0.99, and slopes of 0.90 and 0.70, respectively. The strong linear relationship between  $PM_{10}$  and  
790  $PM_{2.5}$  (higher  $r$  values) suggests common sources of fine and coarse particulates compared to  
791  $PM_1$  vs  $PM_{2.5}$  relationship. While the higher slope values suggest larger contributions of  $PM_1$  to  
792  $PM_{2.5}$  than  $PM_{2.5}$  to  $PM_{10}$ . Overall, both the contribution of  $PM_1$  to  $PM_{2.5}$  and that of  $PM_{2.5}$  to  $PM_{10}$   
793 are smaller over Pakistan than over China (Wang et al. 2015) as indicated by the  $PM_x$  ratios (Figure  
794 9) and slope values (Figure 10). This might be due to a higher contribution of anthropogenic  
795 emissions to the PM concentrations in China than in Pakistan; however, other processes may also  
796 contribute, and unraveling the different contributions requires more detailed research. Figures  
797 10a and 10b show some scattered points, within a red circle or ellipse, which represent the data  
798 from May to September and these scattered points suggest lower contributions of  $PM_1$  in  $PM_{2.5}$   
799 and  $PM_{2.5}$  in  $PM_{10}$ , as also indicated by low  $PM_x$  ratios (Figure 9).



800

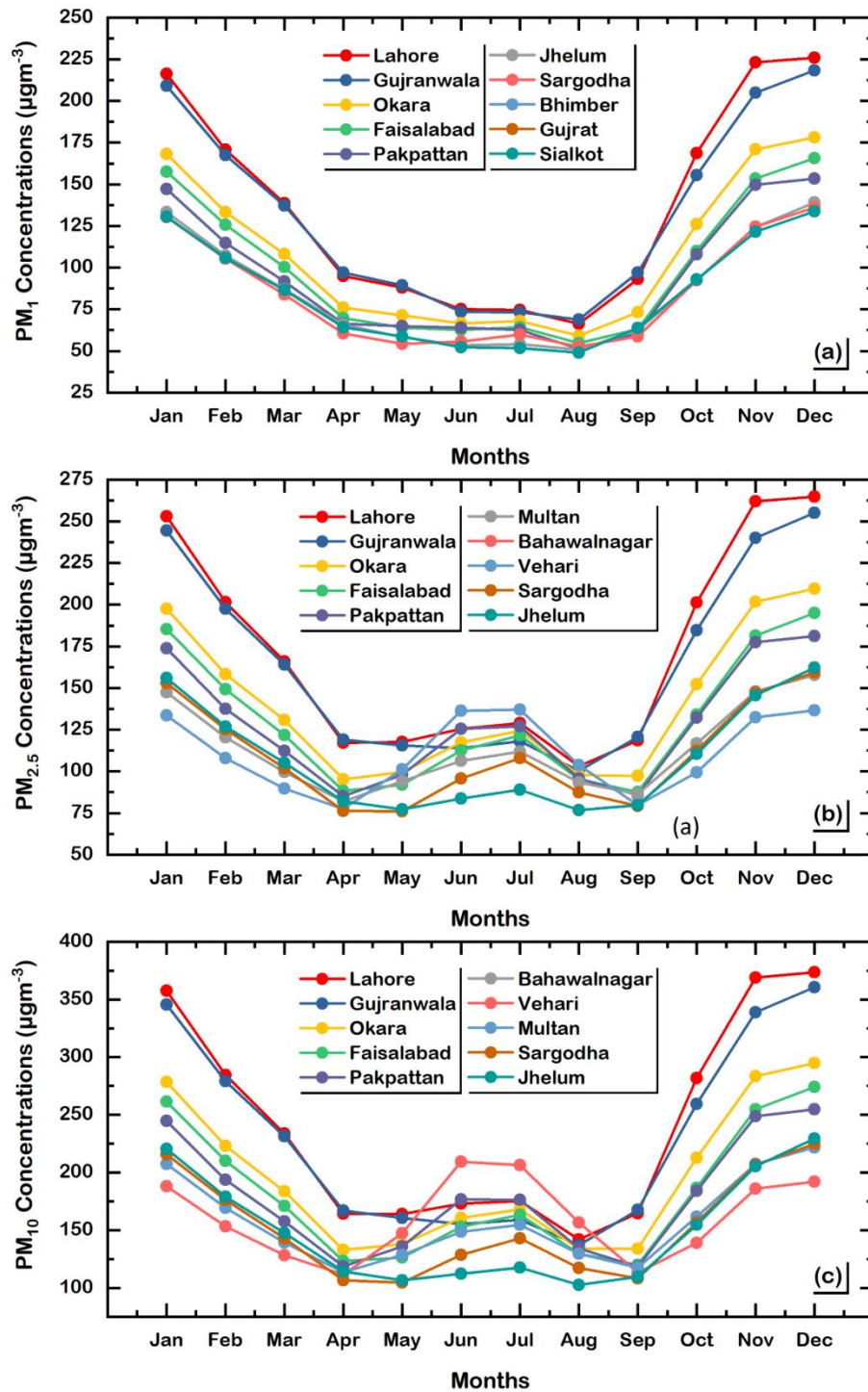
801 Figure 10: Scatter plots between (a)  $PM_1$  vs.  $PM_{2.5}$  and (b)  $PM_{2.5}$  vs.  $PM_{10}$ . The red solid line  
802 represents the regression line and the black dashed line represents the identity line. The data  
803 points in the red circle and ellipse are explained in the text.

#### 804 **5.2.5 Monthly mean temporal trend of $PM_1$ , $PM_{2.5}$ , and $PM_{10}$**

805 The month-to-month variations of the multi-year (2003–2020) monthly mean  $PM_1$ ,  $PM_{2.5}$ , and  
806  $PM_{10}$  concentrations for the top 10 polluted cities are shown in Figure 11. These cities vary  
807 according to population growth, the number of automobiles, urbanization, industrialization, city  
808 size, land cover types, and climatic conditions, and PM concentrations are expected to behave  
809 differently due to these factors. This study follows the hypothesis of our previous study  
810 conducted over Hong Kong (Bilal et al. 2019c) i.e., if the PM concentrations have different  
811 magnitudes but follow the same temporal pattern at different locations, they are influenced by  
812 local as well as regional contributions. Thus for  $PM_1$  concentrations, Figure 11a shows the same  
813 pattern for each of the 10 cities, suggesting that both local and regional sources contribute to  
814  $PM_1$  concentrations. For both  $PM_{2.5}$  (Figure 11b) and  $PM_{10}$  (Figure 11c), similar patterns are only  
815 evident from September to April, and dissimilar patterns due to variation in magnitudes are  
816 evident from May to August, suggesting more local contributions for the summer months of May  
817 to August. This local contribution during summer may be attributed to the frequent dust/sand  
818 storms. Similarly, from October to January, the  $PM_1$ ,  $PM_{2.5}$ , and  $PM_{10}$  concentrations in Lahore  
819 and Gujranwala show similar patterns as in other cities, but with higher concentrations, probably  
820 because Lahore and Gujranwala are the largest cities, with consequently more transport, fossil  
821 fuel, and industrial emissions, and some local and cross-border biomass burning activities in

822 autumn (Ali et al. 2013; Tariq et al. 2015; Tariq et al. 2016), which reinforce the effects of  
823 meteorological impacts, such as shallower boundary layer height and lower wind speed, which  
824 result in the accumulation of particulate matter near the surface (Miao et al. 2019; Miao and Liu  
825 2019; Miao et al. 2018; Qu et al. 2017; Sun et al. 2019; Wang et al. 2018).





826

827

**Figure 11:** Multiyear (2003 - 2020) monthly average variations of PM<sub>1</sub>, PM<sub>2.5</sub>, and PM<sub>10</sub>

828

concentrations in the corresponding top 10 polluted cities (see legend). Cities are plotted with

829

the rank of high to low polluted.

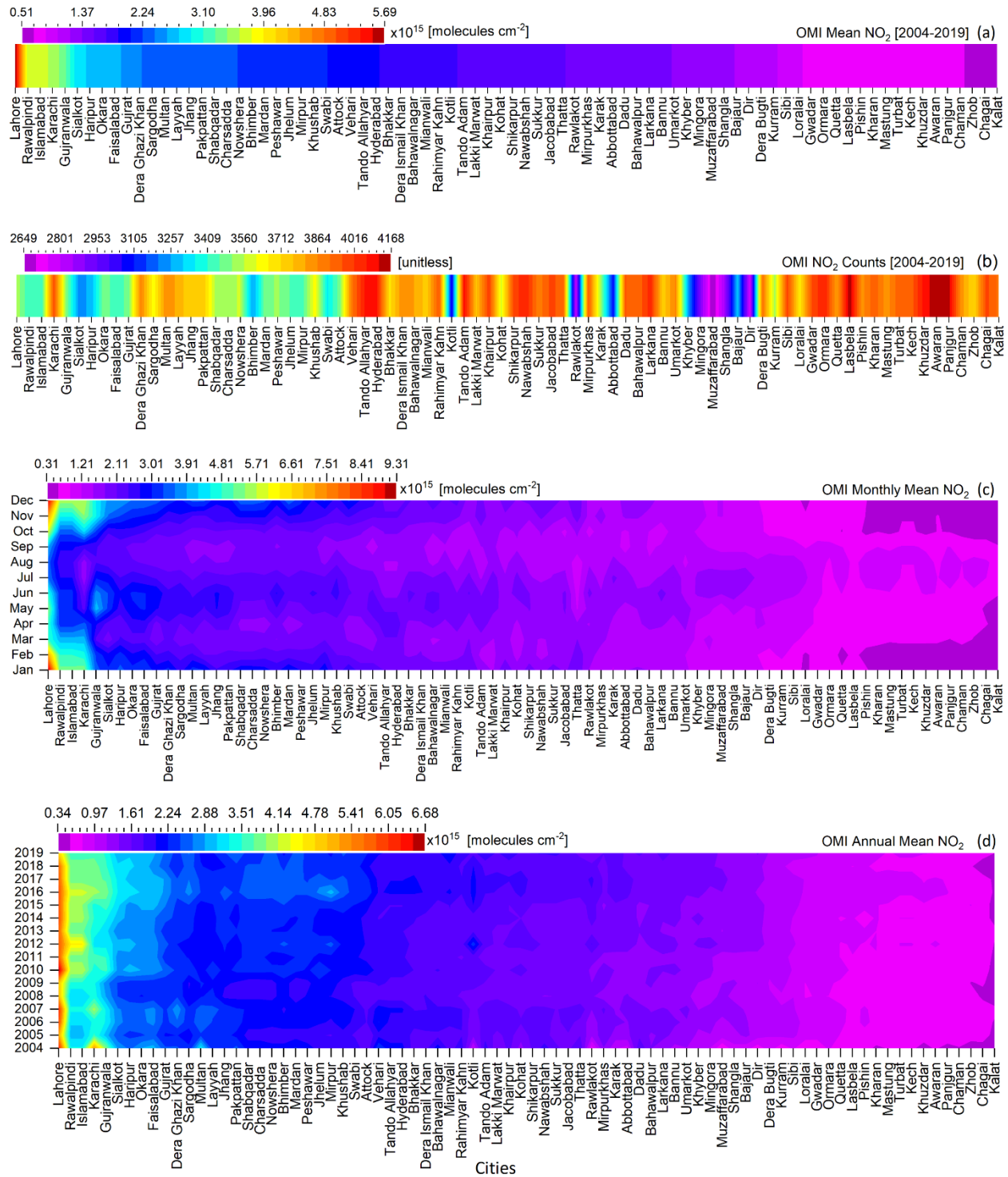
## 830 5.3 OMI vertical column densities of NO<sub>2</sub> and SO<sub>2</sub>

### 831 5.3.1 Characterization of extremely polluted cities using NO<sub>2</sub> data

832 NO<sub>2</sub> is mainly produced from fossil fuel combustion, industrial emission, automobile  
833 emission, biomass burning, natural lightning, and soil microbe emissions (Cheng et al. 2012; Lee  
834 et al. 1997; Olivier et al. 1998; Richter and Burrows 2002). NO<sub>2</sub> has an adverse effect on health  
835 and contributes to low atmospheric visibility, and poor air quality conditions (Khokhar et al. 2015;  
836 ul-Haq et al. 2014). Pakistan's top ten polluted cities according to NO<sub>2</sub>, where we use  
837 Tropospheric vertical column densities (TVCDs) as a proxy, are those with the highest levels of  
838 urbanization, vehicle emissions, and industrialization, suggesting anthropogenic activities to be  
839 the major cause. They are Lahore ( $5.69 \times 10^{15}$  molecules/cm<sup>2</sup>), Rawalpindi ( $3.65 \times 10^{15}$   
840 molecules/cm<sup>2</sup>), Islamabad ( $3.65 \times 10^{15}$  molecules/cm<sup>2</sup>), Karachi ( $3.60 \times 10^{15}$  molecules/cm<sup>2</sup>),  
841 Gujranwala ( $3.32 \times 10^{15}$  molecules/cm<sup>2</sup>), Sialkot ( $2.81 \times 10^{15}$  molecules/cm<sup>2</sup>), Haripur ( $2.73 \times 10^{15}$   
842 molecules/cm<sup>2</sup>), Okara ( $2.72 \times 10^{15}$  molecules/cm<sup>2</sup>), Faisalabad ( $2.72 \times 10^{15}$  molecules/cm<sup>2</sup>), and  
843 Gujrat ( $2.47 \times 10^{15}$  molecules/cm<sup>2</sup>) (Figure 12a). Similar results are reported by Tabinda et al.  
844 (2019), Ashraf et al. (2013), and Khanum et al. (2017). In terms of data availability from OMI,  
845 Figure 12b indicates the largest number of PC available for Lasbela (4168), Awaran (4154), and  
846 Panjgur (4140), all located in Balochistan. On a monthly mean basis, NO<sub>2</sub> (Figure 12c) follows the  
847 same patterns as observed for PM<sub>1</sub> and PM<sub>2.5</sub> concentrations; i.e., higher values in winter,  
848 especially for the extremely polluted cities (Lahore, Rawalpindi, Islamabad, and Karachi), which  
849 are attributed to emissions of automobiles, industries, and fossil fuel combustion, under stable  
850 atmospheric conditions. The NO<sub>2</sub> atmospheric lifetime is higher in winter than in summer due to



851 higher mixing ratio and less sunlight that initiates the breakdown reaction of NO<sub>2</sub>; therefore stays  
852 longer in the atmosphere in winter than in summer. A different trend observed for cities located  
853 in Balochistan, with higher NO<sub>2</sub> in summer, could be due to natural lightning as reported by  
854 Khokhar et al. (2015). Figure 12d shows that Lahore, Rawalpindi, Islamabad, and Karachi are  
855 polluted in all years from 2004 to 2019, subjecting citizens to long-term exposure associated with  
856 respiratory diseases, otitis media, and mortality (Latza et al. 2009).

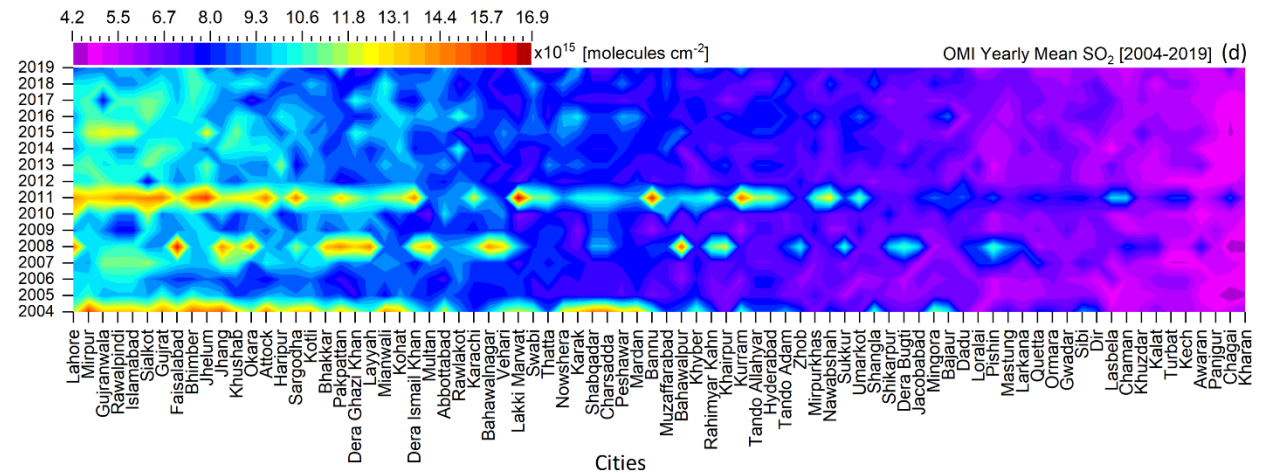
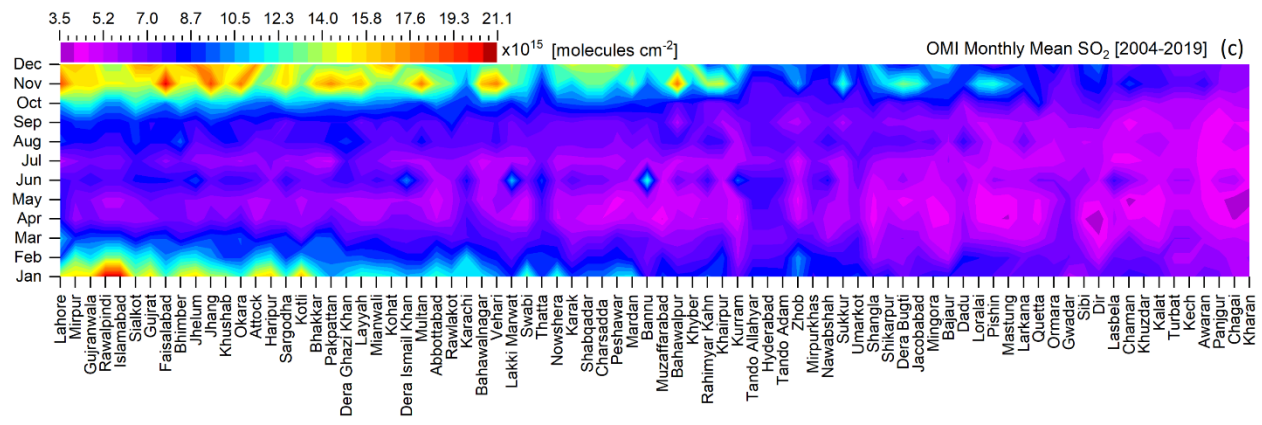
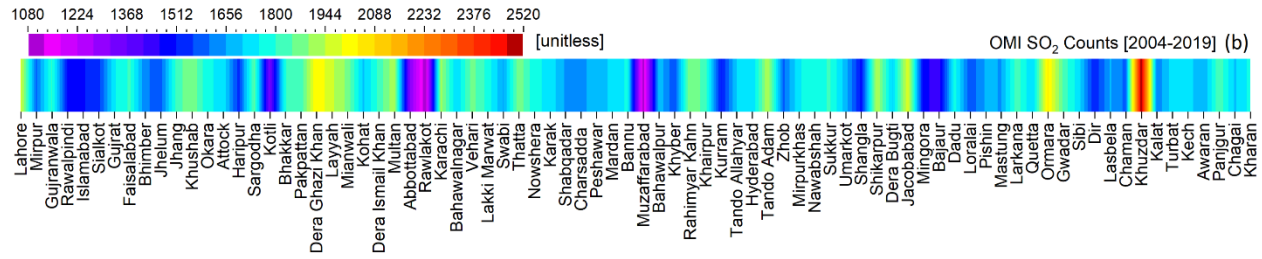
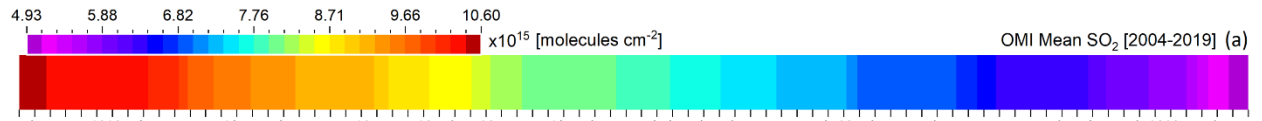


858 **Figure 12:** Ranking of extremely polluted to polluted cities in Pakistan according to OMI NO<sub>2</sub>  
859 TVCDs (molecules/cm<sup>2</sup>) from 2004 to 2019. (a) polluted cities based on mean NO<sub>2</sub>, (b) pixel  
860 counts, (c) polluted months based on mean NO<sub>2</sub>, and (d) polluted years based on mean NO<sub>2</sub>.

### 861 **5.3.2 Characterization of extremely polluted cities using SO<sub>2</sub> data**

862 Power plants, oil and gas refineries, and metal smelters are the major sources of  
863 anthropogenic SO<sub>2</sub> (Dahiya and Myllyvirta 2019). In Figure 13a, extremely polluted to polluted  
864 cities are ranked based on OMI-derived SO<sub>2</sub> vertical column density and the top 10 polluted cities  
865 are Lahore (10.6×10<sup>15</sup> molecules/cm<sup>2</sup>), Mirpur (10.5×10<sup>15</sup> molecules/cm<sup>2</sup>), Gujranwala (10.3×10<sup>15</sup>  
866 molecules/cm<sup>2</sup>), Rawalpindi (10.3×10<sup>15</sup> molecules/cm<sup>2</sup>), Islamabad (10.3×10<sup>15</sup> molecules/cm<sup>2</sup>),  
867 Sialkot (10.3×10<sup>15</sup> molecules/cm<sup>2</sup>), Gujrat (10.3×10<sup>15</sup> molecules/cm<sup>2</sup>), Faisalabad (10.3×10<sup>15</sup>  
868 molecules/cm<sup>2</sup>), Bhimber (10.2×10<sup>15</sup> molecules/cm<sup>2</sup>), and Jhelum (10.2×10<sup>15</sup> molecules/cm<sup>2</sup>).  
869 According to the global SO<sub>2</sub> emission hotspot database (Dahiya and Myllyvirta 2019), five oil  
870 power plants near Lahore are the main sources of high SO<sub>2</sub> emissions over Lahore. The lower  
871 number (1080–2520) of successful SO<sub>2</sub> retrievals (Figure 13b) as compared to NO<sub>2</sub> retrievals  
872 (Figure 12b) is attributed to the high noise level in the OMI-retrieved SO<sub>2</sub> data. Only the relatively  
873 strong SO<sub>2</sub> signal over point sources (e.g., power plants, metal smelters) can be detected.  
874 (Fioletov et al. 2011; Li et al. 2017; Li et al. 2020). The temporal variation of the monthly mean  
875 SO<sub>2</sub> VCDs (Figure 13C) have a pattern similar to that of PM<sub>2.5</sub> and NO<sub>2</sub> TVCD, with high values in  
876 the winter and low in the summer. For the top polluted cities, the high SO<sub>2</sub> observed during  
877 November, December, and January may be attributed to the power plants and brick kilns (Dahiya  
878 and Myllyvirta 2019; Rahman et al. 2000). Brick kilns are considered as major sources of SO<sub>2</sub>

879 resulting in extremely poor air quality. This is clearly observed over Punjab (Adrees et al. 2016;  
880 Colbeck et al. 2010; Pervaiz et al. 2021; Ur Rehman et al. 2019). Therefore, every year during late  
881 autumn and winter, the government of Pakistan bans these kilns to control pollution levels. The  
882 SO<sub>2</sub> accumulates in the BL during the stable atmospheric conditions and shallow BLH at this time  
883 of year, in response to the low solar irradiation resulting in little surface heating and turbulence  
884 mixing. Unlike NO<sub>2</sub>, the contribution of SO<sub>2</sub> to poor air quality in Pakistani cities varies from year  
885 to year, as shown in Figure 13d. The SO<sub>2</sub> VCD is higher in 2004, 2008, and 2011 than in other  
886 years. The investigation of the year-to-year variability requires a separate study.



888 **Figure 13:** Ranking of high to low polluted cities in Pakistan according to OMI SO<sub>2</sub> VCDs  
889 (molecules/cm<sup>2</sup>) from 2004 to 2019. (a) polluted cities based on mean SO<sub>2</sub>, (b) pixel counts, (c)  
890 polluted months based on mean SO<sub>2</sub>, and (d) polluted years based on mean SO<sub>2</sub>.

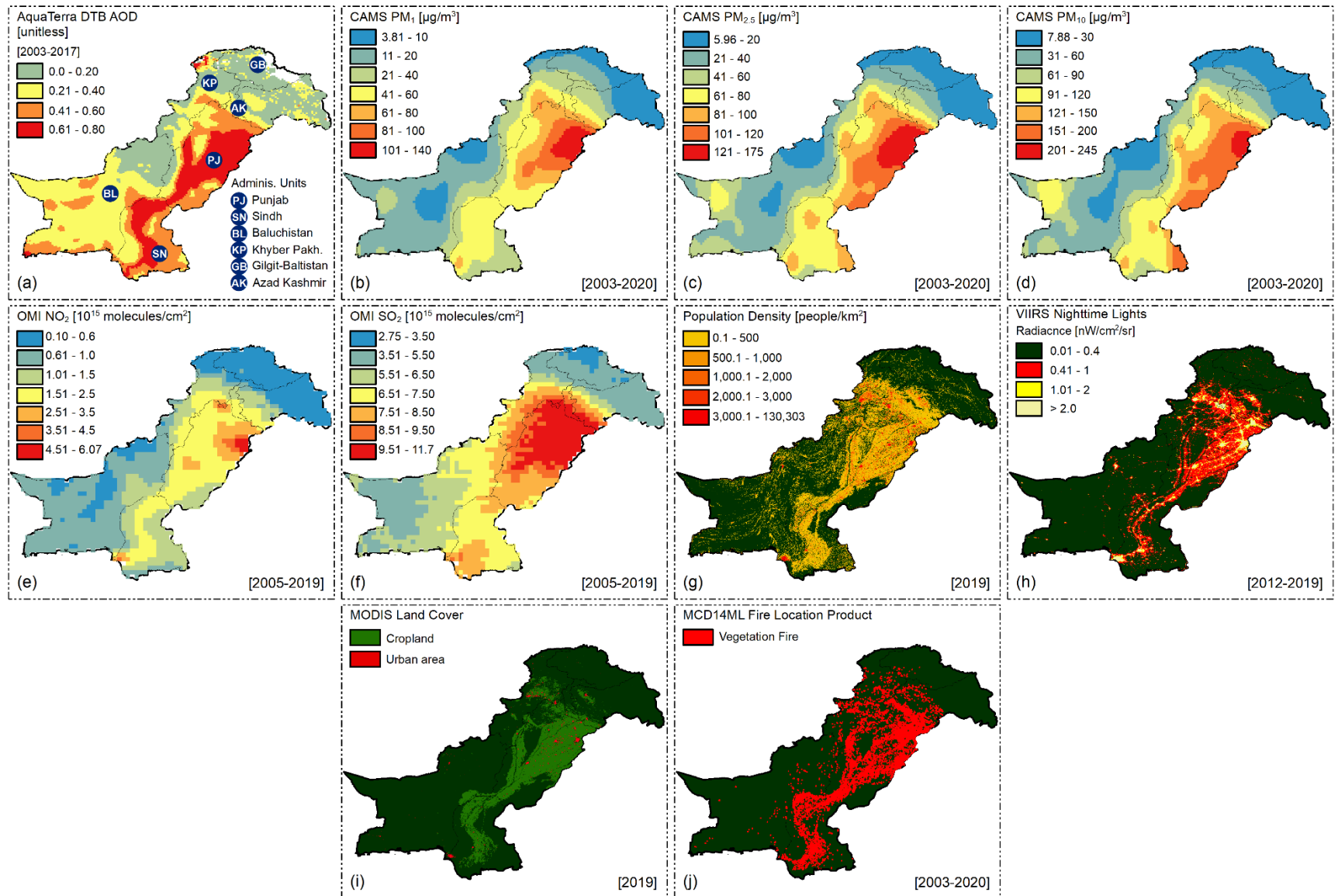
#### 891 **5.4 Spatial distributions of aerosols and trace gases**

892 The purpose of this section is to link the spatial distributions of aerosols and trace gases with  
893 each other as well as with population density, nighttime lights, land cover types (cropland and  
894 urban areas), and presumed vegetation fire activities. Here, the PM<sub>x</sub> data are interpolated using  
895 cubic convolution (Keys 1981) from 0.75° grid size to 0.125° grid size to better show the smooth  
896 spatial distributions over different administrative units. The spatial distributions of the multi-year  
897 averaged concentrations of aerosols (AOD, PM<sub>x</sub>) and trace gases (VCDs) (Figure 14) show that  
898 Punjab is the most polluted region of Pakistan, followed by Sindh. It is significant that other  
899 environmental data including population density (Figure 14g), VIIRS nighttime lights (Figure 14h),  
900 cropland (Figure 14i), and vegetation fires (Figure 14j) show similar spatial patterns. It is obvious  
901 that vegetation fires would have the same spatial pattern as cropland, but not obvious that  
902 population density and nighttime lights would have the same pattern. As nighttime lights and  
903 vegetation fires represent human activities, having the same spatial patterns suggests that the  
904 majority of human settlements including urban, suburban and, industrial regions, are inter-mixed  
905 with cropland. Interestingly, these coincident spatial distributions (population, nighttime lights,  
906 land cover, and fires) correspond to the higher ranges of pollutants i.e., AOD > 0.4, PM<sub>1</sub> > 20  
907 µg/m<sup>3</sup>, PM<sub>2.5</sub> > 40 µg/m<sup>3</sup>, PM<sub>10</sub> > 60 µg/m<sup>3</sup>, NO<sub>2</sub> > 1.0×10<sup>15</sup> molecules/cm<sup>2</sup>, and SO<sub>2</sub> > 6.5×10<sup>15</sup>  
908 molecules/cm<sup>2</sup>. These results suggested that the primary (directly emitted) and the secondary

909 (gas-to-particles formation) aerosol emissions and trace gases are mainly from local  
910 anthropogenic sources such as power plants, oil and gas refineries, vehicular emissions, crop  
911 residue burning, and industrial activities including construction, manufacturing of cement,  
912 ceramic, and bricks, and metals smelting. These anthropogenic sources are mainly responsible  
913 for NO<sub>2</sub>, SO<sub>2</sub>, and PM<sub>x</sub> (Adrees et al. 2016; Shah et al. 2012; Ur Rehman et al. 2019). Among these  
914 anthropogenic sources, brick kilns industries are considered a major source. Small-scale  
915 traditional brick kilns, located in rural and suburban areas, produce large amounts of gaseous  
916 pollutants (NO<sub>2</sub>, SO<sub>2</sub>, O<sub>3</sub>, and CO) and PM<sub>x</sub> due to the usage of low-quality fuels including coal,  
917 oil, wood, rice straw, rice husk, rubber tires, bagasse, and corncobs (Adrees et al. 2016; Ishaq et  
918 al. 2010). Besides this, the combustion of agricultural biomass and crop residue burning are also  
919 contributing to deteriorating rural and urban air quality (Irfan et al. 2015; Irfan et al. 2014). Irfan  
920 et al. (2015) reported that Punjab produced more aerosol pollutants than Sindh from crop  
921 residue burning and among the crop residues, wheat straw is the main contributor of NO<sub>x</sub>, SO<sub>2</sub>,  
922 CO<sub>2</sub>, and CO. Pakistan's 23.6 million vehicles emitted 58% of the country's total NO<sub>2</sub> emission and  
923 34% is emitted by power plants and industries (Amnesty International 2019; Government of  
924 Pakistan 2019; UNDP 2019). Another important source of aerosol pollutants, missed by previous  
925 studies, is the burning of solid waste and street garbage which is a common practice in Pakistan,  
926 even in major urban cities such as Islamabad, Lahore, Rawalpindi, Faisalabad, Gujranwala, Okara,  
927 etc. To support this statement, some illustrations with references are provided in the  
928 supplementary data (Figure S2). Figures 14a to 14d show that deserts (see Figure 1 for locations)  
929 are another source of increasing AOD and PM<sub>x</sub> levels in Pakistan. Although local anthropogenic  
930 activities are the main source of aerosol pollutants and severe air quality problems in Pakistan,

931 transboundary transport of aerosols may also influence Pakistan's air quality. Contributions of  
932 transboundary transport are investigated in section 5.7, using PSCF analyses, integrated with  
933 HYSPLIT backward trajectory analysis and ground-based PM<sub>2.5</sub> measurements.





935 **Figure 14:** Spatial distributions of yearly mean (a) AOD averaged over the years 2003–2017 (b)  
936 PM<sub>1</sub> [2003–2020] (c) PM<sub>2.5</sub> [2003–2020], (d) PM<sub>10</sub> [2003–2020], (e) NO<sub>2</sub> [2005–2019], (f) SO<sub>2</sub>  
937 [2005–2019], (g) Population density [2019], (h) VIIRS Nighttime Lights [2012–2019], (i) Land  
938 cover types [2019], and (j) Presumed vegetation fire data [2003–2020].

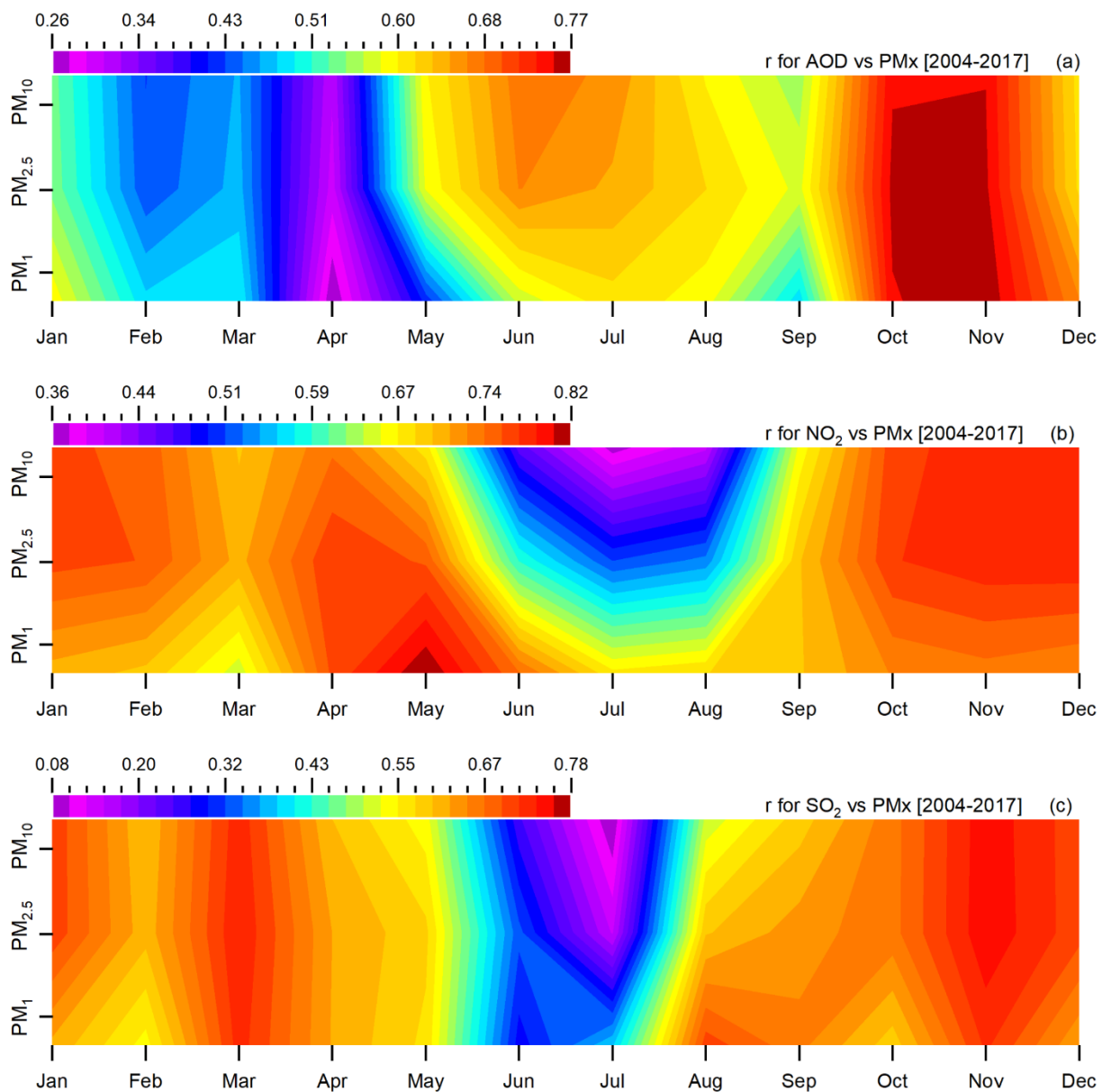
## 939 **5.5 Relationship of PM<sub>x</sub> with AOD, NO<sub>2</sub>, and SO<sub>2</sub>**

940 AOD provides valuable information about the aerosol loading in the atmospheric column,  
941 while the PM<sub>x</sub> represents the aerosol concentrations near the ground. This section assesses how  
942 well satellite-based AOD describes PM<sub>1</sub>, PM<sub>2.5</sub>, and PM<sub>10</sub> by examining the monthly correlation  
943 between AOD and PM<sub>x</sub>. We have also examined the monthly correlation between PM<sub>x</sub> and SO<sub>2</sub>  
944 and NO<sub>2</sub> to understand the common sources that originated mainly from a combustion process.  
945 The relationships between AOD and PM<sub>x</sub> vary spatially and temporally and are influenced by  
946 several factors such as meteorological variables including boundary layer height and relative  
947 humidity, and the vertical distribution of aerosol layer (Li et al. 2016; Mhawish et al. 2021). The  
948 linear correlation between AOD and PM<sub>x</sub> shows a higher correlation coefficient from October to  
949 January (see Figure 15a) when the atmosphere is stably stratified and the boundary layer is  
950 shallow. This suggests that the AOD and PM<sub>x</sub> variability are well agreed during the stable  
951 atmospheric conditions (from Oct to Jan) and AOD can explain > 65% in the PM<sub>x</sub> variability. On  
952 the other hand, during April and May when the atmosphere is unstable and the boundary layer  
953 deeper, the correlation between AOD and PM<sub>x</sub> was smaller ( $r < 0.4$ ). In the rainy season (July to  
954 August), the correlation coefficient between AOD and PM<sub>10</sub> was found higher than PM<sub>2.5</sub> and PM<sub>1</sub>  
955 which may be due to the larger contribution of coarse dust particles to the total aerosol loading

956 than  $PM_{2.5}$  and  $PM_1$ . The high relative humidity in the summer season enhanced the AOD retrieval  
957 due to the hygroscopic growth of aerosol particles. On the other hand, the wash-out of  $PM_x$  due  
958 to precipitation, deeper boundary layer, and strong convection during rainy months leads to a  
959 reduction in the ground-level  $PM_x$  concentrations, while the AOD retrieval remains high under  
960 cloud-free conditions during the inactive rain phase (Mhawish et al. 2021). The results suggested  
961 that using satellite-based AOD to infer the ground-level  $PM_x$  variability is limited to specific  
962 meteorological conditions such as stable atmospheric conditions and dry seasons. On the other  
963 hand, the weak linear relationship between AOD and ground-level  $PM_x$  concentrations found  
964 during unstable conditions in spring and summer and more influenced by meteorological  
965 variables and atmospheric mixing height.

966 Tropospheric  $NO_2$  and  $SO_2$  are precursors for the formation of secondary aerosols which are  
967 produced by anthropogenic activities such as fossil fuel burning and power plants. The strong  
968 correlation coefficient between  $PM_x$  vs.  $SO_2$  and  $NO_2$  in the spring months suggests that  
969 photochemical reactions can contribute to the formation of  $PM_x$ . The strong correlation in winter  
970 suggests that both trace gases  $NO_2$  and  $SO_2$  originated from the same emission sources of  $PM_x$ ,  
971 mainly domestic heating, industrial activities, and vehicular emissions. While the lower  
972 correlation in the summer monsoon may be attributed to the higher contribution of natural  
973 sources of  $PM_x$  and the deeper boundary layer that enhance the dispersion of air pollutants.

974



975

976

**Figure 15:** Relationship from PM<sub>x</sub> with (a) AOD, (b) NO<sub>2</sub>, and (c) SO<sub>2</sub> from 2004-2017.

977

## 5.6 Trends of aerosol and trace gas concentrations

978

This section presents the annual trends in the six parameters used to assess the air quality in

979

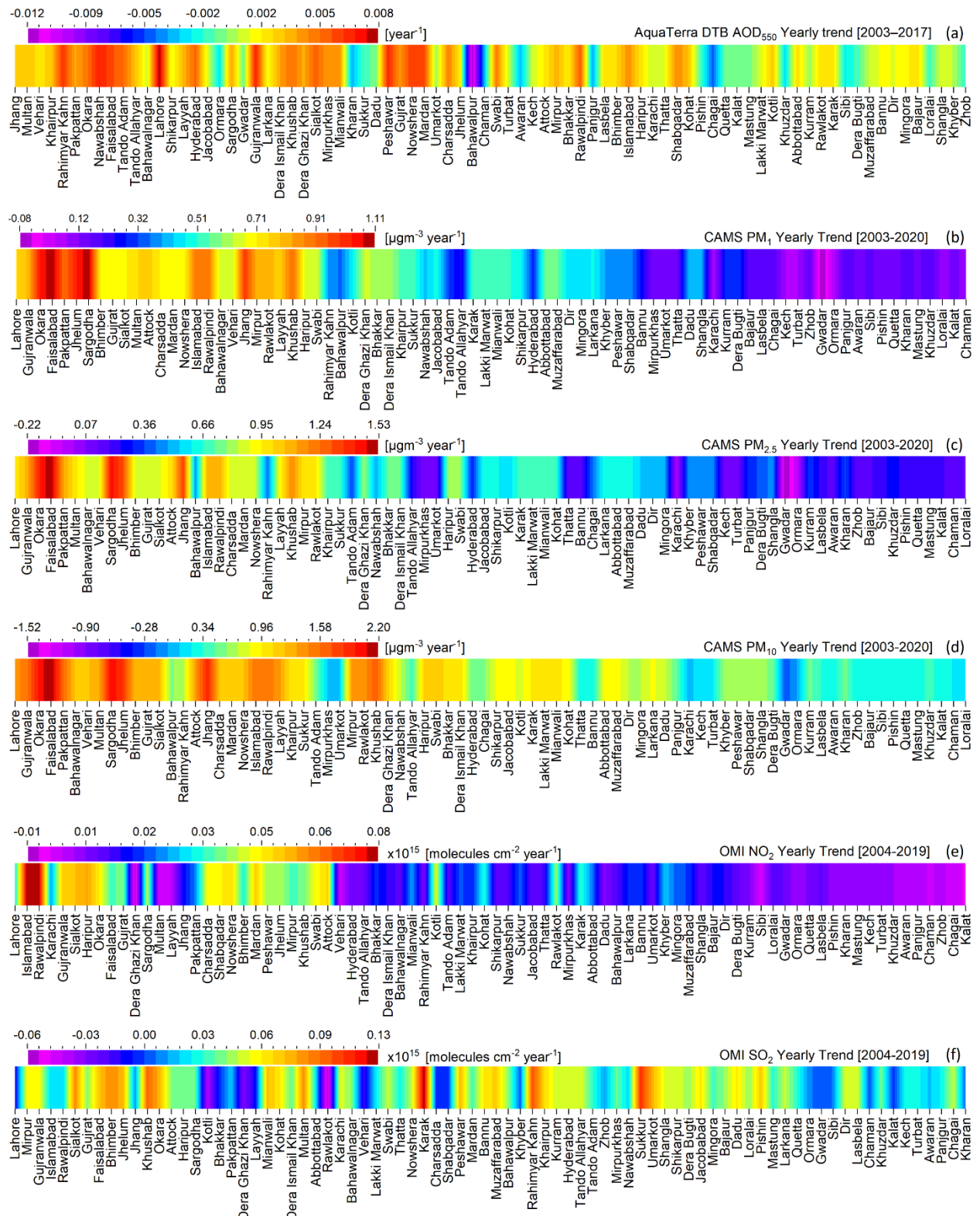
each city of Pakistan. The annual trends were calculated after removing the seasonality from the

980

monthly mean time series data which also accounted for temporal autocorrelation. Figure 16

981 shows the magnitude of the trends as Theil-Sen's slope over each individual city, for the periods  
982 indicated at the top of each Figure. A significant positive trend in  $PM_x$  was found over most cities,  
983 particularly in Punjab, Khyber Pakhtunkhwa, and the Islamabad Capital Territory. The  $PM_x$  trends  
984 found over cities in Punjab range from  $+0.35$  to  $+1.10 \mu\text{g}/\text{m}^3 \text{yr}^{-1}$ ,  $+0.42$  to  $+1.52 \mu\text{g}/\text{m}^3 \text{yr}^{-1}$  and  
985  $+0.57$  to  $+2.20 \mu\text{g}/\text{m}^3 \text{yr}^{-1}$  for  $PM_1$ ,  $PM_{2.5}$  and  $PM_{10}$ , respectively. Correspondingly, the AOD trend  
986 in Punjab cities was positive, with the strongest increase over Lahore ( $0.008 \text{yr}^{-1}$ ). Over cities in  
987 Khyber Pakhtunkhwa and Azad Kashmir, the AOD trend was also positive, but smaller than in  
988 Punjab. The positive trends in  $PM_x$  and AOD, particularly over cities in Punjab, may be due to  
989 increasing aerosol emissions and/or secondary aerosol formation. Anthropogenic activities and  
990 biomass burning are considered major sources of ultrafine and fine particles ( $PM_1$  and  $PM_{2.5}$ ) over  
991 the region (Alam et al. 2015; Stone et al. 2010). Anthropogenic activities also result in the  
992 production of  $\text{NO}_2$  and  $\text{SO}_2$  and  $\sim 91\%$ , and  $\sim 88\%$  of the cities the trends in the  $\text{NO}_2$  and  $\text{SO}_2$ ,  
993 respectively, are positive. This increase in trace gas concentrations would be a further source of  
994 increased particulate pollution, as trace gases facilitate secondary aerosol formation via gas-to-  
995 particle conversion reactions (Seinfeld and Pandis 1998).

996 In terms of monthly trends, the common feature is that the statistically significant positive  
997 trends of  $PM_x$  were largest during the cold months (November to February), particularly over  
998 major Punjab cities (Lahore, Faisalabad, and Gujranwala) and Islamabad (Figure S3). In contrast,  
999 during the summer months, the trends over many cities are negative. The overall positive annual  
1000 trends indicate that the increase of the  $PM_x$  concentrations in the winter is stronger than the  
1001 decrease in the summer. The reasons for these opposing trends are beyond the scope of the  
1002 current study and require further, more detailed investigation.



1003

1004 **Figure 16:** Annual mean trend in aerosols and trace gas concentrations for (a) AOD, (b) PM<sub>1</sub>, (c)

1005 PM<sub>2.5</sub>, (d) PM<sub>10</sub>, (e) NO<sub>2</sub>, and (f) SO<sub>2</sub>. The trends were calculated over different periods of time,

1006 which are indicated on top of each figure on the right-hand side, together with the type of  
1007 species.

## 1008 **5.7 Potential Source Contribution Function (PSCF) Analysis**

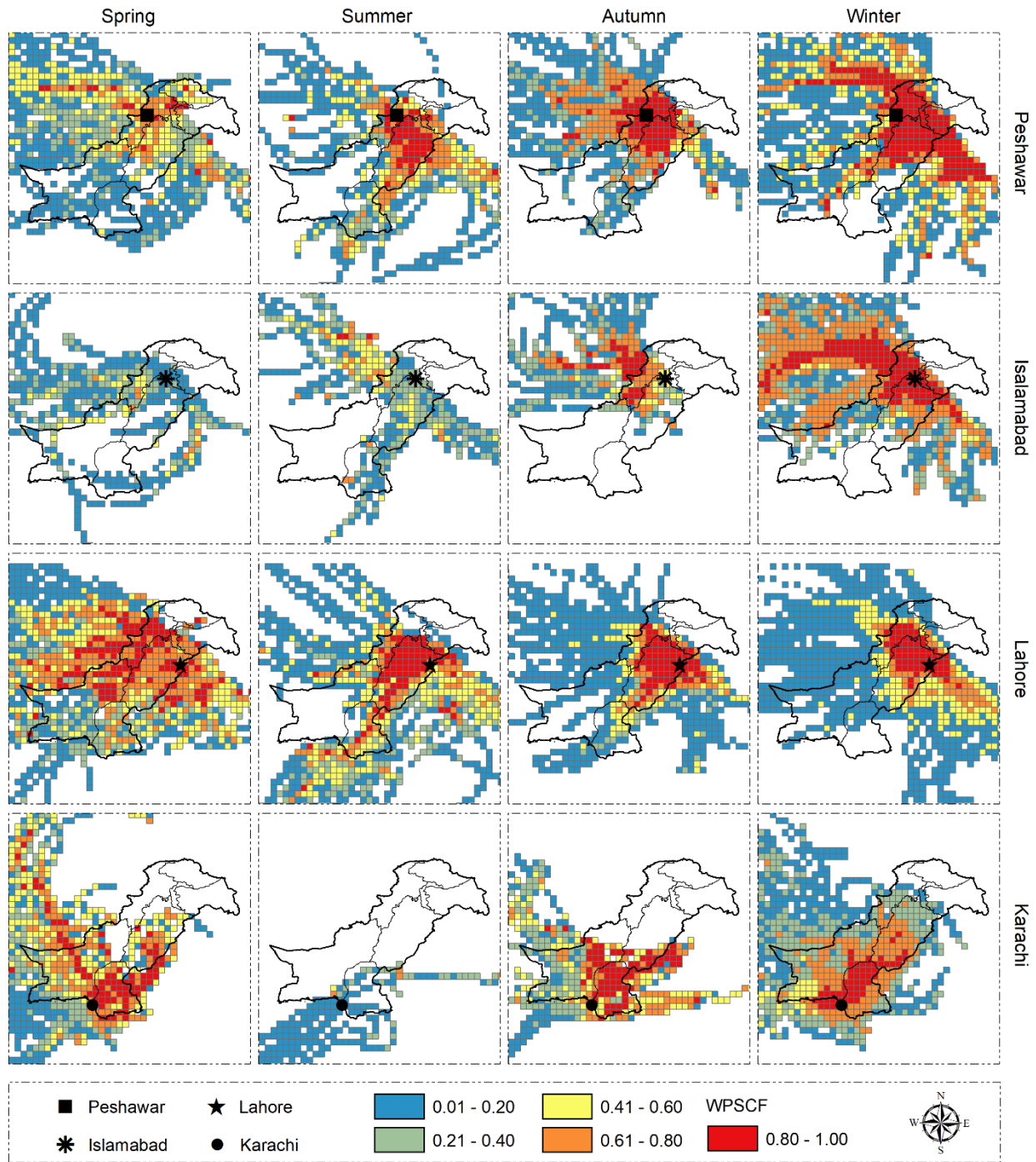
1009 PSCF analysis was used to identify the potential source areas for PM<sub>2.5</sub> at four receptor cities:  
1010 Peshawar, Islamabad, Lahore, and Karachi, for the period from March 2020 to February 2021. 72  
1011 hours HYSPLIT backward trajectories were computed for each receptor site, arriving every 6  
1012 hours at the height of 500 m above ground level (AGL). The results were grouped by season as  
1013 shown in Figure 17. The results show strong differences between cities and seasons. Starting with  
1014 Peshawar, in spring there are some local sources regions around the city, within a few hundreds  
1015 of km, but also strong contributions from the WNW (West-NorthWest) in Afghanistan and from  
1016 the SE in India. In the summer, the source regions are mostly located in Pakistan, but with a  
1017 contribution from sources to the SE (SouthEast), in India. In contrast, in the autumn the  
1018 contributions from India are very small but those from Afghanistan, both to the NW (NorthWest)  
1019 and W (West) are relatively large. Whereas, in the winter source regions in NW and SE directions  
1020 (Afghanistan and India, respectively) are stronger than in other seasons. In Islamabad, not far  
1021 from Peshawar, the situation is quite different. In the spring, the source regions have a rather  
1022 low PSCF, and are distributed over specific directions to the W (West) into Afghanistan and  
1023 toward the SE in India, with few local sources. In the summer, the source regions are similar to  
1024 those in Peshawar, but with low PSCF except for the source regions in Afghanistan which seem  
1025 to contribute most to the air pollution in Islamabad in the summer, but still with moderate PSCF.  
1026 In the autumn sources to the W and N dominate with stronger contributions from Afghanistan  
1027 than from the local sources. In the winter, the source regions redistributed over a much larger  
1028 area than in other seasons, with strong contributions from both local sources and Afghanistan,  
1029 as well as some contributions from India. The situation in Lahore is remarkably different, with  
1030 the strongest contributions from sources inside Pakistan (PJ and KP), some contributions from

1031 sources to the SE in India, during all seasons, and in the spring a strong contribution from sources  
1032 in Afghanistan. The situation in Karachi is again different, both as regards source regions and  
1033 seasonal behaviour. The strongest contributions come from local sources within a few hundreds  
1034 of km in Pakistan, except in the summer when all source regions are weak contributors (PSCF  
1035 <0.2) and almost all located over the ocean. In the spring, source regions to the NW, reaching far  
1036 into Afghanistan, contribute to the PM<sub>2.5</sub> in Karachi. Oceanic sources also contribute some to  
1037 the PM<sub>2.5</sub> in other seasons

1038 In summary, the values of PSCF indicate the regional transport of aerosol from source regions  
1039 in Afghanistan and India (see Figure 1 for locations). Karachi is influenced by fine dust particles  
1040 from the Cholistan and Thar deserts (see Figure 1 for locations). Figure 17 shows that the PM<sub>2.5</sub>  
1041 in Lahore, the top polluted city of Pakistan, is mainly influenced by source areas in Pakistan,  
1042 during all seasons. This suggests that increases in local anthropogenic activities play an important  
1043 role in the worsening of Lahore's air quality. Overall, the higher values of PSCF > 0.6 identify  
1044 potential source areas which are located both inside and outside of Pakistan, which indicates that  
1045 the air quality in Pakistan is not only influenced by local sources but also influenced by transport  
1046 from regional sources areas.

1047





1048

1049 **Figure 17:** Potential source contribution function plots for PM<sub>2.5</sub> at seasonal scales from March  
 1050 2020 to February 2021 for four receptor cities namely, Peshawar, Islamabad, Lahore, and  
 1051 Karachi (see legend for identification).

## 1052 **6. Conclusions**

1053 In this study, long-term (2003–2020) remote sensing, ground-based, and model simulation  
1054 datasets were combined to provide the most comprehensive and extensive evaluation ever, of  
1055 air quality conditions over Pakistan. Long-term spatio-temporal distributions of aerosol  
1056 pollutants and trace gases, recent long-term trends at the city level, ranking of cities in terms of  
1057 air pollution levels into three categories (extremely polluted, highly polluted, polluted cities), and  
1058 the potential sources of air pollution across Pakistan were reported.

1059 The highest AOD was observed in the summer months (June to August), mainly attributed to  
1060 the hygroscopic growth of aerosol particles during the humid summer season. High AOD levels  
1061 were also observed during cold months (October to January), mainly over biomass burning  
1062 affected regions such as Punjab. For PM<sub>x</sub> and trace gases, the highest values were observed  
1063 during cold months from October to February, when the atmosphere is stably stratified and the  
1064 boundary layer is shallow, and emissions from anthropogenic activities and biomass burning are  
1065 higher than in other seasons.

1066 The CAMS PM<sub>2.5</sub> data are in better agreement with ground-based PM<sub>2.5</sub> concentrations than  
1067 MERRA-2 reanalysis PM<sub>2.5</sub> data and were therefore used to rank the cities in terms of  
1068 concentrations of particulate matter (PM<sub>x</sub>). The 18 years average of the PM<sub>2.5</sub> concentrations for  
1069 the 80 cities of Pakistan show that a total of 21 cities fall within the category of extremely polluted  
1070 cities ( $PM_{2.5} > 92.84$ ) (namely Punjab: 17, Khyber Pakhtunkhwa: 3, Azad Kashmir: 1), 40 cities fall  
1071 within the category of highly polluted cities ( $45.69 < PM_{2.5} < 92.84$ ) (namely 6 in Punjab, 14 in  
1072 Sindh, 3 in Balochistan, 13 in Khyber Pakhtunkhwa and 4 in Azad Kashmir); 19 cities fall within

1073 the category of polluted cities ( $PM_{2.5} < 45.69$ ) (16 in Balochistan and 3 in Khyber Pakhtunkhwa).  
1074 No single city in Pakistan falls within the  $PM_{2.5}$  standards defined by Pak-NEQS and WHO, and the  
1075 values of  $PM_1$  and  $PM_{2.5}$  for the top 10 cities are 5.6 (8.4) to 9.0 (13.5) times and 7.2 (10.8) to  
1076 11.4 (17.1) times larger than the Pak-NEQS (WHO AQG). The map of annual average  $PM_{2.5}$  shows  
1077 that people in the whole country are exposed to high  $PM_{2.5}$  concentrations for many years, with  
1078 the annual mean concentrations for all cities exceeding the Pak-NEQS ( $<15 \mu\text{g}/\text{m}^3$ ), and 68, 73,  
1079 and 80 cities exceeding the WHO Interim Target-1 ( $<35 \mu\text{g}/\text{m}^3$ ), Target-2 ( $<25 \mu\text{g}/\text{m}^3$ ), and  
1080 Target-3 ( $<15 \mu\text{g}/\text{m}^3$ ), respectively. In terms of pollution sources, the study indicates that  
1081 biomass (crop residue) burning activities may not be the main source of severe air quality  
1082 conditions in Pakistan: the highest  $PM_x$  concentrations were observed in December and January  
1083 when also the  $\text{NO}_2$  TVCD and  $\text{SO}_2$  VCD, used as proxies for  $\text{NO}_2$  and  $\text{SO}_2$  concentrations, were  
1084 highest. The emissions of these trace gases are known to be associated with anthropogenic  
1085 activities including transport, industrial activities, and power generation. Interestingly, higher  
1086 levels of AOD,  $PM_1$ ,  $PM_{2.5}$ ,  $PM_{10}$ ,  $\text{NO}_2$ ,  $\text{SO}_2$ , population density, nighttime lights, and vegetation  
1087 fire activities showed the same spatial pattern as cropland: most of the major cities, as well as  
1088 rural areas in Pakistan, are surrounded by cropland and transport of pollutants generated from  
1089 anthropogenic activities mix with aerosol and trace gases generated from agricultural activities,  
1090 biomass burning and natural aerosols such as dust, to produce a rather smooth mixture of the  
1091 metrics reported in this study. These findings suggest that Pakistan's extreme air pollution  
1092 problems are strongly influenced by anthropogenic activities within Pakistan. This is also  
1093 confirmed by the PSCF ( $> 0.6$ ) analysis based on HYSPLIT air parcel back trajectories and ground-

1094 based PM<sub>2.5</sub> concentrations. In addition, meteorological factors have a strong influence on the  
1095 occurrence of pollution episodes.

1096 Significant positive trends in the concentrations of AOD, PM<sub>1</sub>, PM<sub>2.5</sub>, PM<sub>10</sub>, NO<sub>2</sub>, and SO<sub>2</sub> were  
1097 observed from November to February, particularly over Lahore, Islamabad, Gujranwala, and  
1098 Faisalabad.

1099 The final remark of this study is that all cities in Pakistan have been exposed to long-term  
1100 PM<sub>x</sub>, NO<sub>2</sub>, and SO<sub>2</sub> concentrations throughout the last two decades. The pollution levels in these  
1101 cities imply extremely poor air quality conditions, mainly due to local anthropogenic activities,  
1102 which severely threaten human life. This comprehensive study, based on long-term multi-source  
1103 information on aerosols and trace gases may be considered a baseline study by the Ministry of  
1104 Climate Change, Pakistan, and other policymakers, to mitigate air pollution problems in Pakistan.

#### 1105 **CRedit authorship contribution statement**

1106 **Muhammad Bilal:** Conceptualization, Data curation, Methodology, Formal analysis,  
1107 Investigation, Validation, Visualization, Writing - original draft. **Janet E. Nichol:** Supervision,  
1108 Investigation, Writing - review & editing. **Zhongfeng Qiu:** Supervision, Investigation, Writing -  
1109 review & editing. **Alaa Mhawish:** Data curation, Writing - review & editing. **Majid Nazeer:** Data  
1110 curation, Writing - review & editing. **Md. Arfan Ali:** Data curation, Writing - review & editing.  
1111 **Gerrit de Leeuw:** Supervision, Writing - review & editing. **Robert C. Levy:** Writing - review &  
1112 editing. **Yu Wang:** Data curation. **Yang Chen:** Data curation. **Lunche Wang:** Data curation. **Yuan**

1113 **Shi:** Writing - review & editing. **Max P. Bleiweiss:** Supervision, Investigation, **Luqman Atique:**  
1114 Visualization. **Usman Mazhar:** Visualization.

## 1115 **Declaration of competing interest**

1116 The authors declare that they have no known competing financial interests or personal  
1117 relationships that could have appeared to influence the work reported in this paper.

## 1118 **Acknowledgment**

1119 The authors would like to acknowledge NASA's Level-1 and Atmosphere Archive and  
1120 Distribution System (LAADS) Distributed Active Archive Center (DAAC)  
1121 (<https://ladsweb.modaps.eosdis.nasa.gov/>) for MODIS data, the Copernicus Atmosphere  
1122 Monitoring Service (CAMS) for air quality data (PM<sub>1</sub>, PM<sub>2.5</sub>, and PM<sub>10</sub>), the Goddard Earth Science  
1123 DISC (<https://daac.gsfc.nasa.gov/>) for OMI data, Principal Investigators of Lahore AERONET site,  
1124 and the NOAA Air Resources Laboratory (ARL) for the provision of the HYSPLIT air parcel back  
1125 trajectories (<https://www.ready.noaa.gov>) used in this publication. The authors are grateful to  
1126 Mr. Abid Omar, founder of Pakistan Air Quality Initiative (PAQI), and gratefully acknowledge the  
1127 U.S. Department of State for providing the open access ground-based PM<sub>2.5</sub> data. The authors  
1128 also acknowledge the use of data from NASA's Fire Information for Resource Management  
1129 System (FIRMS) (<https://earthdata.nasa.gov/firms>), part of NASA's Earth Observing System Data  
1130 and Information System (EOSDIS). The authors are thankful to Mr. Pravash Tiwari for helping in  
1131 PSCF analysis and Dr. Devin White (Oak Ridge National Laboratory) for MODIS Conversion Tool  
1132 Kit (MCTK).

1133

1134 **Funding**

1135 This work was supported by the National Key Research and Development Program of China  
1136 (2016YFC1400901), the Special Project of Jiangsu Distinguished Professor (R2018T22), the  
1137 National Natural Science Foundation of China (41976165), Jiangsu Technology Project of Nature  
1138 Resources (KJXM2019042), and the Startup Foundation for Introduction Talent of NUIST  
1139 (2017r107). Additional support came from the New Mexico State University College of  
1140 Agriculture Consumer and Environmental Sciences' Agricultural Experiment Station.

1141 **References**

1142 Adrees, M., Ibrahim, M., Shah, A.M., Abbas, F., Saleem, F., Rizwan, M., Hina, S., Jabeen, F., & Ali, S. (2016).  
1143 Gaseous pollutants from brick kiln industry decreased the growth, photosynthesis, and yield of  
1144 wheat (*Triticum aestivum* L.). *Environ Monit Assess*, *188*, 267

1145 Alam, K., Rahman, N., Khan, H.U., Haq, B.S., & Rahman, S. (2015). Particulate Matter and Its Source  
1146 Apportionment in Peshawar, Northern Pakistan. *Aerosol and Air Quality Research*, *15*, 634-647

1147 Ali, M., Tariq, S., Mahmood, K., Daud, A., Batool, A., & Zia ul, H. (2013). A study of aerosol properties over  
1148 Lahore (Pakistan) by using AERONET data. *Asia-Pacific Journal of Atmospheric Sciences*, *50*, 153-  
1149 162

1150 Ali, M.A., & Assiri, M. (2019). Analysis of AOD from MODIS-Merged DT-DB Products Over the Arabian  
1151 Peninsula. *Earth Systems and Environment*, *3*, 625-636

1152 Amnesty International (2019). Pakistan: Hazardous air puts lives at risk. In

1153 Ashraf, N., Mushtaq, M., Sultana, B., Iqbal, M., Ullah, I., & Shahid, S.A. (2013). Preliminary monitoring of  
1154 tropospheric air quality of Lahore City in Pakistan. *Int. J. Chem. Biochem. Sci.*, *3*, 19-28

1155 Begum, A.B., Kim, E., Jeong, C.-H., Lee, D.-W., & Hopke, P.K. (2005). Evaluation of the potential source  
1156 contribution function using the 2002 Quebec forest fire episode. *Atmospheric Environment*, 39,  
1157 3719-3724

1158 Bilal, M., Nazeer, M., Nichol, J.E., Bleiweiss, M.P., Qiu, Z., Jäkel, E., Campbell, J.R., Atique, L., Huang, X., &  
1159 Lolli, S. (2019a). A Simplified and Robust Surface Reflectance Estimation Method (SREM) for Use  
1160 over Diverse Land Surfaces Using Multi-Sensor Data. *Remote Sensing*, 11

1161 Bilal, M., Nazeer, M., Nichol, J.E., Qiu, Z., Wang, L., Bleiweiss, M.P., Shen, X., Campbell, J.R., & Lolli, S.  
1162 (2019b). Evaluation of Terra-MODIS C6 and C6.1 Aerosol Products against Beijing, XiangHe, and  
1163 Xinglong AERONET Sites in China during 2004-2014. *Remote Sensing*, 11, 486

1164 Bilal, M., Nazeer, M., Qiu, Z., Ding, X., & Wei, J. (2018a). Global Validation of MODIS C6 and C6.1 Merged  
1165 Aerosol Products over Diverse Vegetated Surfaces. *Remote Sensing*, 10

1166 Bilal, M., & Nichol, J. (2017). Evaluation of the NDVI-Based Pixel Selection Criteria of the MODIS C6 Dark  
1167 Target and Deep Blue Combined Aerosol Product. *IEEE Journal of Selected Topics in Applied Earth  
1168 Observations and Remote Sensing*, 10, 3448 - 3453

1169 Bilal, M., Nichol, J., & Wang, L. (2017). New customized methods for improvement of the MODIS C6 Dark  
1170 Target and Deep Blue merged aerosol product. *Remote Sensing of Environment*, 197, 115–124

1171 Bilal, M., Nichol, J.E., Bleiweiss, M.P., & Dubois, D. (2013). A Simplified high resolution MODIS Aerosol  
1172 Retrieval Algorithm (SARA) for use over mixed surfaces. *Remote Sensing of Environment*, 136, 135-  
1173 145

1174 Bilal, M., Nichol, J.E., & Chan, P.W. (2014). Validation and accuracy assessment of a Simplified Aerosol  
1175 Retrieval Algorithm (SARA) over Beijing under low and high aerosol loadings and dust storms.  
1176 *Remote Sensing of Environment*, 153, 50-60

1177 Bilal, M., Nichol, J.E., & Nazeer, M. (2016). Validation of Aqua-MODIS C051 and C006 Operational Aerosol  
1178 Products Using AERONET Measurements Over Pakistan. *IEEE Journal of Selected Topics in Applied  
1179 Earth Observations and Remote Sensing*, 9, 2074-2080

1180 Bilal, M., Nichol, J.E., Nazeer, M., Shi, Y., Wang, L., Kumar, K.R., Ho, H.C., Mazhar, U., Bleiweiss, M.P., Qiu,  
1181 Z., Khedher, K.M., & Lolli, S. (2019c). Characteristics of Fine Particulate Matter (PM<sub>2.5</sub>) over Urban,  
1182 Suburban, and Rural Areas of Hong Kong. *Atmosphere*, 10

1183 Bilal, M., Qiu, Z., Campbell, J.R., Spak, S., Shen, X., & Nazeer, M. (2018b). A New MODIS C6 Dark Target  
1184 and Deep Blue Merged Aerosol Product on a 3 km Spatial Grid. *Remote Sensing*, 10, 463

1185 Buchard, V., da Silva, A.M., Randles, C.A., Colarco, P., Ferrare, R., Hair, J., Hostetler, C., Tackett, J., &  
1186 Winker, D. (2016). Evaluation of the surface PM<sub>2.5</sub> in Version 1 of the NASA MERRA Aerosol  
1187 Reanalysis over the United States. *Atmospheric Environment*, *125*, 100-111

1188 Buchard, V., Randles, C.A., da Silva, A.M., Darmenov, A., Colarco, P.R., Govindaraju, R., Ferrare, R., Hair, J.,  
1189 Beyersdorf, A.J., Ziemba, L.D., & Yu, H. (2017). The MERRA-2 Aerosol Reanalysis, 1980 Onward.  
1190 Part II: Evaluation and Case Studies. *J Clim*, *30*, 6851-6872

1191 Carn, S.A., Fioletov, V.E., McLinden, C.A., Li, C., & Krotkov, N.A. (2017). A decade of global volcanic SO<sub>2</sub>  
1192 emissions measured from space. *Sci Rep*, *7*, 44095

1193 Che, H., Yang, L., Liu, C., Xia, X., Wang, Y., Wang, H., Wang, H., Lu, X., & Zhang, X. (2019). Long-term  
1194 validation of MODIS C6 and C6.1 Dark Target aerosol products over China using CARSNET and  
1195 AERONET. *Chemosphere*, *236*, 124268

1196 Chen, G., Li, S., Zhang, Y., Zhang, W., Li, D., Wei, X., He, Y., Bell, M.L., Williams, G., Marks, G.B., Jalaludin,  
1197 B., Abramson, M.J., & Guo, Y. (2017). Effects of ambient PM<sub>1</sub> air pollution on daily emergency  
1198 hospital visits in China: an epidemiological study. *The Lancet Planetary Health*, *1*, e221-e229

1199 Cheng, M.M., Jiang, H., & Guo, Z. (2012). Evaluation of long-term tropospheric NO<sub>2</sub> columns and the effect  
1200 of different ecosystem in Yangtze River Delta. *Procedia Environmental Sciences*, *13*, 1045-1056

1201 Chin, M., Ginoux, P., Kinne, S., Torres, O., Holben, B.N., Duncan, B.N., Martin, R.V., Logan, J.A., Higurashi,  
1202 A., & Nakajima, T. (2002). Tropospheric Aerosol Optical Thickness from the GOCART Model and  
1203 Comparisons with Satellite and Sun Photometer Measurements. *Journal of the Atmospheric*  
1204 *Sciences*, *59*, 461-483

1205 Colarco, P., da Silva, A., Chin, M., & Diehl, T. (2010). Online simulations of global aerosol distributions in  
1206 the NASA GEOS-4 model and comparisons to satellite and ground-based aerosol optical depth.  
1207 *Journal of Geophysical Research*, *115*

1208 Colbeck, I., Nasir, Z.A., & Ali, Z. (2010). The state of ambient air quality in Pakistan--a review. *Environ Sci*  
1209 *Pollut Res Int*, *17*, 49-63

1210 Cuevas, E., Camino, C., Benedetti, A., Basart, S., Terradellas, E., Baldasano, J.M., Morcrette, J.J.,  
1211 Marticorena, B., Goloub, P., Mortier, A., Berjón, A., Hernández, Y., Gil-Ojeda, M., & Schulz, M.  
1212 (2015). The MACC-II 2007–2008 reanalysis: atmospheric dust evaluation and characterization over  
1213 northern Africa and the Middle East. *Atmospheric Chemistry and Physics*, *15*, 3991-4024

1214 Dahiya, S., & Myllyvirta, L. (2019). Global SO<sub>2</sub> emission hotspot database: Ranking the world's worst  
1215 sources of SO<sub>2</sub> pollution. In K. Ford, N. Sivalingam, S. Ayeche, & A. Jacobsen (Eds.)



1216 de Leeuw, G., Sogacheva, L., Rodriguez, E., Kourtidis, K., Georgoulas, A.K., Alexandri, G., Amiridis, V.,  
1217 Proestakis, E., Marinou, E., Xue, Y., & van der A, R. (2018). Two decades of satellite observations of  
1218 AOD over mainland China using ATSR-2, AATSR and MODIS/Terra: data set evaluation and large-  
1219 scale patterns. *Atmospheric Chemistry and Physics*, *18*, 1573-1592

1220 Dickerson, R.R., Kondragunta, S., Stenchikov, G., Civerolo, K.L., Doddridge, B.G., & Holben, B.N. (1997).  
1221 The impact of aerosols on solar ultraviolet radiation and photochemical smog. *Science*, *278*, 827-  
1222 830

1223 Ding, A.J., Huang, X., Nie, W., Sun, J.N., Kerminen, V.M., Petaja, T., Su, H., Cheng, Y.F., Yang, X.Q., Wang,  
1224 M.H., Chi, X.G., Wang, J.P., Virkkula, A., Guo, W.D., Yuan, J., Wang, S.Y., Zhang, R.J., Wu, Y.F., Song,  
1225 Y., Zhu, T., Zilitinkevich, S., Kulmala, M., & Fu, C.B. (2016). Enhanced haze pollution by black carbon  
1226 in megacities in China. *Geophysical Research Letters*, *43*, 2873-2879

1227 Eck, T.F., Holben, B.N., Reid, J.S., Dubovik, O., Smirnov, A., O'Neill, N.T., Slutsker, I., & Kinne, S. (1999).  
1228 Wavelength dependence of the optical depth of biomass burning, urban, and desert dust aerosols.  
1229 *Journal of Geophysical Research: Atmospheres*, *104*, 31333-31349

1230 Elvidge, C.D., Zhizhin, M., Ghosh, T., Hsu, F.-C., & Taneja, J. (2021). Annual Time Series of Global VIIRS  
1231 Nighttime Lights Derived from Monthly Averages: 2012 to 2019. *Remote Sensing*, *13*

1232 Fan, A., Chen, W., Liang, L., Sun, W., Lin, Y., Che, H., & Zhao, X. (2017). Evaluation and Comparison of Long-  
1233 Term MODIS C5.1 and C6 Products against AERONET Observations over China. *Remote Sensing*, *9*,  
1234 1269

1235 Filonchyk, M., Yan, H., Zhang, Z., Yang, S., Li, W., & Li, Y. (2019). Combined use of satellite and surface  
1236 observations to study aerosol optical depth in different regions of China. *Sci Rep*, *9*, 6174

1237 Fioletov, V.E., McLinden, C.A., Krotkov, N., Moran, M.D., & Yang, K. (2011). Estimation of SO<sub>2</sub> emissions  
1238 using OMI retrievals. *Geophysical Research Letters*, *38*, n/a-n/a

1239 Fleming, Z.L., Monks, P.S., & Manning, A.J. (2012). Review: Untangling the influence of air-mass history in  
1240 interpreting observed atmospheric composition. *Atmospheric Research*, *104-105*, 1-39

1241 Flemming, J., Benedetti, A., Inness, A., Engelen, R.J., Jones, L., Huijnen, V., Remy, S., Parrington, M., Suttie,  
1242 M., Bozzo, A., Peuch, V.-H., Akritidis, D., & Katragkou, E. (2017). The CAMS interim Reanalysis of  
1243 Carbon Monoxide, Ozone and Aerosol for 2003–2015. *Atmospheric Chemistry and Physics*, *17*,  
1244 1945-1983

1245 Flemming, J., Huijnen, V., Arteta, J., Bechtold, P., Beljaars, A., Blechschmidt, A.M., Diamantakis, M.,  
1246 Engelen, R.J., Gaudel, A., Inness, A., Jones, L., Josse, B., Katragkou, E., Marecal, V., Peuch, V.H.,

1247 Richter, A., Schultz, M.G., Stein, O., & Tsikerdekis, A. (2015). Tropospheric chemistry in the  
1248 Integrated Forecasting System of ECMWF. *Geoscientific Model Development*, 8, 975-1003

1249 Giles, D.M., Sinyuk, A., Sorokin, M.G., Schafer, J.S., Smirnov, A., Slutsker, I., Eck, T.F., Holben, B.N., Lewis,  
1250 J.R., Campbell, J.R., Welton, E.J., Korkin, S.V., & Lyapustin, A.I. (2019). Advancements in the Aerosol  
1251 Robotic Network (AERONET) Version 3 database – automated near-real-time quality control  
1252 algorithm with improved cloud screening for Sun photometer aerosol optical depth (AOD)  
1253 measurements. *Atmospheric Measurement Techniques*, 12, 169-209

1254 Government of Pakistan, F.D. (2019). Pakistan Economic Survey 2018-19. In

1255 Granier, C., Bessagnet, B., Bond, T., D'Angiola, A., Denier van der Gon, H., Frost, G.J., Heil, A., Kaiser, J.W.,  
1256 Kinne, S., Klimont, Z., Kloster, S., Lamarque, J.-F., Liousse, C., Masui, T., Meleux, F., Mieville, A.,  
1257 Ohara, T., Raut, J.-C., Riahi, K., Schultz, M.G., Smith, S.J., Thompson, A., van Aardenne, J., van der  
1258 Werf, G.R., & van Vuuren, D.P. (2011). Evolution of anthropogenic and biomass burning emissions  
1259 of air pollutants at global and regional scales during the 1980–2010 period. *Climatic Change*, 109,  
1260 163-190

1261 Gupta, P., Khan, M.N., da Silva, A., & Patadia, F. (2013). MODIS aerosol optical depth observations over  
1262 urban areas in Pakistan: quantity and quality of the data for air quality monitoring. *Atmospheric  
1263 Pollution Research*, 4, 43-52

1264 Hamed, K.H., & Ramachandra Rao, A. (1998). A modified Mann-Kendall trend test for autocorrelated data.  
1265 *Journal of Hydrology*, 204, 182-196

1266 Harper, W.V. (2016). Reduced Major Axis Regression. *Wiley StatsRef: Statistics Reference Online* (pp. 1-6)

1267 He, L., Lin, A., Chen, X., Zhou, H., Zhou, Z., & He, P. (2019). Assessment of MERRA-2 Surface PM<sub>2.5</sub> over  
1268 the Yangtze River Basin: Ground-based Verification, Spatiotemporal Distribution and  
1269 Meteorological Dependence. *Remote Sensing*, 11

1270 He, L., Wang, L., Lin, A., Zhang, M., Bilal, M., & Wei, J. (2018). Performance of the NPP-VIIRS and aqua-  
1271 MODIS Aerosol Optical Depth Products over the Yangtze River Basin. *Remote Sensing*, 10, 117

1272 Health Effects Institute (2019). State of Global Air 2019: A Special Report On Global Exposure to Air  
1273 Pollution and Its Disease Burden. In. Boston, MA

1274 Holben, B.N., Eck, T.F., Slutsker, I., Tanré, D., Buis, J.P., Setzer, A., Vermote, E., Reagan, J.A., Kaufman, Y.J.,  
1275 Nakajima, T., Lavenu, F., Jankowiak, I., & Smirnov, A. (1998). AERONET—A Federated Instrument  
1276 Network and Data Archive for Aerosol Characterization. *Remote Sensing of Environment*, 66, 1-16

1277 Holben, N., Tanr, D., Smirnov, A., Eck, T.F., Slutsker, I., Newcomb, W.W., Schafer, J.S., Chatenet, B., Lavenu,  
1278 F., Kaufman, J., Castle, J.V., Setzer, A., Markham, B., Clark, D., Halthore, R., Karneli, A., Neill, N.T.O.,

1279 Pietras, C., Pinker, T., Voss, K., & Zibordi, G. (2001). An emerging ground-based aerosol climatology  
1280 : Aerosol optical depth from AERONET. *Journal of Geophysical Research: Atmospheres*, *106*, 12067-  
1281 12097

1282 Hsu, N.C., Jeong, M.-J., Bettenhausen, C., Sayer, A.M., Hansell, R., Seftor, C.S., Huang, J., & Tsay, S.-C.  
1283 (2013). Enhanced Deep Blue aerosol retrieval algorithm: The second generation. *Journal of*  
1284 *Geophysical Research: Atmospheres*, *118*, 9296-9315

1285 Inness, A., Ades, M., Agustí-Panareda, A., Barré, J., Benedictow, A., Blechschmidt, A.-M., Dominguez, J.J.,  
1286 Engelen, R., Eskes, H., Flemming, J., Huijnen, V., Jones, L., Kipling, Z., Massart, S., Parrington, M.,  
1287 Peuch, V.-H., Razinger, M., Remy, S., Schulz, M., & Suttie, M. (2019). The CAMS reanalysis of  
1288 atmospheric composition. *Atmospheric Chemistry and Physics*, *19*, 3515-3556

1289 Irfan, M., Riaz, M., Arif, M.S., Shahzad, S.M., Hussain, S., Akhtar, M.J., van den Berg, L., & Abbas, F. (2015).  
1290 Spatial distribution of pollutant emissions from crop residue burning in the Punjab and Sindh  
1291 provinces of Pakistan: uncertainties and challenges. *Environ Sci Pollut Res Int*, *22*, 16475-16491

1292 Irfan, M., Riaz, M., Arif, M.S., Shahzad, S.M., Saleem, F., Rahman, N.-u., van den Berg, L., & Abbas, F.  
1293 (2014). Estimation and characterization of gaseous pollutant emissions from agricultural crop  
1294 residue combustion in industrial and household sectors of Pakistan. *Atmospheric Environment*, *84*,  
1295 189-197

1296 Ishaq, M., Khan, M.A., Jan, F.A., & Ahmad, I. (2010). Heavy metals in brick kiln located area using atomic  
1297 absorption spectrophotometer: a case study from the city of Peshawar, Pakistan. *Environ Monit*  
1298 *Assess*, *166*, 409-420

1299 Islam, M.N., Ali, M.A., & Islam, M.M. (2019). Spatiotemporal Investigations of Aerosol Optical Properties  
1300 Over Bangladesh for the Period 2002–2016. *Earth Systems and Environment*, *3*, 563-573

1301 Jacob, D.J., & Winner, D.A. (2009). Effect of climate change on air quality. *Atmospheric Environment*, *43*,  
1302 51-63

1303 Jain, S., Sharma, S.K., Vijayan, N., & Mandal, T.K. (2020). Seasonal characteristics of aerosols (PM<sub>2.5</sub> and  
1304 PM<sub>10</sub>) and their source apportionment using PMF: A four year study over Delhi, India. *Environ*  
1305 *Pollut*, *262*, 114337

1306 Janssens-Maenhout, G., Pagliari, V., Guizzardi, D., & Muntean, M. (2013). Global emission inventories in  
1307 the Emission Database for Global Atmospheric Research (EDGAR) – Manual (I), Gridding: EDGAR  
1308 emissions distribution on global gridmaps. In. Luxembourg: Publications Office of the European  
1309 Union

1310 Jethva, H., Torres, O., Field, R.D., Lyapustin, A., Gautam, R., & Kayetha, V. (2019). Connecting Crop  
1311 Productivity, Residue Fires, and Air Quality over Northern India. *Sci Rep*, *9*, 16594

1312 Kendall, M., & Gibbons, J.D. (1990). *Rank Correlation Methods*. (5th Edition ed.). London: Edward Arnold

1313 Keys, R. (1981). Cubic convolution interpolation for digital image processing. *IEEE Transactions on*  
1314 *Acoustics, Speech, and Signal Processing*, *29*, 1153-1160

1315 Khanum, F., Chaudhry, M.N., & Kumar, P. (2017). Characterization of five-year observation data of fine  
1316 particulate matter in the metropolitan area of Lahore. *Air Qual Atmos Health*, *10*, 725-736

1317 Khokhar, M.F., Mehdi, H., Abbas, Z., & Javed, Z. (2016). Temporal Assessment of NO<sub>2</sub> Pollution Levels in  
1318 Urban Centers of Pakistan by Employing Ground-Based and Satellite Observations. *Aerosol and Air*  
1319 *Quality Research*, *16*, 1854-1867

1320 Khokhar, M.F., Yasmin, N., Fatima, N., Beirle, S., & Wagner, T. (2015). Detection of Trends and Seasonal  
1321 Variation in Tropospheric Nitrogen Dioxide over Pakistan. *Aerosol and Air Quality Research*, *15*,  
1322 2508-2524

1323 Krotkov, N.A., Lamsal, L.N., Celarier, E.A., Swartz, W.H., Marchenko, S.V., Bucsela, E.J., Chan, K.L., Wenig,  
1324 M., & Zara, M. (2017). The version 3 OMI NO<sub>2</sub> standard product.  
1325 *Atmospheric Measurement Techniques*, *10*, 3133-3149

1326 Krotkov, N.A., McLinden, C.A., Li, C., Lamsal, L.N., Celarier, E.A., Marchenko, S.V., Swartz, W.H., Bucsela,  
1327 E.J., Joiner, J., Duncan, B.N., Boersma, K.F., Veefkind, J.P., Levelt, P.F., Fioletov, V.E., Dickerson, R.R.,  
1328 He, H., Lu, Z., & Streets, D.G. (2016). Aura OMI observations of regional SO<sub>2</sub> and NO<sub>2</sub> pollution  
1329 changes from 2005 to 2015. *Atmospheric Chemistry and Physics*, *16*, 4605-4629

1330 Kulmala, M., Dada, L., Daellenbach, K.R., Yan, C., Stolzenburg, D., Kontkanen, J., Ezhova, E., Hakala, S.,  
1331 Tuovinen, S., Kokkonen, T.V., Kurppa, M., Cai, R., Zhou, Y., Yin, R., Baalbaki, R., Chan, T., Chu, B.,  
1332 Deng, C., Fu, Y., Ge, M., He, H., Heikkinen, L., Junninen, H., Liu, Y., Lu, Y., Nie, W., Rusanen, A.,  
1333 Vakkari, V., Wang, Y., Yang, G., Yao, L., Zheng, J., Kujansuu, J., Kangasluoma, J., Petaja, T., Paasonen,  
1334 P., Jarvi, L., Worsnop, D., Ding, A., Liu, Y., Wang, L., Jiang, J., Bianchi, F., & Kerminen, V.M. (2020).  
1335 Is reducing new particle formation a plausible solution to mitigate particulate air pollution in  
1336 Beijing and other Chinese megacities? *Faraday Discuss*

1337 Latza, U., Gerdes, S., & Baur, X. (2009). Effects of nitrogen dioxide on human health: systematic review of  
1338 experimental and epidemiological studies conducted between 2002 and 2006. *Int J Hyg Environ*  
1339 *Health*, *212*, 271-287

1340 Le Blond, J.S., Woskie, S., Horwell, C.J., & Williamson, B.J. (2017). Particulate matter produced during  
1341 commercial sugarcane harvesting and processing: A respiratory health hazard? *Atmospheric*  
1342 *Environment*, *149*, 34-46

1343 Lee, D.S., Köhler, I., Grobler, E., Rohrer, F., Sausen, R., Gallardo-Klenner, L., Olivier, J.G.J., Dentener, F.J., &  
1344 Bouwman, A.F. (1997). Estimations of global no, emissions and their uncertainties. *Atmospheric*  
1345 *Environment*, *31*, 1735-1749

1346 Levy, R.C., Mattoo, S., Munchak, L.A., Remer, L.A., Sayer, A.M., Patadia, F., & Hsu, N.C. (2013). The  
1347 Collection 6 MODIS aerosol products over land and ocean. *Atmospheric Measurement Techniques*,  
1348 *6*, 2989-3034

1349 Levy, R.C., Remer, L.a., Kleidman, R.G., Mattoo, S., Ichoku, C., Kahn, R., & Eck, T.F. (2010). Global evaluation  
1350 of the Collection 5 MODIS dark-target aerosol products over land. *Atmospheric Chemistry and*  
1351 *Physics*, *10*, 10399-10420

1352 Li, C., Krotkov, N.A., Carn, S., Zhang, Y., Spurr, R.J.D., & Joiner, J. (2017). New-generation NASA Aura Ozone  
1353 Monitoring Instrument (OMI) volcanic SO<sub>2</sub> dataset: algorithm description,  
1354 initial results, and continuation with the Suomi-NPP Ozone Mapping and Profiler Suite (OMPS).  
1355 *Atmospheric Measurement Techniques*, *10*, 445-458

1356 Li, C., Krotkov, N.A., Leonard, P.J.T., Carn, S., Joiner, J., Spurr, R.J.D., & Vasilkov, A. (2020). Version 2 Ozone  
1357 Monitoring Instrument SO<sub>2</sub> product (OMSO2 V2): new anthropogenic  
1358 SO<sub>2</sub> vertical column density dataset. *Atmospheric Measurement*  
1359 *Techniques*, *13*, 6175-6191

1360 Li, L., & Wang, Y. (2014). What drives the aerosol distribution in Guangdong--the most developed province  
1361 in Southern China? *Sci Rep*, *4*, 5972

1362 Li, L., Wu, J., Ghosh, J.K., & Ritz, B. (2013). Estimating Spatiotemporal Variability of Ambient Air Pollutant  
1363 Concentrations with A Hierarchical Model. *Atmos Environ (1994)*, *71*, 54-63

1364 Li, Z.Q., Zhang, Y., Shao, J., Li, B.S., Hong, J., Liu, D., Li, D.H., Wei, P., Li, W., Li, L., Zhang, F.X., Guo, J., Deng,  
1365 Q., Wang, B.X., Cui, C.L., Zhang, W.C., Wang, Z.Z., Lv, Y., Xu, H., Chen, X.F., Li, L., & Qie, L.L. (2016).  
1366 Remote sensing of atmospheric particulate mass of dry PM<sub>2.5</sub> near the ground: Method validation  
1367 using ground-based measurements. *Remote Sensing of Environment*, *173*, 59-68

1368 Liu, L., Breitner, S., Schneider, A., Cyrys, J., Bruske, I., Franck, U., Schlink, U., Marian Leitte, A., Herbarth,  
1369 O., Wiedensohler, A., Wehner, B., Pan, X., Wichmann, H.E., & Peters, A. (2013). Size-fractioned  
1370 particulate air pollution and cardiovascular emergency room visits in Beijing, China. *Environ Res*,  
1371 *121*, 52-63

1372 Livingston, J.M., Redemann, J., Shinozuka, Y., Johnson, R., Russell, P.B., Zhang, Q., Mattoo, S., Remer, L.,  
1373 Levy, R., Munchak, L., & Ramachandran, S. (2014). Comparison of MODIS 3 km and 10 km  
1374 resolution aerosol optical depth retrievals over land with airborne sunphotometer measurements  
1375 during ARCTAS summer 2008. *Atmospheric Chemistry and Physics*, *14*, 2015-2038

1376 Mann, H.B. (1945). Nonparametric Tests Against Trend. *Econometrica*, *13*

1377 Mannucci, P.M., & Franchini, M. (2017). Health Effects of Ambient Air Pollution in Developing Countries.  
1378 *Int J Environ Res Public Health*, *14*

1379 Mehta, M., Singh, R., Singh, A., Singh, N., & Anshumali (2016). Recent global aerosol optical depth  
1380 variations and trends - A comparative study using MODIS and MISR level 3 datasets. *Remote*  
1381 *Sensing of Environment*, *181*, 137-150

1382 Mei, L., Zhao, C., de Leeuw, G., Che, H., Che, Y., Rozanov, V., Vountas, M., & Burrows, J.P. (2019).  
1383 Understanding MODIS dark-target collection 5 and 6 aerosol data over China: Effect of surface  
1384 type, aerosol loading and aerosol absorption. *Atmospheric Research*, *228*, 161-175

1385 Meng, X., Ma, Y., Chen, R., Zhou, Z., Chen, B., & Kan, H. (2013). Size-fractionated particle number  
1386 concentrations and daily mortality in a Chinese city. *Environ Health Perspect*, *121*, 1174-1178

1387 Mhawish, A., Banerjee, T., Broday, D.M., Misra, A., & Tripathi, S.N. (2017). Evaluation of MODIS Collection  
1388 6 aerosol retrieval algorithms over Indo-Gangetic Plain: Implications of aerosols types and mass  
1389 loading. *Remote Sensing of Environment*, *201*, 297-313

1390 Mhawish, A., Banerjee, T., Sorek-Hamer, M., Bilal, M., Lyapustin, A.I., Chatfield, R., & Broday, D.M. (2020).  
1391 Estimation of High-Resolution PM<sub>2.5</sub> over the Indo-Gangetic Plain by Fusion of Satellite Data,  
1392 Meteorology, and Land Use Variables. *Environmental science & technology*, *54*, 7891-7900

1393 Mhawish, A., Banerjee, T., Sorek-Hamer, M., Lyapustin, A., Broday, D.M., & Chatfield, R. (2019).  
1394 Comparison and evaluation of MODIS Multi-angle Implementation of Atmospheric Correction  
1395 (MAIAC) aerosol product over South Asia. *Remote Sensing of Environment*, *224*, 12-28

1396 Mhawish, A., Sorek-Hamer, M., Chatfield, R., Banerjee, T., Bilal, M., Kumar, M., Sarangi, C., Franklin, M.,  
1397 Chau, K., Garay, M., & Kalashnikova, O. (2021). Aerosol Characteristics from Earth Observation  
1398 Systems: A Comprehensive Investigation over South Asia (2000-2019). *Remote Sensing of*  
1399 *Environment*, (in press)

1400 Miao, Y., Li, J., Miao, S., Che, H., Wang, Y., Zhang, X., Zhu, R., & Liu, S. (2019). Interaction Between Planetary  
1401 Boundary Layer and PM<sub>2.5</sub> Pollution in Megacities in China: a Review. *Current Pollution Reports*, *5*,  
1402 261-271

1403 Miao, Y., & Liu, S. (2019). Linkages between aerosol pollution and planetary boundary layer structure in  
1404 China. *Sci Total Environ*, 650, 288-296

1405 Miao, Y., Liu, S., Guo, J., Huang, S., Yan, Y., & Lou, M. (2018). Unraveling the relationships between  
1406 boundary layer height and PM2.5 pollution in China based on four-year radiosonde measurements.  
1407 *Environ Pollut*, 243, 1186-1195

1408 More, S., Kumar, P.P., Gupta, P., Devara, P., & Aher, G. (2013). Comparison of Aerosol Products Retrieved  
1409 from AERONET, MICROTOPS and MODIS over a Tropical Urban City, Pune, India. *Aerosol and Air*  
1410 *Quality Research*, 13, 107-121

1411 Navinya, C.D., Vinoj, V., & Pandey, S.K. (2020). Evaluation of PM2.5 Surface Concentrations Simulated by  
1412 NASA's MERRA Version 2 Aerosol Reanalysis over India and its Relation to the Air Quality Index.  
1413 *Aerosol and Air Quality Research*, 20, 1329-1339

1414 Nichol, J., & Bilal, M. (2016). Validation of MODIS 3 km Resolution Aerosol Optical Depth Retrievals Over  
1415 Asia. *Remote Sensing*, 8, 328

1416 Nichol, J.E., Bilal, M., Ali, M.A., & Qiu, Z. (2020). Air Pollution Scenario over China during COVID-19. *Remote*  
1417 *Sensing*, 12

1418 Olivier, J.G.J., Bouwman, A.F., Van der Hoek, K.W., & Berdowski, J.J.M. (1998). Global air emission  
1419 inventories for anthropogenic sources of NO<sub>x</sub>, NH<sub>3</sub> and N<sub>2</sub>O in 1990. *Environmental Pollution*, 102,  
1420 135-148

1421 PAQI (2018). LahoreSmog, Just how bad is it? In: Pakistan Air Quality Initiative

1422 Pervaiz, S., Akram, M.A.N., Khan, F.Z., Javid, K., & Zahid, Y. (2021). Brick Sector and Air Quality: An  
1423 Integrated Assessment towards 2020 Challenge of Environment Development. *Environment and*  
1424 *Natural Resources Journal*, 19, 153-164

1425 Pope, C.A., Burnett, R.T., Thun, M.J., Calle, E.E., Krewski, D., Ito, K., & Thurston, G.D. (2002). Lung cancer,  
1426 cardiopulmonary mortality, and long-term exposure to fine particulate air pollution. *JAMA : the*  
1427 *journal of the American Medical Association*, 287, 1132-1141

1428 Provencal, S., Buchard, V., da Silva, A.M., Leduc, R., Barrette, N., Elhacham, E., & Wang, S.H. (2017).  
1429 Evaluation of PM2.5 surface concentration simulated by Version 1 of the NASA's MERRA Aerosol  
1430 Reanalysis over Israel and Taiwan. *Aerosol Air Qual Res*, 17, 253-261

1431 Purohit, P., Munir, T., & Rafaj, P. (2013). Scenario analysis of strategies to control air pollution in Pakistan.  
1432 *Journal of Integrative Environmental Sciences*, 10, 77-91

1433 Qu, Y., Han, Y., Wu, Y., Gao, P., & Wang, T. (2017). Study of PBLH and Its Correlation with Particulate  
1434 Matter from One-Year Observation over Nanjing, Southeast China. *Remote Sensing*, 9

1435 Rahman, U., Awan, M.A., Hassan, S.T., & Khattak, M.M. (2000). Mosses as Indicators of Atmospheric  
1436 Pollution of Trace Metals (Cd, Cu, Pb, Mn and Zn) in the Vicinity of Coal-Fired Brick Kilns in North-  
1437 Eastern Suburbs of Islamabad, Pakistan. *Journal of Radioanalytical and Nuclear Chemistry*, 246,  
1438 331-336

1439 Randles, C.A., Da Silva, A.M., Buchard, V., Colarco, P.R., Darmenov, A., Govindaraju, R., Smirnov, A.,  
1440 Holben, B., Ferrare, R., Hair, J., Shinozuka, Y., & Flynn, C.J. (2017). The MERRA-2 Aerosol Reanalysis,  
1441 1980 - onward, Part I: System Description and Data Assimilation Evaluation. *J Clim*, 30, 6823-6850

1442 Remer, L.A., Mattoo, S., Levy, R.C., & Munchak, L.A. (2013). MODIS 3 km aerosol product: algorithm and  
1443 global perspective. *Atmospheric Measurement Techniques*, 6, 1829-1844

1444 Rémy, S., Kipling, Z., Flemming, J., Boucher, O., Nabat, P., Michou, M., Bozzo, A., Ades, M., Huijnen, V.,  
1445 Benedetti, A., Engelen, R., Peuch, V.-H., & Morcrette, J.-J. (2019). Description and evaluation of the  
1446 tropospheric aerosol scheme in the European Centre for Medium-Range Weather Forecasts  
1447 (ECMWF) Integrated Forecasting System (IFS-AER, cycle 45R1). *Geoscientific Model Development*,  
1448 12, 4627-4659

1449 Richter, A., & Burrows, J.P. (2002). Tropospheric NO<sub>2</sub> from GOME measurements. *Advances in Space*  
1450 *Research*, 29, 1673-1683

1451 Rose, A.N., McKee, J.J., Sims, K.M., Bright, E.A., Reith, A.E., & Urban, M.L. (2020). LandScan 2019. In. Oak  
1452 Ridge, TN: Oak Ridge National Laboratory

1453 Salmi, T., Määttä, A., Anttila, P., Ruoho-Airola, T., Amnell, T., & Maatta, A. (2002). *Detecting Trends of*  
1454 *Annual Values of Atmospheric Pollutants by the Mann-Kendall Test and Sen's Solpe Estimates the*  
1455 *Excel Template Application MAKESENS*. Helsinki: Finnish Meteorological Institute, Air Quality  
1456 Research

1457 Sayer, A.M., Hsu, N.C., Bettenhausen, C., & Jeong, M.-J. (2013). Validation and uncertainty estimates for  
1458 MODIS Collection 6 “Deep Blue” aerosol data. *Journal of Geophysical Research: Atmospheres*, 118,  
1459 7864-7872

1460 Sayer, A.M., Munchak, L.A., Hsu, N.C., Levy, R.C., Bettenhausen, C., & Jeong, M.J. (2014). MODIS Collection  
1461 6 aerosol products: Comparison between Aqua's e-Deep Blue, Dark Target, and “merged” data  
1462 sets, and usage recommendations. *Journal of Geophysical Research: Atmospheres*, 119, 13965-  
1463 13989

1464 Sayer, A.M., USA, N.G.S.F.C.G.M., USA, U.S.R.A.G.E.S.T.a.R.G.G.M., Hsu, N.C., USA, N.G.S.F.C.G.M.,  
1465 Bettenhausen, C., USA, N.G.S.F.C.G.M., Science Systems and Applications, I.L.M.U., Jeong, M.J.,  
1466 Korea, G.W.N.U.G.C., Meister, G., & USA, N.G.S.F.C.G.M. (2015). Effect of MODIS Terra radiometric



1467 calibration improvements on Collection 6 Deep Blue aerosol products: Validation and Terra/Aqua  
1468 consistency. *Journal of Geophysical Research: Atmospheres*, *120*, 12157-12174

1469 Seinfeld, J.H., & Pandis, S.N. (1998). *Atmospheric Chemistry and Physics, from Air Pollution to climate*  
1470 *Change*. New York: John Wiley and Sons

1471 Sen, P.K. (1968). Estimates of the Regression Coefficient Based on Kendall's Tau. *Journal of the American*  
1472 *Statistical Association*, *63*, 1379-1389

1473 Shah, M.H., Shaheen, N., & Nazir, R. (2012). Assessment of the trace elements level in urban atmospheric  
1474 particulate matter and source apportionment in Islamabad, Pakistan. *Atmospheric Pollution*  
1475 *Research*, *3*, 39-45

1476 Shen, X., Bilal, M., Qiu, Z., Sun, D., Wang, S., & Zhu, W. (2018). Validation of MODIS C6 Dark Target Aerosol  
1477 Products at 3 km and 10 km Spatial Resolutions Over the China Seas and the Eastern Indian Ocean.  
1478 *Remote Sensing*, *10*

1479 Shi, Y., Bilal, M., Ho, H.C., & Omar, A. (2020). Urbanization and regional air pollution across South Asian  
1480 developing countries – A nationwide land use regression for ambient PM<sub>2.5</sub> assessment in  
1481 Pakistan. *Environmental Pollution*, *266*

1482 Shi, Y., Zhang, J., Reid, J.S., Hyer, E.J., & Hsu, N.C. (2013). Critical evaluation of the MODIS Deep Blue  
1483 aerosol optical depth product for data assimilation over North Africa. *Atmospheric Measurement*  
1484 *Techniques*, *6*, 949-969

1485 Singh, N., Mhawish, A., Deboudt, K., Singh, R.S., & Banerjee, T. (2017). Organic aerosols over Indo-Gangetic  
1486 Plain: Sources, distributions and climatic implications. *Atmospheric Environment*, *157*, 59-74

1487 Smirnov, A., Holben, B.N., Eck, T.F., Dubovik, O., & Slutsker, I. (2000). Cloud-Screening and Quality Control  
1488 Algorithms for the AERONET Database. *Remote Sensing of Environment*, *73*, 337-349

1489 Sogacheva, L., de Leeuw, G., Rodriguez, E., Kolmonen, P., Georgoulas, A.K., Alexandri, G., Kourtidis, K.,  
1490 Proestakis, E., Marinou, E., Amiridis, V., Xue, Y., & van der A, R.J. (2018). Spatial and seasonal  
1491 variations of aerosols over China from two decades of multi-satellite observations – Part 1: ATSR  
1492 (1995–2011) and MODIS C6.1 (2000–2017). *Atmospheric Chemistry and Physics*, *18*, 11389-11407

1493 Song, Z., Fu, D., Zhang, X., Wu, Y., Xia, X., He, J., Han, X., Zhang, R., & Che, H. (2018). Diurnal and seasonal  
1494 variability of PM<sub>2.5</sub> and AOD in North China plain: Comparison of MERRA-2 products and ground  
1495 measurements. *Atmospheric Environment*, *191*, 70-78

1496 Stein, A.F., Draxler, R.R., Rolph, G.D., Stunder, B.J.B., Cohen, M.D., & Ngan, F. (2015). NOAA's HYSPLIT  
1497 Atmospheric Transport and Dispersion Modeling System. *Bulletin of the American Meteorological*  
1498 *Society*, *96*, 2059-2077

1499 Stone, E., Schauer, J., Quraishi, T.A., & Mahmood, A. (2010). Chemical characterization and source  
1500 apportionment of fine and coarse particulate matter in Lahore, Pakistan. *Atmospheric*  
1501 *Environment*, *44*, 1062-1070

1502 Sun, T., Che, H., Qi, B., Wang, Y., Dong, Y., Xia, X., Wang, H., Gui, K., Zheng, Y., Zhao, H., Ma, Q., Du, R., &  
1503 Zhang, X. (2019). Characterization of vertical distribution and radiative forcing of ambient aerosol  
1504 over the Yangtze River Delta during 2013-2015. *Sci Total Environ*, *650*, 1846-1857

1505 Tabinda, A.B., Ali, H., Yasar, A., Rasheed, R., Mahmood, A., & Iqbal, A. (2019). Comparative Assessment of  
1506 Ambient Air Quality of Major Cities of Pakistan. *Mapan*, *35*, 25-32

1507 Tariq, S., & Ali, M. (2015). Spatio-temporal distribution of absorbing aerosols over Pakistan retrieved from  
1508 OMI onboard Aura satellite. *Atmospheric Pollution Research*, *6*, 254-266

1509 Tariq, S., ul-Haq, Z., & Ali, M. (2015). Analysis of optical and physical properties of aerosols during crop  
1510 residue burning event of October 2010 over Lahore, Pakistan. *Atmospheric Pollution Research*, *6*,  
1511 969-978

1512 Tariq, S., Zia, u.-H., & Ali, M. (2016). Satellite and ground-based remote sensing of aerosols during intense  
1513 haze event of October 2013 over Lahore, Pakistan. *Asia-Pacific Journal of Atmospheric Sciences*, *52*,  
1514 25-33

1515 Theil, H. (1992). A Rank-Invariant Method of Linear and Polynomial Regression Analysis. *Henri Theil's*  
1516 *Contributions to Economics and Econometrics* (pp. 345-381)

1517 Tong, Y., Feng, L., Sun, K., & Tang, J. (2020). Assessment of the Representativeness of MODIS Aerosol  
1518 Optical Depth Products at Different Temporal Scales Using Global AERONET Measurements.  
1519 *Remote Sensing*, *12*

1520 Torres, O., Ahn, C., & Chen, Z. (2013). Improvements to the OMI near-UV aerosol algorithm using A-train  
1521 CALIOP and AIRS observations. *Atmospheric Measurement Techniques*, *6*, 3257-3270

1522 Torres, O., Tanskanen, A., Veihelmann, B., Ahn, C., Braak, R., Bhartia, P.K., Veefkind, P., & Levelt, P. (2007).  
1523 Aerosols and surface UV products from Ozone Monitoring Instrument observations: An overview.  
1524 *Journal of Geophysical Research*, *112*, D24S47

1525 Ukhov, A., Mostamandi, S., da Silva, A., Flemming, J., Alshehri, Y., Shevchenko, I., & Stenchikov, G. (2020).  
1526 Assessment of natural and anthropogenic aerosol air pollution in the Middle East using MERRA-2,  
1527 CAMS data assimilation products, and high-resolution WRF-Chem model simulations. *Atmospheric*  
1528 *Chemistry and Physics*, *20*, 9281-9310

1529 ul-Haq, Z., Tariq, S., & Ali, M. (2017). Spatiotemporal assessment of CO<sub>2</sub> emissions and its satellite remote  
1530 sensing over Pakistan and neighboring regions. *Journal of Atmospheric and Solar-Terrestrial*  
1531 *Physics*, 152-153, 11-19

1532 ul-Haq, Z., Tariq, S., Ali, M., Mahmood, K., Batool, S.A., & Rana, A.D. (2014). A study of tropospheric NO<sub>2</sub>  
1533 variability over Pakistan using OMI data. *Atmospheric Pollution Research*, 5, 709-720

1534 Ul\_Haq, Z., Tariq, S., Rana, A.D., Ali, M., Mahmood, K., & Shahid, P. (2015). Satellite remote sensing of  
1535 total ozone column (TOC) over Pakistan and neighbouring regions. *International Journal of Remote*  
1536 *Sensing*, 36, 1038-1054

1537 UNDP (2019). Sustainable Urbanization. In: Development Advocate Pakistan

1538 Ur Rehman, S.A., Cai, Y., Siyal, Z.A., Mirjat, N.H., Fazal, R., & Kashif, S.U.R. (2019). Cleaner and Sustainable  
1539 Energy Production in Pakistan: Lessons Learnt from the Pak-TIMES Model. *Energies*, 13

1540 Veefkind, J.P., de Haan, J.F., Brinksma, E.J., Kroon, M., & Levelt, P.F. (2006). Total ozone from the Ozone  
1541 Monitoring Instrument (OMI) using the DOAS technique. *IEEE Transactions on Geoscience and*  
1542 *Remote Sensing*, 44, 1239–1244

1543 Wang, H., Lu, K., Chen, X., Zhu, Q., Wu, Z., Wu, Y., & Sun, K. (2018). Fast particulate nitrate formation via  
1544 N<sub>2</sub>O<sub>5</sub> uptake aloft in winter in Beijing. *Atmospheric Chemistry and Physics*, 18, 10483-10495

1545 Wang, Q., Sun, L., Wei, J., Yang, Y., Li, R., Liu, Q., & Chen, L. (2017). Validation and Accuracy Analysis of  
1546 Global MODIS Aerosol Products over Land. *Atmosphere*, 8, 155

1547 Wang, Y., Yuan, Q., Li, T., Shen, H., Zheng, L., & Zhang, L. (2019). Evaluation and comparison of MODIS  
1548 Collection 6.1 aerosol optical depth against AERONET over regions in China with multifarious  
1549 underlying surfaces. *Atmospheric Environment*, 200, 280-301

1550 Wang, Y.Q., Zhang, X.Y., & Draxler, R.R. (2009). TrajStat: GIS-based software that uses various trajectory  
1551 statistical analysis methods to identify potential sources from long-term air pollution measurement  
1552 data. *Environmental Modelling & Software*, 24, 938-939

1553 Wang, Y.Q., Zhang, X.Y., Sun, J.Y., Zhang, X.C., Che, H.Z., & Li, Y. (2015). Spatial and temporal variations of  
1554 the concentrations of PM<sub>10</sub>, PM<sub>2.5</sub> and PM<sub>1</sub> in China. *Atmospheric Chemistry and Physics*, 15,  
1555 13585-13598

1556 WHO (2018a). 9 out of 10 people worldwide breathe polluted air, but more countries are taking action.  
1557 In. Geneva

1558 WHO (2018b). WHO Global Ambient Air Quality Database (update 2018). In. Geneva

- 1559 Xiao, Q., Zhang, H., Choi, M., Li, S., Kondragunta, S., Kim, J., Holben, B., Levy, R.C., & Liu, Y. (2016).  
1560 Evaluation of VIIRS, GOCI, and MODIS Collection 6 AOD retrievals against ground sunphotometer  
1561 observations over East Asia. *Atmospheric Chemistry and Physics*, *16*, 1255-1269
- 1562 Xie, Y., Zhang, Y., Xiong, X., Qu, J.J., & Che, H. (2011). Validation of MODIS aerosol optical depth product  
1563 over China using CARSNET measurements. *Atmospheric Environment*, *45*, 5970-5978
- 1564 Zhang, M., Su, B., Bilal, M., Atique, L., Usman, M., Qiu, Z., Ali, M.A., & Han, G. (2020). An Investigation of  
1565 Vertically Distributed Aerosol Optical Properties over Pakistan Using CALIPSO Satellite Data.  
1566 *Remote Sensing*, *12*
- 1567 Zhang, R., Sun, X., Shi, A., Huang, Y., Yan, J., Nie, T., Yan, X., & Li, X. (2018). Secondary inorganic aerosols  
1568 formation during haze episodes at an urban site in Beijing, China. *Atmospheric Environment*, *177*,  
1569 275-282
- 1570